Stony Brook University

A Study of TeV-Scale Physics Beyond the Standard Model, LHC Signals and Dark Matter Implications

A Dissertation Presented

by

Ning Chen

to

The Graduate School

in Partial Fulfillment of the Requirements

for the Degree of

Doctor of Philosophy

in

Physics

Stony Brook University

May 2011

Stony Brook University

The Graduate School

Ning Chen

We, the dissertation committee for the above candidate for the Doctor of Philosophy degree, hereby recommend acceptance of this dissertation.

Robert E. Shrock - Advisor – Dissertation Advisor
Professor, Department of Physics and Astronomy

Peter van Nieuwenhuizen - Committee Chair – Chairperson of Defense
Distinguished Professor, Department of Physics and Astronomy

Robert L. McCarthy
Professor, Department of Physics and Astronomy

Jiangyong Jia
Assistant Professor, Department of Chemistry

Pran Nath
Matthews Distinguished Professor of Physics, Physics Department,
Northeastern University

This dissertation is accepted by the Graduate School.

Lawrence Martin
Dean of the Graduate School

Abstract of the Dissertation

A Study of TeV-Scale Physics Beyond the Standard Model, LHC Signals and Dark Matter Implications

by

Ning Chen

Doctor of Philosophy

in

Physics

Stony Brook University

2011

This thesis is devoted to the study of two major scenarios of physics beyond the Standard Model (SM), namely TeV-scale supersymmetric models and models with dynamical electroweak symmetry breaking.

For the supersymmetric models, we will concentrate on supergravity-mediated grand unification models. We analyze the mass spectra and collider signatures for minimal supergravity (mSUGRA) models. We also study benchmark models with non-universal masses in the gaugino sector. We are particularly interested in some collider signatures that can be discovered in the early LHC experiments with center of mass energy of 7 TeV in operation in the years 2011 and 2012. In addition, we will discuss the dark matter implications

for these benchmark models. For models with dynamical symmetry breaking, we study prospects for the unification of different gauge groups.

To my parents

Contents

List of Figures

List of Tables

Acknowledgements

I would like to express my gratitude to everyone who has supported and helped me during my five years' graduate life in Stony Brook University. Particularly, I would like to address the following people.

My advisor, Prof. Robert Shrock. You suggested various topics in phenomenology and provided me persistent guidance through my research work here. I have learned a lot from you about the methodology of theoretical research from which I will benefit throughout my life.

Prof. Pran Nath in Northeastern University. You helped me a lot for the projects on the supersymmetric model buildings and phenomenology. I learned a lot about the supersymmetric phenomenology through these projects. Your pioneer work on various topics on phenomenology will inspire my future research work all the time. And I would like to thank you for your hospitality in the SUSY09 meeting in Boston.

Prof. Peter van Nieuwenhuizen. It is great pleasure for me to take your series of lectures on various topics in theoretical physics. The crystal lecture notes and your way of explaining physics are the most precious lessons I have taken in Stony Brook and will benefit me a lot in my future research work.

Prof. George Sterman and all other faculty members and staff of YITP. You helped me in many different aspects. Most importantly it is all of you together who offered me this great opportunity to be part of the prestigious YITP and I enjoyed my research and life here very much.

I would like to thank my collaborators in the past two years, Dr. Liu Zuowei here, Dr. Daniel Feldman in MCTP, Baris Altunkaynak and Gregg Peim in Northeastern University. I appreciate your enthusiasm on the work and nice communication with you all.

My friends in the Physics and Astronomy Department, Leo Almeida, Tom Berlijn, Fong Chee-Sheng, Abhijit Gadde, Huang Yu-tin, Li Li, Lin Shu, Itai Ryb, Elli Pomoni, Ilmo Sung, Wang Jue, and Yan Wenbin. It has been such a great pleasure to discuss with you guys about topics in physics as well as everything. I would thank many of my other friends inside or outside of physics. They are Bai Yang, Chen Wei, Dong Hui, Li Ye, Li Yichen, Li Zhaofeng, Liu Hongliang, Liu Jia, Liu Tao, and Zhu Xi.

Lastly, I am extremely grateful to my parents and all family members for a lot of love you give to me. And I would like to thank my cousin Yuan Yu, her husband Dr. Xu Zhen-Ming, and their lovely girls Calla and Elaina.

Chapter 1

Motivations for Physics Beyond Standard Model

In this chapter, we will review the structure of the Standard Model including the Higgs mechanism for the electroweak symmetry breaking. We will motivate why physics above the ~ 100 GeV scale is needed both from theoretical considerations and experimental evidence.

1.1 Brief Review of The Standard Model

1.1.1 Gauge fields and Higgs mechanism

The Standard Model is a gauge theory with gauge symmetry by a direct product of three gauge groups: $\mathcal{G}_{\rm SM} = {\rm SU}(3)_c \times {\rm SU}(2)_L \times {\rm U}(1)_Y$, which stands for color strong interaction and electroweak interaction respectively. The pure gauge sector is described by the Yang-Mills theory with the Lagrangian as follows:

$$\mathcal{L}_{\rm YM} = -\frac{1}{4}\sum_{a=1}^{3}(G^a_{\mu\nu})^2 - \frac{1}{4}\sum_{a=1}^{3}(W^a_{\mu\nu})^2 - \frac{1}{4}(B_{\mu\nu})^2 \tag{1.1}$$

where the field strengths for each gauge symmetry read:

$$G^a_{\mu\nu} = \partial_{[\mu} G^a_{\nu]} + g_s f^{abc} G^b_\mu G^c_\nu \tag{1.2}$$

$$W_{\mu\nu} = \partial_{[\mu} W^a_{\nu]} + g \epsilon^{abc} W^b_\mu W^c_\nu \tag{1.3}$$

$$B_{\mu\nu} = \partial_{[\mu} B_{\nu]} \tag{1.4}$$

Here f^{abc} and ϵ^{abc} are structure constants for $\mathrm{SU}(3)_c$ and $\mathrm{SU}(2)_L$ gauge groups respectively. g_s and g are couplings for $\mathrm{SU}(3)_c$ and $\mathrm{SU}(2)_L$. We also denote the coupling constant for $\mathrm{U}(1)_Y$ as g'.

Next we shall introduce a complex Higgs field φ for the electroweak symmetry breaking (EWSB) [4]. It is chosen to be $\varphi \in 2_1$ representation under the $\mathrm{SU}(2)_L \times \mathrm{U}(1)_Y$, hence this is a proper candidate for the EWSB. Here we use the metric $(-,+,+,+)$. The part of Lagrangian for the Higgs field reads:

$$\mathcal{L}_{\text{higgs}} = -|D_\mu \varphi|^2 - V(\varphi) \tag{1.5}$$

where the covariant derivative is:

$$D_\mu \varphi = \partial_\mu \varphi - i(g \vec{W}_\mu \cdot \frac{\vec{\sigma}}{2} + g' B_\mu \frac{1}{2}) \varphi \tag{1.6}$$

and the Higgs potential is:

$$V(\varphi) = \frac{\lambda}{4} (\varphi^\dagger \varphi - \frac{1}{2} v^2)^2. \tag{1.7}$$

Notice here, the $\lambda > 0$ is required to have the Higgs potential bounded from below. The minimum of this potential gives φ a non-zero vev as $v/\sqrt{2}$. We denote the Higgs doublet explicitly as follows:

$$\varphi \equiv \begin{pmatrix} \phi^+ \\ \phi_0 \end{pmatrix} = \frac{1}{\sqrt{2}} \begin{pmatrix} i\chi^1 + \chi^2 \\ v + h - i\chi^3 \end{pmatrix} \tag{1.8}$$

where $\chi^{1,2,3}$ are the Nambu-Goldstone bosons (NGBs) to be eaten by the $W^{\pm}$ and Z. Ignoring the NGB's and putting (1.8) back into (1.7), one gets terms for Higgs field as:

$$-\mathcal{L}(h) = \frac{\lambda}{4}v^2h^2 + \frac{\lambda}{4}vh^3 + \frac{\lambda}{16}h^4 \tag{1.9}$$

where the first term is the Higgs boson mass $m_h^2 = \frac{1}{2}\lambda v^2$, and the Higgs boson can interact with itself in the form of three-point and four-point vertices. By taking the vev back to the (1.5), one has the mass terms for gauge bosons from the Higgs kinematic terms. With the gauge fields in their mass eigenstate defined as:

$$W_\mu^{\pm} \equiv \frac{1}{\sqrt{2}}(W_\mu^1 \mp iW_\mu^2) \tag{1.10}$$

$$Z_\mu \equiv \cos\theta_w W_\mu^3 - \sin\theta_w B_\mu \tag{1.11}$$

$$A_\mu \equiv \sin\theta_w W_\mu^3 + \cos\theta_w B_\mu \tag{1.12}$$

where the Weinberg mixing angle θ_w is defined as[1]:

$$\tan\theta_w \equiv g'/g \tag{1.13}$$

one gets the mass terms as:

$$\mathcal{L}_{\text{mass}} = -\frac{g^2}{4}v^2W^{+\mu}W_\mu^- - \frac{1}{4}(g'^2+g^2)v^2Z^\mu Z_\mu \tag{1.14}$$

i.e.,

$$M_W = \frac{1}{2}gv \qquad M_Z = \frac{1}{2}\sqrt{g'^2+g^2}v \tag{1.15}$$

[1]Later we use the short notations: $s_w = \sin\theta_w$ and $c_w = \cos\theta_w$.

1.1.2 Matter fields

The Standard Model matter fields coupled to the $\mathcal{G}_{\rm SM}$ gauge fields can be summarized in the following table:

fermions	$\mathrm{SU}(3)_c \times \mathrm{SU}(2)_L \times \mathrm{U}(1)_Y$ representation
$q^a_{i,L}: \binom{u^a}{d^a}_L, \binom{c^a}{s^a}_L, \binom{t^a}{b^a}_L$	$(3,2)_{1/3}$
$u^a_R,\ c^a_R,\ t^a_R$	$(3,1)_{4/3}$
$d^a_R,\ s^a_R,\ b^a_R$	$(3,1)_{-2/3}$
$l_{i,L}: \binom{\nu_e}{e}_L, \binom{\nu_\mu}{\mu}_L, \binom{\nu_\tau}{\tau}_L$	$(1,2)_{-1}$
$e_R,\ \mu_R,\ \tau_R$	$(1,1)_{-2}$

Table 1.1: Standard Model matter fields and their representations under the $\mathcal{G}_{\rm SM}$.

The gauge-invariant Standard Model fermion terms contain the kinematic terms for all fermions. We write down them explicitly:

$$\begin{aligned}
\mathcal{L}(f,G) \;=\; & -(\overline{u}_L, \overline{d}_L)\gamma^\mu(\partial_\mu - ig_s G^a_\mu T^a - ig\vec{W}_\mu\cdot\frac{\vec{\sigma}}{2} - ig'B_\mu\frac{1}{6})\begin{pmatrix} u_L \\ d_L \end{pmatrix} \\
& -\overline{u}_R\gamma^\mu(\partial_\mu - ig_s G^a_\mu T^a - ig'B_\mu\frac{2}{3})u_R \\
& -\overline{d}_R\gamma^\mu(\partial_\mu - ig_s G^a_\mu T^a + ig'B_\mu\frac{1}{3})d_R \\
& -(\overline{\nu}_L, e_L)\gamma^\mu(\partial_\mu - ig\frac{\vec{\sigma}}{2}\cdot\vec{W}_\mu + ig'B_\mu\frac{1}{2})\begin{pmatrix} \nu_L \\ e_L \end{pmatrix} \\
& -\overline{e}_R\gamma^\mu(\partial_\mu + ig'B_\mu)e_R
\end{aligned} \tag{1.16}$$

Bare fermion mass terms are not gauge-invariant. Instead, one can write down gauge-invariant Dirac fermion masses through Yukawa couplings. To have both up-type and down-type quarks and charged leptons get Yukawa couplings, one has to define a charge conjugated Higgs doublet:

$$\tilde{\varphi} \;=\; i\sigma_2\varphi^* = \begin{pmatrix} \phi_0^* \\ -\phi^- \end{pmatrix} \tag{1.17}$$

which is $\tilde{\varphi} \in 2_{-1}$ of the $\mathrm{SU}(2)_L \times \mathrm{U}(1)_Y$ gauge symmetry. Hence the gauge-invariant Yukawa couplings for Standard Model fermions are:

$$\mathcal{L}(f,\varphi) \;=\; y_{ij}^{(e)}\overline{l_{i,L}}\varphi e_{j,R} + y_{ij}^{(u)}\overline{q_{i,L}}\tilde{\varphi}u_{j,R} + y_{ij}^{(d)}\overline{q_{i,L}}\varphi d_{j,R} + h.c. \quad (1.18)$$

where y_{ij}'s are the 3×3 Yukawa coupling matrices for different flavors.

1.2 Problems with the SM Higgs mechanism

A central question for physics beyond the Standard Model is the mechanism for electroweak symmetry breaking. The Standard Model does not explain this, since it does not give any reason for picking the coefficient of the quadratic term in the Higgs potential to be negative instead of the *a priori* an equally likely positive value. Furthermore, even if one accepts this sign choice, there is a very serious problem with the Higgs potential of the Standard Model, namely its instability to radiative corrections. This problem is called the naturalness, fine-tuning or gauge hierarchy problem. Recall that the tree-level Higgs boson mass square reads $\frac{1}{2}\lambda v^2$ from the (1.9). The self-energy correction to the higgs mass at the one-loop level from the (1.9) yields a term that is quadratically sensitive to a high-energy cutoff Λ_{UV}, namely $\delta m_h^2 \sim \lambda\Lambda_{\mathrm{UV}}^2$, where we view this Higgs sector as a low-energy effective field theory. For typical high values of this UV cutoff, one must then carry out an extreme fine-tuning to arrange that the sum of the tree-level contribution to the higgs mass squared combines with the one (and higher) loop contributions in such a manner as to yield a sensible result. This result for the Higgs mass cannot be arbitrarily high. In particular, if it were higher than a value of order a TeV, then the partial wave amplitudes for longitudinally polarized vector boson scattering would violate perturbative unitarity [5]. The Standard Model by itself does not contain any mechanism to protect the Higgs mass squared from a huge radiative shift, of order $\lambda\Lambda_{\mathrm{UV}}^2$.

A related problem in the Standard Model is that the Higgs sector is not asymptotically free. Thus for a fixed high-energy boundary value, $\lambda(Q) > 0$,

the effective, running coupling $\lambda(Q_0) \to 0$ as the momentum scale at which this coupling is evaluated, Q_0 goes to 0. This is the so-called "triviality" problem (called the Landau "zero-charge" problem in the case of quantum electrodynamics, where a similar problem occurs). Phrased in a different but equivalent manner, if one fixes $\lambda(Q_0)$ at some low-energy scale Q_0, and then tracks the evolution of the running quartic coupling at higher momentum scales Q, $\lambda(Q)$ will eventually diverge at a sufficiently large Q. This is called the *Landau pole*. This is one of the reasons why one envisions that the Standard Model with its Higgs sector is not a complete theory but instead is a low-energy effective theory, valid up to some UV cutoff scale where it is embedded in a more complete theory where these difficulties could be removed. For example, this could be the scale of supersymmetry (SUSY) breaking, so that above this scale, the theory is supersymmetric. As will be seen below, at least in the simplest supersymmetric extension of the Standard Model, the quartic coupling λ is replaced by sums of squares of the two electroweak gauge couplings for the $SU(2)_L$ and $U(1)_Y$ gauge groups, $(1/2)(g^2 + g'^2)$, removing both the triviality problem. A supersymmetric extension also removes the quadratic sensitivity of the higgs mass squared to the UV physics.

These problems with the Higgs potential of the Standard Model motivated people to consider alternatives to the Standard Model Higgs mechanism for electroweak symmetry breaking. One possibility is to have some new symmetry to protect Higgs mass from quantum corrections. This possibility is realized in supersymmetric extensions of the Standard Model. Due to the fact that the fermionic loop gives an opposite sign relative to the scalar loop, the supersymmetry solves the gauge hierarchy problem. Furthermore, in the simplest supersymmetric extension of the Standard Model, the quartic Higgs coupling is replaced by $(1/2)(g^2 + g'^2)$, removing the problem with triviality and the Landau pole. Although the supersymmetry must be broken, if it remains exact down to scales of order the electroweak scalar of ~ 300 GeV, then it can achieve its purpose of protecting the Higgs mass from large corrections.

Another possibility is to have a theory in which the electroweak symmetry breaking is not due to the vev of a fundamental Higgs field, but instead is produced dynamically as a nonzero value of a bilinear condensate of fermion

fields. Indeed, in two of the main precursors to electroweak symmetry breaking that we know of, namely the breaking of $U(1)_{em}$ gauge invariance in a superconductor below the phase transition temperature, and the breaking of global $SU(2)_L \times SU(2)_R$ chiral symmetry in hadronic physics (below the deconfinement temperature), phenomenological models were constructed using scalar fields (the Ginzburg-Landau free energy functional for superconductivity and the Gell-Mann Lévy sigma model for hadronic chiral symmetry breaking), and the symmetry breaking was produced by the arranged nonzero vevs of these scalar fields. But in both cases, the microscopic physics was not due to vevs of such hypothetical scalar fields; instead, it was due to the formation of bilinear fermion condensates. In the case of superconductivity, these are the Cooper pairs, and in the case of hadronic symmetry breaking they are the $\langle \bar{q}q \rangle$ quark condensates. In the same way, technicolor theories of electroweak symmetry breaking produce this by positing a new, asymptotically free gauge interaction that gets strong on the TeV scale and produces bilinear condensates of technifermions.

The Large Hadron Collider (LHC) currently running at CERN was designed to elucidate the origin of electroweak symmetry breaking and the physics of the TeV scale. Its first run in 2010 and its continuing run starting in the spring of 2011 has a center-of-mass energy $\sqrt{s} = 7$ TeV, and it is continually increasing the luminosity toward 10^{32} cm^{-2} s^{-1}. After a shutdown, it then plans to upgrade to the full $\sqrt{s} = 14$ TeV and 10^{34} cm^{-2} s^{-1} luminosity. It has already sent important limits on both supersymmetric and dynamical EWSB scenarios for physics beyond the Standard Model.

1.3 Problems of The SM Fermions

1.3.1 Fermion Generations and Mass Hierarchies

Another basic problem in the Standard Model is that it gives no explanation of the number of fermion generations ($N_{gen} = 3$), and it accommodates, but does not explain the observed fermion masses. In particular, it produces the masses of quarks and charged leptons via Yukawa couplings to the Higgs, but

this requires a huge range of magnitudes of Yukawa couplings from 10^{-5} to unity, without any explanation. It fails to explain either the intergenerational fermion mass hierarchies of the mass splittings within each Standard Model generation.

1.3.2 Neutrino masses

The original Standard Model made a prediction for neutrino masses, and it was that they are zero. Hence, the evidence for neutrino masses and lepton mixing that accumulated from the late 1960's with the original solar neutrino Chlorine experiment of Ray Davis and collaborators through to the compelling evidence obtained by the SuperKamiokande experiment in 1998 from both its solar and atmospheric neutrino data have been the first confirmed evidence for physics beyond the Standard Model. This evidence has forced a modification of this model to include neutrino masses and lepton mixing. The results from the Davis and the SuperKamiokande experiments have been confirmed by later experiments, including the K2K and MINOS accelerator experiments, the Sudbury Neutrino Observatory (SNO) solar neutrino experiment, and the KamLAND reactor antineutrino experiment. Defining $\Delta m_{ij} = m(\nu_i)^2 - m(\nu_j)^2$, the existing neutrino data [62] gives $|\Delta m_{32}| \simeq 2.4 \times 10^{-3}$ eV^2, and $|\Delta m_{21}| \simeq 7.6 \times 10^{-5}$ eV^2. Several leptonic mixing angles have also been measured, with the results $\sin^2(2\theta_{23}) \simeq 1$, $\sin^2(2\theta_{12}) \simeq 0.9$, with an upper bound $\sin^2(2\theta_{13}) \lesssim 0.15$. There are a number of theoretical approaches to explaining very small neutrino masses. For example, one can use a seesaw mechanism in the context of supersymmetric grand unification [8] and also (with different Majorana and Dirac neutrino energy scales) in the context of technicolor [121] [123].

1.4 Other Problems of the Standard Model

The Standard Model gauge sector has three gauge couplings (g_s, g, g') for three subgroups. Their strengths at the M_Z^2 scale were precisely measured at the Large Electron-Positron (LEP) and Stanford Linear Collider (SLAC) as follows

[61]:

$$g_s^2(M_Z) \simeq 1.495, \qquad g^2(M_Z) \simeq 0.424, \qquad g'^2(M_Z) \simeq 0.1277 \qquad (1.19)$$

or equivalently,

$$\alpha_s(M_Z) \simeq 0.118, \qquad \alpha(M_Z) \simeq 3.37 \times 10^{-2}, \qquad \alpha'(M_Z) \simeq 1.02 \times 10^{-2}, \quad (1.20)$$

where $\alpha_s = g_s^2/(4\pi)$, etc. The Standard Model itself does not predict the magnitudes for three different gauge couplings. A complete theory would predict the values of these couplings, or at least their ratios. One appealing approach is a supersymmetric grand unification theory (GUT), where the $\mathcal{G}_{\rm SM}$ is embedded into a larger simple non-Abelian gauge group, e.g. SU(5) or SO(10) [6] [7].

In the Standard Model, the electric charge Q is given by $Q = T_3 + (Y/2)$, where T_3 and Y refer to weak isospin and hypercharge. Because the weak hypercharge is an abelian $\mathrm{U}(1)_Y$ group, this means that the Standard Model does not explain the observed quantization of electric charge. Again, this can be done in a grand unified theory. Other problems that the Standard Model does not explain include the fact that, because of instantons, QCD does not automatically conserve P or T (equivalently, CP).

A particularly important problem for the Standard Model is the issue of dark matter. In the 1930s Zwicky analyzed the motions of galaxies in the Coma cluster and found that these motions were considerably greater than could be accounted for by visible matter [88] [89]. Since this time there has been a progressive accumulation of evidence for dark matter. Among the more recent pieces of evidence was the measurement of velocity rotation curves for several galaxies by Rubin et al., which showed that these velocities were again much greater than could be accounted for by the visible matter. From these and other pieces of observational evidence, it has been concluded that baryonic matter comprises only about $\sim 4\%$ of all of the mass/energy in the Universe. Approximately $\sim 23\%$ is inferred to be composed of dark matter, while $\sim 70\%$

is "dark energy" associated with the observed accelerated expansion of the universe [88] [89]. (At present, this dark energy is consistent with being a cosmological constant.) Clearly, a dark matter candidate particle should have a lifetime comparable with the age of the universe. This property may be built into a model if that model has some exact discrete parity that prevents the particle from decaying. In addition, the dark matter particle should be a color singlet and have zero electric charge, or else it would not be dark. Aside from primordial black holes, the Standard Model does not contain a candidate for this dark matter, so this strongly suggests further physics beyond the Standard Model. There are many possible candidates for dark matter particles. In gravity-mediated supersymmetric models, the lightest sparticle (LSP) is generically the lightest neutralino $\tilde{\chi}_1^0$ with mass $\sim \mathcal{O}(100 \text{ GeV})$. Such a particle can satisfy basic requirements of a dark matter candidate.

Another relevant quantity from astrophysics and cosmology is the average baryon asymmetry in the universe. To generate a non-zero baryon number from the initially baryon symmetric state, three conditions (called *Sakharov conditions*) [85] are necessary: (i) baryon number violation, (ii) C and CP violation, and (iii) non-equilibrium condition.

Chapter 2

The Minimal Supersymmetric Standard Model (MSSM)

We shall apply the WZ theory and SYM theory to construct a supersymmetric extension of the Standard Model. In this chapter, we focus on the minimal extension, called the Minimal Supersymmetric Standard Model (MSSM). During this construction, we shall use the Standard Model gauge symmetry $\mathcal{G}_{\rm SM} = {\rm SU}(3)_c \times {\rm SU}(2)_L \times {\rm U}(1)_Y$ and the necessary matter representations. The inclusion of soft SUSY-breaking terms will be shown in this chapter, and their origins in the ultraviolet later in this thesis. We will also discuss the mass spectrum of the supersymmetric particles (sparticles) in this MSSM model.

2.1 Field Contents of The MSSM

Now we list the field content of the MSSM. From the discussion of WZ theory and SYM theory, the matter fields form chiral supermultiplets of the generic form (ϕ, ψ, F) and the gauge fields form Lie-algebra valued vector supermultiplets of the generic form (λ, A_μ, D). Each component of the supermultiplet transforms according to the same representation of the relevant gauge group. Hence it is straightforward to list all MSSM fields[1] in the gauge sector and matter sector. The fermion fields are written in left-handed holomorphic form.

[1] We indicate the representation of all fields by their dimensions.

Our notation is $\psi_L^c \equiv (\psi_R)^c$. The subscripts L on the scalar components refer to their correspondence to the chiral fermion fields.

vector multiplet and field strength	spin 1/2	spin 1	$\mathrm{SU}(3)_c$, $\mathrm{SU}(2)_L$, $\mathrm{U}(1)_Y$
V_G, W_G	$\tilde{g}$	g	$(8,1)_0$
V_W, W_W	$\tilde{W}$	W	$(1,3)_0$
V_Y, W_Y	$\tilde{B}$	B	$(1,1)_0$

Table 2.1: MSSM superfields in the gauge sector.

chiral multiplet	spin 0	spin 1/2	$\mathrm{SU}(3)_c$, $\mathrm{SU}(2)_L$, $\mathrm{U}(1)_Y$
$Q_{i,L}$	$(\tilde{u}, \tilde{d})_L$	$(u,d)_L$	$(3,2)_{1/3}$
$\bar{U}_{i,L}$	$\tilde{u}_L^c$	u_L^c	$(\overline{3},1)_{-4/3}$
$\bar{D}_{i,L}$	$\tilde{d}_L^c$	d_L^c	$(\overline{3},1)_{2/3}$
$L_{i,L}$	$(\tilde{\nu}, \tilde{e})_L$	$(\nu, e)_L$	$(1,2)_{-1}$
$\bar{E}_{i,L}$	$\tilde{e}_L^c$	e_L^c	$(1,1)_2$
H_u	(h_u^+, h_u^0)	$(\tilde{H}_u^+, \tilde{H}_u^0)$	$(1,2)_1$
H_d	(h_d^0, h_d^-)	$(\tilde{H}_d^0, \tilde{H}_d^-)$	$(1,2)_{-1}$

Table 2.2: MSSM superfields in the matter sector. $i = 1,2,3$ are indices for three generations of sfermions and fermions.

The MSSM contains two Higgs doublets and each is responsible for giving mass to the up-type or down-type matters (i.e., both fermions and sfermions). This is also necessary for the gauge anomaly cancellation.

2.2 Anatomy of The MSSM Lagrangian

The full Lagrangian of the MSSM is more complicated than the Standard Model one. A most general form of the MSSM Lagrangian contains two parts:

$$\mathcal{L}_{\mathrm{MSSM}} \;=\; \mathcal{L}_{\mathrm{SUSY}} + \mathcal{L}_{\mathrm{soft}} \tag{2.1}$$

One can denote all vector multiplets and their field strength as $(V_A, W_A) = (V_A^a, W_A^a)T^a$, and denote all chiral matter fields as Φ_i. The supersymmetric part contains the pure gauge sector, matter-YM coupling part, and the superpotential term for the chiral fields:

$$\begin{aligned}\mathcal{L}_{\rm SUSY} &= \frac{1}{4}(\int d^2\theta W_A^\alpha W_{A,\alpha} + h.c.) + \int d^4\theta \Phi_i^\dagger (e^{gV})_j^i \Phi_j \\ &+ \int d^2\theta (h_i\Phi_i + \frac{1}{2}\mu_{ij}\Phi_i\Phi_j + \frac{1}{3!}f_{ijk}\Phi_i\Phi_j\Phi_k) + h.c. \end{aligned} \tag{2.2}$$

The most general soft SUSY-breaking terms are written as:

$$\begin{aligned}\mathcal{L}_{\rm soft} &= -(m^2)_{ij}\phi_i^\dagger\phi_j - (\frac{1}{3!}\mathcal{A}_{ijk}\phi_i\phi_j\phi_k + \frac{1}{2}\mathcal{B}_{ij}\phi_i\phi_j + \mathcal{C}_i\phi_i + h.c.) \\ &-(\frac{1}{2}M\lambda^a\lambda^a + h.c.) \end{aligned} \tag{2.3}$$

with ϕ_i being the scalar component of Φ_i and λ^a being the gaugino fields. The m_{ij}^2-term and the $M-$term are the soft masses for sfermions and gauginos. The $\mathcal{A}_{ijk}$, $\mathcal{B}_{ij}$, and $\mathcal{C}_i$ are the most general soft terms for the scalar fields one can write down as long as they are gauge invariant. In particular, the $\mathcal{C}_i$ term requires that the scalar field ϕ_i itself to be gauge invariant. Since we do not have a gauge invariant field in the MSSM, this linear term is not considered in the soft term.

2.2.1 Supersymmetric terms

The $\mathcal{L}_{\rm SUSY}$ stands for the renormalizable supersymmetric part, which is just SYM and WZ theories with the Standard Model gauge group and proper quantum number assignment to matter fields following Table (2.1). Explicitly, the pure gauge sector (SYM) of the MSSM has the following Lagrangian containing three separate superspace field strengths:

$$\mathcal{L}_{\rm SYM} = \frac{1}{4}\int d^2\theta (W_G^\alpha W_{G,\alpha} + W_W^\alpha W_{W,\alpha} + W_Y^\alpha W_{Y,\alpha}) + h.c. \tag{2.4}$$

The gauge fields also couple to the matter fields (both sfermion-fermion multiplets and higgs-higgsino multiplets) in forms of the (A.14):

$$\begin{aligned}\mathcal{L}_{\rm matter} = &\int d^4\theta (Q_{i,L}^\dagger \exp(g_s V_G + g V_W + g' V_Y Y) Q_{i,L} + \\ &+ U_{i,R}^\dagger \exp(g_s V_G + g' V_Y Y) U_{i,R} + D_{i,R}^\dagger \exp(g_s V_G + g' V_Y Y) D_{i,R} \\ &+ L_{i,L}^\dagger \exp(g V_W + g' V_Y Y) L_{i,L} + E_{i,R}^\dagger \exp(g' V_Y Y) E_{i,R} \\ &+ \sum_{p=u,d} H_p^\dagger \exp(g V_W + g' V_Y Y) H_p)\end{aligned} \tag{2.5}$$

The MSSM superpotential contains all matter fields listed in Table (2.1) as:

$$\begin{aligned}\mathcal{W}_{\rm MSSM} = &-(y_u)_{ij} Q_{i,L} H_u U_{j,R} - (y_d)_{ij} Q_{i,L} H_d D_{j,R} - (y_e)_{ij} L_{i,L} H_d E_{j,R} \\ &+ \mu H_u H_d\end{aligned} \tag{2.6}$$

with y_u, y_d and y_e being the 3×3 dimensionless Yukawa coupling matrices in the generation space.

2.2.2 Soft breaking terms

Without explaining the dynamical origin yet, we will simply write down the most general soft SUSY-breaking terms for the MSSM. The soft SUSY-breaking terms can be decomposed into four parts:

$$\mathcal{L}_{\rm soft} = \mathcal{L}_{\tilde{f}} + \mathcal{L}_A + \mathcal{L}_\lambda + \mathcal{L}_h \tag{2.7}$$

where $\mathcal{L}_{\tilde{f}}$ contains the sfermion mass terms, $\mathcal{L}_A$ contains the trilinear couplings between sfermions and MSSM Higgs, $\mathcal{L}_\lambda$ contains the gaugino (Majorana) mass terms, and $\mathcal{L}_h$ contains the MSSM Higgs mass terms. Their explicit expressions read:

$$\begin{aligned}
\mathcal{L}_{\tilde{f}} &= -\tilde{q}^\dagger_{iL}(M^2_{\tilde{q}})_{ij}\tilde{q}_{jL} - \tilde{u}^\dagger_{iR}(M^2_{\tilde{u}})_{ij}\tilde{u}_{jR} - \tilde{d}^\dagger_{iR}(M^2_{\tilde{d}})_{ij}\tilde{d}_{jR} \\
&\quad -\tilde{l}^\dagger_{iL}(M^2_{\tilde{l}})_{ij}\tilde{l}_{jL} - \tilde{e}^\dagger_{iR}(M^2_{\tilde{e}})_{ij}\tilde{e}_{jR} \qquad (2.8) \\
\mathcal{L}_A &= -H_d \cdot \tilde{l}_{iL}(y_e A_e)_{ij}\tilde{e}^\dagger_{jR} - H_d \cdot \tilde{q}_{iL}(y_d A_d)_{ij}\tilde{d}^\dagger_{jR} \\
&\quad -H_u \cdot \tilde{q}_{iL}(y_u A_u)_{ij}\tilde{u}^\dagger_{jR} + h.c. \qquad (2.9) \\
\mathcal{L}_h &= -m^2_{H_u}|H_u|^2 - m^2_{H_d}|H_d|^2 - (bH_u H_d + h.c.) \qquad (2.10) \\
\mathcal{L}_\lambda &= -\frac{1}{2}(M_3\tilde{g}\tilde{g} + M_2\tilde{W}\tilde{W} + M_1\tilde{B}\tilde{B} + h.c.) \qquad (2.11)
\end{aligned}$$

2.3 Sparticle Spectrum

In this part of discussion, we will present the sparticle spectrum based upon the discussion of the general MSSM structures, including MSSM Higgs, charginos, neutralinos, and sfermions.

2.3.1 MSSM Higgs

The Higgs spectrum in the context of MSSM is more complicated than the Standard Model case in that: there are two complex Higgs doublets, which yield five MSSM Higgs fields after the EWSB; there are both supersymmetric and soft term contributions to the Higgs masses. The scalar potential for the Higgs fields is the following:

$$\begin{aligned}
V &= (|\mu|^2 + m^2_{H_u})(|h^0_u|^2 + |h^+_u|^2) + (|\mu|^2 + m^2_{H_d})(|h^0_d|^2 + |h^-_d|^2) \\
&\quad +\frac{1}{8}(g^2 + g'^2)(|h^0_u|^2 + |h^+_u|^2 - |h^0_d|^2 - |h^-_d|^2)^2 \\
&\quad +b(h^+_u h^-_d - h^0_u h^0_d) + h.c. + \frac{1}{2}g^2|h^+_u h^{0*}_d + h^0_u h^{-*}_d|^2 \qquad (2.12)
\end{aligned}$$

where the MSSM higgs fields are in their gauge eigenstates following from Table (2.1). The $|\mu|^2$ terms come from the F-terms of the Higgs doublets inside the MSSM superpotential (2.6). The $m^2_{H_u}$, $m^2_{H_d}$, and b are the soft mass terms shown in the (2.10). Different from the Standard Model, the Higgs also get contributions proportional to g^2 and g'^2 as from the D-terms of the Higgs chiral multiplets coupling to the vector multiplets (2.5).

Clearly the minima of the (2.12) should be electrically neutral, which means one should set their vev's to be $\langle h_u^+ \rangle = \langle h_d^- \rangle = 0$. Hence the (2.12) is simplified into:

$$\begin{aligned} V &= (|\mu|^2 + m^2_{H_u})|h_u^0|^2 + (|\mu|^2 + m^2_{H_d})|h_d^0|^2 - (b h_u^0 h_d^0 + h.c.) \\ &\quad + \frac{1}{8}(g^2 + g'^2)(|h_u^0|^2 - |h_d^0|^2)^2 \end{aligned} \tag{2.13}$$

Two requirements should be made on the (2.13): (i) this potential should be bounded from below; (ii) a linear combination of h_u^0 and h_d^0 should yield negative mass square to trigger the EWSB. These two conditions are therefore:

$$\begin{aligned} 2b &< 2|\mu|^2 + m^2_{H_u} + m^2_{H_d} \\ b^2 &> (|\mu|^2 + m^2_{H_u})(|\mu|^2 + m^2_{H_d}) \end{aligned} \tag{2.14}$$

With necessary conditions (2.14) for h_u^0 and h_d^0 to get their vev's, one can assign them as:

$$\langle h_u^0 \rangle = v_u = v \sin\beta \qquad \langle h_d^0 \rangle = v_d = v \cos\beta \tag{2.15}$$

which are related to the W mass as:

$$m_W^2 = \frac{1}{2} g^2 v^2 = \frac{1}{2} g^2 (v_u^2 + v_d^2) \tag{2.16}$$

and the ratio between two vev's reads:

$$\tan\beta \equiv \frac{v_u}{v_d} \tag{2.17}$$

One can write down the conditions $\partial V/\partial h_u^0 = \partial V/\partial h_d^0 = 0$ which minimize the potential (2.13) as follows:

$$\begin{aligned} |\mu|^2 + m_{H_u}^2 - b\cot\beta - \frac{m_Z^2}{2}\cos(2\beta) = 0 \\ |\mu|^2 + m_{H_d}^2 - b\tan\beta + \frac{m_Z^2}{2}\cos(2\beta) = 0 \end{aligned} \tag{2.18}$$

However, these relations imply the so-called "μ problem" [14] immediately. μ should be a supersymmetric parameter since it shows up in the MSSM superpotential, while the other quantities m_{H_u}, m_{H_d}, and b are soft-breaking parameters. In other words, the $|\mu|^2$ parameter should be fine-tuned into a similar size with other soft parameters $m_{H_u}^2$, $m_{H_d}^2$, b, and also m_Z^2.

Now we shall give the Higgs mass terms in their mass eigenstates. Two complex Higgs doublets contain eight real components. After the EWSB, three of them (one neutral G^0 and two with ± 1 charges $G^\pm$) are eaten by the $W^\pm$ and Z. Five real components (three neutral ones and two charged ones) shall consist of two CP-even scalars h^0 and H^0, one CP-odd scalar A^0, and two charged ones $H^\pm$. In particular, CP- is only used to refer the MSSM Higgs sector here since the MSSM itself introduces CP-violation sources. Explicitly we denote them as:

$$\begin{pmatrix} h_u^0 \\ h_d^0 \end{pmatrix} = \begin{pmatrix} v_u \\ v_d \end{pmatrix} + \frac{1}{\sqrt{2}} R_\alpha \begin{pmatrix} h^0 \\ H^0 \end{pmatrix} + \frac{i}{\sqrt{2}} R_{\beta_0} \begin{pmatrix} G^0 \\ A^0 \end{pmatrix} \tag{2.19}$$

$$\begin{pmatrix} h_u^+ \\ h_d^{-*} \end{pmatrix} = R_{\beta_\pm} \begin{pmatrix} G^+ \\ H^+ \end{pmatrix} \tag{2.20}$$

with R_α, R_{β_0}, and $R_{\beta_\pm}$ being the rotation matrices between the corresponding gauge eigenstates and the mass eigenstates. Plugging the (2.19) and (2.20)

into the (2.12), it is easy to obtain the tree-level Higgs masses as:

$$
\begin{aligned}
m^2_{A^0} &= 2|\mu|^2 + m^2_{H_u} + m^2_{H_d} && (2.21)\\
m^2_{h^0,H^0} &= \frac{1}{2}\left(m^2_{A^0} + m^2_Z \mp \sqrt{(m^2_{A^0} - m^2_Z)^2 + 4m^2_Z m^2_{A^0}\sin^2(2\beta)}\right) && (2.22)\\
m^2_{H^\pm} &= m^2_{A^0} + m^2_W && (2.23)
\end{aligned}
$$

However, another problem emerges from the (2.22), namely the lightest Higgs h^0 has an unacceptable mass upper bound at the tree level:

$$m_{h^0} < m_Z|\cos(2\beta)| \tag{2.24}$$

If the (2.24) were true, the lightest MSSM Higgs boson should have been discovered at LEP2. From the above inequality, the lightest CP-even higgs mass can approach to m_Z when $\tan\beta \gg 1$. However, it was shown that the quantum corrections from the top quark loop and the stop loop turn out to be significant. For example in the limit of small stop mixings and $m_{\tilde{t}_{1,2}} \gg m_t$, one gets:

$$\delta(m^2_{h^0}) = \frac{3}{4\pi^2}\cos^2\alpha y_t^2 m_t^2 \log\frac{m_{\tilde{t}_1} m_{\tilde{t}_2}}{m_t^2} \tag{2.25}$$

2.3.2 Chargino

The gauge eigenstates for the chargino sector are $\psi^\pm \equiv (\tilde{W}^+, \tilde{H}_u^+, \tilde{W}^-, \tilde{H}_d^-)$, with the mass term expressed as:

$$\mathcal{L}_{\tilde{C}} = -\frac{1}{2}(\psi^\pm)^T M_{\tilde{C}} \psi^\pm + h.c. \tag{2.26}$$

where,

$$M_{\tilde{C}} = \begin{pmatrix} \mathbf{0} & \mathbf{X}^T \\ \mathbf{X} & \mathbf{0} \end{pmatrix} \tag{2.27}$$

with

$$\mathbf{X} = \begin{pmatrix} M_2 & \sqrt{2} m_W \sin\beta \\ \sqrt{2} m_W \cos\beta & \mu \end{pmatrix} \tag{2.28}$$

It is straightforward to diagonalize the (2.28) to obtain two chargino masses:

$$\begin{aligned} m^2_{\tilde{C}_1,\tilde{C}_2} &= \frac{1}{2}(M_2^2 + |\mu|^2 + 2m_W^2 \\ &\quad \mp \sqrt{(M_2^2 + |\mu|^2 + 2m_W^2)^2 - 4|\mu M_2 - m_W^2 \sin 2\beta|^2}) \end{aligned} \tag{2.29}$$

Taking μ to be real by absorbing the phases into the gauginos and Higgs chiral fields, and the limit of $m_Z \ll (\mu, M_2)$, their masses are simplified into:

$$m_{\tilde{C}_1} = M_2 - \frac{m_W^2(M_2 + \mu \sin 2\beta)}{\mu^2 - M_2^2} + ... \tag{2.30}$$

$$m_{\tilde{C}_2} = \mu + \frac{m_W^2 I(\mu + M_2 \sin 2\beta)}{\mu^2 - M_2^2} + ... \tag{2.31}$$

with $I \equiv \mathrm{sgn}(\mu)$ and ... stands for terms in higher order of $(m_Z/M_2)^2$ and $(m_Z/\mu)^2$.

2.3.3 Neutralino

In terms of the gauge eigenstates $\psi^0 \equiv (\tilde{B}, \tilde{W}, \tilde{H}_d^0, \tilde{H}_u^0)$, one gets the neutralino mass terms as:

$$\mathcal{L}_{\tilde{N}} = -\frac{1}{2}(\psi^0)^T M_{\tilde{N}} \psi^0 + h.c. \tag{2.32}$$

It is easy to see that the $M_{\tilde{N}}$ contains three parts: the $\mathrm{SU}(2)_L \times \mathrm{U}(1)_Y$ gaugino soft masses $M_{1,2}$, the higgsino μ terms, and the off-diagonal terms from the higgsino-gaugino-higgs coupling after $\langle h_d^0 \rangle$ and $\langle h_u^0 \rangle$ getting their vev's. The explicit matrix reads:

$$M_{\tilde{N}} = \begin{pmatrix} M_1 & 0 & -c_\beta s_W m_Z & s_\beta s_W m_Z \\ 0 & M_2 & c_\beta c_W m_Z & -s_\beta c_W m_Z \\ -c_\beta s_W m_Z & c_\beta c_W m_Z & 0 & -\mu \\ s_\beta s_W m_Z & -s_\beta c_W m_Z & -\mu & 0 \end{pmatrix} \tag{2.33}$$

By a unitary transformation, the (2.33) is diagonalized and the gauge eigenstates are transformed into four mass eigenstates: $\tilde{\chi}_i^0 = Z_{ij}\psi_j^0$ with $i, j = 1, 2, 3, 4$ for four neutralino components. The Z_{1i} entries measure the eigen contents of the lightest neutralino $\tilde{\chi}_1^0$ (or the LSP in the context of supergravity models): Z_{11} for bino $\tilde{B}$, Z_{12} for wino $\tilde{W}$, and (Z_{13}, Z_{14}) for higgsinos $(\tilde{H}_d^0, \tilde{H}_u^0)$. These components will turn out to play important roles in the discussion of dark matter in the supergravity-mediation framework.

2.3.4 Sfermions

In the case of the MSSM, one would expect three 6×6 matrices for the up-type squarks, down-type squarks, and the charged sleptons; together with one 3×3 matrix for the sneutrinos. However, the third generations can get very different masses since they get important contributions due to the large Yukawa couplings (y_t, y_b, y_τ) and soft parameters (A_t, A_b, A_τ).

The spectra for the first two generations of squarks and sleptons are the following:

$$m^2_{\tilde{u}_L,\tilde{d}_L} = M_0^2 + K_3 + K_2 + \frac{1}{36}K_1 + \Delta_{\tilde{u}_L,\tilde{d}_L} \tag{2.34}$$

$$m^2_{\tilde{u}_R} = M_0^2 + K_3 + \frac{4}{9}K_1 + \Delta_{\tilde{u}_R} \tag{2.35}$$

$$m^2_{\tilde{d}_R} = M_0^2 + K_3 + \frac{1}{9}K_1 + \Delta_{\tilde{d}_R} \tag{2.36}$$

$$m^2_{\tilde{e}_L,\tilde{\nu}_L} = M_0^2 + K_2 + \frac{1}{4}K_1 + \Delta_{\tilde{e}_L,\tilde{\nu}_L} \tag{2.37}$$

$$m^2_{\tilde{e}_R} = M_0^2 + K_2 + \frac{1}{4}K_1 + \Delta_{\tilde{e}_R} \tag{2.38}$$

Some explanation is needed for three different contributions to sfermion masses. Implicitly we have assumed a universal scalar squared mass M_0^2 appearing for all squark flavors. Such an assumption is quite natural in the minimal supergravity mediation (mSUGRA) models, which will be discussed in detail in the next chapter. The contributions of $K_{1,2,3}$ are due to the chiral supermultiplets coupling to the gauginos. Explicitly, they read:

$$K_\alpha(Q^2) \;\; = \;\; C_{2,\alpha} \times \frac{1}{2\pi^2} \int_{\log Q}^{\log Q_0} dt g_\alpha^2(t) |M_\alpha(t)|^2 \tag{2.39}$$

where α denotes different gauge symmetry contributions without summation. The $g_\alpha(t)$ and $M_\alpha(t)$ should run according to their RGE's to be discussed soon. The coefficients $C_{2,\alpha} = (3/5, 3/4, 4/3)$ for $\alpha = 1, 2, 3$ are the quadratic Casimir invariants for the $\mathrm{SU}(3)_c$ and $\mathrm{SU}(2)_L$ respectively; while 3/5 for the $K_1(Q^2)$ is due to the U(1) coupling rescaling for the GUT model. Q_0 is the input RG scale where boundary conditions to the soft parameters are imposed, and Q is typically the scale around the sfermion masses below 1 TeV. Specifically when a universal gaugino mass is imposed at the GUT scale, one can easily obtain that $K_3 \gg K_2 \gg K_1$. This implies that squarks are generally heavier than sleptons with this assumption. Furthermore, there is a hyperfine splitting term $\Delta_{\tilde{f}}$ within each generation of squarks and sleptons due to the sfermion couplings to the Higgs doublets $\sim \tilde{f}^* \tilde{f} H_{u,d}$ after Higgs doublets picking up the vev's. For particular sfermion $\tilde{f}$, this reads:

$$\Delta_{\tilde{f}} = (T_{3\tilde{f}} - Q_{\tilde{f}} s_W^2)\cos(2\beta) m_Z^2 \tag{2.40}$$

The spectra for the third generation of squarks and sleptons are different. We shall take stop mass matrix for our illustration. First, there are usual diagonal terms for $\tilde{t}_L^* \tilde{t}_L$ and $\tilde{t}_R^* \tilde{t}_R$ like the first two generations of squarks. In addition, there is m_t^2 contribution due to the large top Yukawa coupling. Second, there are soft trilinear coupling contributions from the $A^t \tilde{q}_3 H_u^0 \tilde{t} + h.c.$. Third, there are contribution from the combined Higgs F-terms of $y_u Q_L H_u U_R$ and $\mu H_u H_d$. Such terms are neglected for the first two generational sfermions since their Yukawa couplings are small. Therefore, the stop mass matrix reads:

$$m_{\tilde{t}}^2 = \begin{pmatrix} M_0^2 + K_3 + K_2 + \frac{1}{36}K_1 & v(A_t^* \sin\beta - \mu y_t \cos\beta) \\ \quad + \Delta_{\tilde{u}_L} + m_t^2 & \\ & M_0^2 + K_3 + \frac{4}{9}K_1 \\ v(A_t \sin\beta - \mu^* y_t \cos\beta) & \quad + \Delta_{\tilde{u}_R} + m_t^2 \end{pmatrix} \tag{2.41}$$

It is easy to diagonalize the (2.41) by a unitary transformation into the mass eigenstates:

$$\begin{pmatrix} \tilde{t}_1 \\ \tilde{t}_2 \end{pmatrix} = \begin{pmatrix} c_{\tilde{t}} & -s_{\tilde{t}} \\ s_{\tilde{t}} & c_{\tilde{t}} \end{pmatrix} \begin{pmatrix} \tilde{t}_L \\ \tilde{t}_R \end{pmatrix} \tag{2.42}$$

The significant off-diagonal entries for the third generation squark here would generally induce a strong mixing between the left and right components. Therefore the $\tilde{t}_1$ is the lightest squark among all.

2.4 Renormalization Group Equations (RGE) in The MSSM

Having demonstrated the structure of the MSSM sparticle mass spectra, one needs the one-loop RGE's of soft parameters in the MSSM to derive them from some UV theories. This is summarized in the Ref. [12] with two-loop effects taken into account. Here we will only focus on the gauge coupling evolution in the MSSM, where three gauge couplings unify at a GUT scale $M_U \simeq 2 \times 10^{16}$ GeV. And we also mention the implication to the gaugino masses at the electroweak scale.

We start from the one-loop RGE's for the gauge couplings in the MSSM. Recall that the one-loop β function for the non-supersymmetric YM coupling (with $t = \log \mu$, where μ is the momentum scale) reads:

$$8\pi^2 \frac{dg^2}{dt} = \left(-\frac{11}{3} C_2(\mathcal{G}) + \frac{2}{3} \sum_i T(\mathcal{R}_i) + \frac{1}{3} \sum_\alpha T(\mathcal{R}_\alpha) \right) g^4 \quad (2.43)$$

Here $C_2(\mathcal{G})$ is the quadratic Casimir invariant of the gauge group $\mathcal{G}$, which reads $C_2(\mathcal{G}) = N$ for non-Abelian gauge group $\mathcal{G} = \mathrm{SU}(N)$ and vanishes for Abelian gauge group U(1). $T(\mathcal{R}_i)$ and $T(\mathcal{R}_\alpha)$ are trace invariants from the chiral fermions in the representation $\mathcal{R}_i$ and complex scalars in the representation $\mathcal{R}_\alpha$. In SM/MSSM case, matter fields are either in the fundamental representation of the non-Abelian gauge group or charged under the $\mathrm{U}(1)_Y$. Hence $T(\mathcal{R}) = 1/2$ for the non-Abelian fundamental representation, or $T(\mathcal{R}) = Y^2/4$ for the $\mathrm{U}(1)_Y$ charges.

The one-loop β function for the SYM (coupled with chiral matters) coupling is simply obtained from the above (2.43) by the fact that fields within a chiral supermultiplet (ϕ, ψ) and fields within vector multiplets (λ_α, A_μ) are in the same representation. For the vector multiplet, its components are in the adjoint representation of the $\mathcal{G}$ in particular. Therefore, one simply takes the contribution from the chiral fermion into the gauge sector and complex scalars respectively. Hence the one-loop β function for the SYM coupling reads:

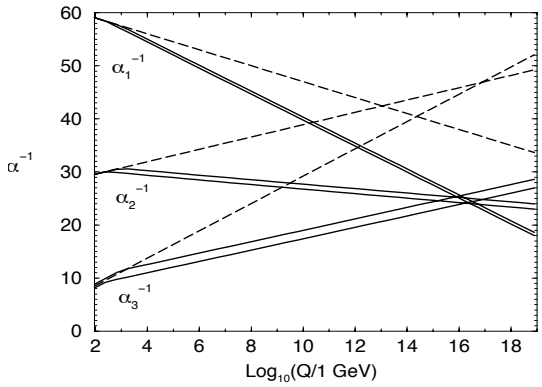

Figure 2.1: Gauge coupling constant evolution for the SM (dashed lines) and the MSSM (double solid lines). Two-loop effects are included.

$$8\pi^2 \frac{dg^2}{dt} = \left(-3C_2(\mathcal{G}) + \sum_\alpha T(\mathcal{R}_\alpha) \right) g^4 \equiv b^{(1)} g^4 \tag{2.44}$$

where one sums over all chiral matter multiplets in the trace invariants. Its solution is then simply:

$$g^2(Q) = g^2(Q_0) \left(1 - \frac{1}{8\pi^2} b^{(1)} g^2(Q_0) \log \frac{Q}{Q_0} \right)^{-1} \tag{2.45}$$

For the MSSM with $\mathcal{G} = \mathrm{SU}(3)_c \times \mathrm{SU}(2)_L \times \mathrm{U}(1)_Y$, we can easily give the one-loop coefficients[2]: $b^{(1)}(g_s^2) = -3$, $b^{(1)}(g^2) = 1$, and $b^{(1)}(g'^2) = 11$. In comparison, the one-loop β coefficients for the SM read: $b^{(1)}(g_s^2) = -7$, $b^{(1)}(g^2) = -\frac{19}{6}$, and $b^{(1)}(g'^2) = \frac{41}{6}$. One remarkable feature of the MSSM gauge coupling RGE's is that they demonstrate the gauge coupling unification. Using the (1.19) as the boundary conditions for the set of one-loop gauge coupling RGE's (2.45), one gets the following gauge coupling evolutions for the Standard Model case and the MSSM case respectively (2.1).

Notice that the U(1) coupling appearing in the Fig. (2.1) is $g_1 = \sqrt{\frac{5}{3}} g'$.

[2]Explicit computation of the one-loop β coefficients for the MSSM is: $b^{(1)}(g_s^2) = -3 \times 3 + \frac{1}{2} \times 2 \times 6 = -3$, $b^{(1)}(g^2) = -3 \times 2 + \frac{1}{2} \times (4 \times 3 + 2) = 1$, and $b^{(1)}(g'^2) = \frac{1}{4}((\frac{1}{9} \times 2 + \frac{16}{9} + \frac{4}{9}) \times 3 + 2 + 4) \times 3 + \frac{1}{4} \times 4 = 11$.

This is natural in the context of a grand unified theory. The MSSM prediction of gauge coupling unification happens at $M_U \simeq 2\times 10^{16}$ GeV, where the unified gauge coupling is $\alpha^2_{\rm GUT} \simeq 0.041$.

The one-loop RGE's for the gaugino masses simply read:

$$\frac{d(M_\alpha/g^2_\alpha)}{dt} = 0 \tag{2.46}$$

with α denoting different subgroups of the MSSM. This means that the gaugino masses roughly evolve with the gauge coupling evolution. Assuming a universal gaugino mass input at the M_U as in the mSUGRA case to be discussed later, one easily gets the following gaugino mass relation at the M_Z scale with the (1.19):

$$M_1 : M_2 : M_3 \approx 1 : 2 : 7 \tag{2.47}$$

One should have other RGE's for the general soft SUSY breaking parameters, e.g. the sfermion soft masses, the trilinear couplings, the Yukawa couplings, and so on. Their RGE's are presented in the Ref. [11].

2.5 Flavor Constraints for The MSSM

In this section, we shall mention the flavor constraint for the MSSM in general. The expressions (2.8) and (2.9) imply complicated flavor structure for the sfermions. As one diagonalizes them to get the mass eigenstates, one gets sfermion mixings. Such mixings would generically introduce new contributions to the flavor-changing neutral current (FCNC) processes. In other words, various FCNC processes give constraints to the MSSM parameters. For example, the dominant supersymmetric contribution [16] of gluino box to the $\Delta S = 2$ $K^0 - \overline{K}^0$ mixing amplitude is proportional to :

$$\frac{g_s^4}{\tilde{m}^6}|\sum_i U_{di}^{\tilde{d}} U_{is}^{\tilde{d}\dagger} \Delta m_{\tilde{d}}^2|^2 \tag{2.48}$$

where $\tilde{m} = \text{Max}(m_{\tilde{q}}, m_{\tilde{g}})$, and U's are elements from the mixing matrix for the down-type sfermions. In a simple two-generation version of the Standard Model, the contribution to the $K^0 - \overline{K}^0$ mixing amplitude reads:

$$\frac{g^4 \sin^2\theta_c \cos^2\theta_c}{m_W^4}(m_c - m_u)^2 \tag{2.49}$$

where θ_c is the Cabbibo mixing angle. This exhibits the Glashow-Iliopoulos-Maiani (GIM) suppression to this flavor-changing neutral current process. This generalizes in the full three-generation version of the Standard Model, and the resulting prediction for $K^0 - \overline{K}^0$ mixing agrees with experiments well (to within the uncertainties inherent in the estimate of the hadronic matrix element of the relevant four-quark operator). Therefore, it is natural to require the (2.48) amplitude to be smaller than the (2.49), which leads to:

$$|\sum U_{di}^{\tilde{d}} U_{is}^{\tilde{d}\dagger} \frac{\Delta m^2}{\tilde{m}^2}| < \frac{g^2 \sin^2\theta_c \cos^2\theta_c}{g_s^2} \frac{(m_c - m_u)\tilde{m}}{m_W^2} \tag{2.50}$$

Using the (1.19), $\sin\theta_c = 0.22$, $m_W = 80.4$ GeV and $m_c = 1.3$ GeV, one gets the following constraint:

$$|\sum U_{di}^{\tilde{d}} U_{is}^{\tilde{d}\dagger} \frac{\Delta m^2}{\tilde{m}^2}| \lesssim 9.8 \times 10^{-4} \frac{\tilde{m}}{100 \text{ GeV}} \tag{2.51}$$

In a more predictive theory from the ultraviolet, such SUSY contributions to the FCNC processes should be suppressed adequately. The suppression can be achieved in several ways. As is evident from the (2.51), a direct method is to take the overall squark masses much larger than the gaugino and Higgs masses, say $\tilde{m} \gtrsim 1$ TeV. This kind of "brute force" solution can appear for special

parameter values in gravity-mediated SUSY-breaking models, which are called the *focus point models* [23]. Sometimes models of this class are referred as *more minimal superysmmetry*, since the first two generation sfermions decouple from the accessible energy scale of the LHC. The other possibility is to assume the off-diagonal components of $U^{\tilde{d}}_{ji}$ are extremely small, say $\lesssim 10^{-3}$. A third possibility is that a high degeneracy among sfermions exists to make the $\Delta m^2_{\tilde{d}}$ very small. This implies that some generation symmetry besides of the gauge symmetries is needed for this to happen. Such a possibility is quite natural in the framework of the gauge-mediation SUSY-breaking models[3] where the scale of flavor symmetry breaking is presumably above the SUSY-breaking scale[4].

[3]The gauge-mediation SUSY breaking (GMSB) is reviewed on Ref. [17] and other references therein. The minimal GMSB [18] contains only five free parameters, and more general GMSB [19] scenario gives more possibilities to the spectrum.

[4]In the gauge-mediation, the SUSY breaking scale is typically $\Lambda_S \sim 10^3 - 10^4$ TeV; while it becomes about $10^7 - 10^8$ TeV in the gravity-mediation models.

Chapter 3

SUSY and Higgs Signatures Implied by Cancellations in $b \longrightarrow s\gamma$

In this chapter we discuss a recent re-evaluation of the Standard Model contribution to $\mathrm{Br}(b \to s\gamma)$ which hints at a positive correction from new physics. It is found that under the HFAG (Heavy Flavor Averaging Group) constraints and with re-evaluated Standard Model results, large cancellations between the charged Higgs and the chargino contributions in supersymmetric models occur. Such cancellations then correlate the charged Higgs and the chargino masses, often implying both are light. Inclusion of the more recent evaluation of $g_\mu - 2$ is also considered. The combined constraints imply the existence of several light sparticles. Signatures arising from these light sparticles are investigated and the analysis indicates the possibility of their early discovery at the LHC in a significant part of the parameter space. We also show that for certain restricted regions of the parameter space, such as for very large $\tan\beta$ under the 1σ HFAG constraints, the signatures from Higgs production supersede those from sparticle production and may become the primary signatures for the discovery of supersymmetry. The main results presented here were published in Ref. [47] co-authored with Dr. Daniel Feldman, Dr. Zuowei Liu and Prof. Pran Nath.

3.1 Introduction and Analysis

Recently a re-evaluation of the Standard Model result for the branching ratio for the flavor changing neutral current (FCNC) process $b \to s\gamma$ including NNLO corrections in QCD has been given [73]; this is $\mathrm{Br}(b \to s\gamma) = (3.15 \pm 0.23) \times 10^{-4}$. Here, $b \to s\gamma$ means the sum of inclusive decays of the form $B_s \to X_s\gamma$, where X_s denotes a final state with strangeness $S = -1$. This new estimate lies lower than the current experimental value which is given by the Heavy Flavor Averaging Group (HFAG) [74] along with the BABAR, Belle and CLEO experimental results: $\mathrm{Br}(B \to X_s\gamma) = (352 \pm 23 \pm 9) \times 10^{-6}$. The above result hints at a positive contribution to this process arising from new physics. It is known from the early days that the experimental value of the branching ratio $b \to s\gamma$ is a very strong constraint on the parameter space of most classes of SUSY models [75, 76] (for more recent theoretical evaluations of $\mathrm{Br}(b \to s\gamma)$ in supersymmetry see [77]). A positive contribution to $\mathrm{Br}(b \to s\gamma)$ suggests either the existence of a light charged Higgs exchange, which always gives a positive contribution [78], or the existence of a light chargino, which can give either a positive or a negative contribution [79]. A significant cancellation between the charged Higgs loop contribution and the chargino contribution implies that individual contributions from the charged Higgs loops and the gaugino loops are generically larger than their sum. Such cancellations then necessarily imply that some of the sparticles that enter in the supersymmetric contributions to the FCNC loops must be relatively light and thus should be accessible in early runs at the LHC.

In addition to the above, recently the difference between experiment and the standard model prediction of the anomalous magnetic moment of the muon, $a_\mu = (g_\mu - 2)/2$, seem to converge [80] towards roughly a 3σ deviation from the SM value. Thus the most recent analysis gives $\delta a_\mu = a_\mu^{exp} - a_\mu^{SM}$ as [80] $\delta a_\mu = (24.6 \pm 8.0) \times 10^{-10}$. It is well known that supersymmetric electroweak contributions to $g_\mu - 2$ can be as large or larger than the Standard Model electroweak corrections [81]. Further, a large deviation of $g_\mu - 2$ from the Standard Model is a harbinger [82], for the observation of low lying sparticles [83**?** , 84] at colliders with the experimental data putting upper limits on

some of the sparticle masses in SUGRA models [83]. The positive correction to $b \to s\gamma$ which is of size $(1-1.5)\sigma$ together with the 3σ level deviation of $g_\mu - 2$ from the Standard Model value points to the existence of some of the sparticles being light.

In this work we investigate the implications of the revised constraints in the framework of supergravity grand unified models [20, 21] following the analysis of [24, 40] with the parameter space characterized by parameters $m_0, m_{1/2}, A_0, \tan\beta$, sign$(\mu)$ where for Monte Carlo simulations we have assumed the following range: $m_0 < 4$ TeV, $m_{1/2} < 2$ TeV, $|A_0/m_0| < 10$, and $1 < \tan\beta < 60$ with $\mu > 0$ for three million candidate models. For the purpose of selecting viable models from the large scan, we impose the following set of constraints: (conservative bounds are given here to illustrate the constraining effects and also to account for experimental and theoretical uncertainties) (i) The 5-year WMAP data constrains the relic density of dark matter so that $\Omega_{\rm DM}h^2 = 0.1131 \pm 0.0034$ [87]. The bound $0.0855 < \Omega_{\tilde{\chi}_1^0}h^2 < 0.1189$ is taken; (ii) A 3 σ constraint for $b \to s\gamma$ is taken around the HFAG value (a stricter constraint will be considered later); (iii) The 95% (90%) C.L. limit reported by CDF in Br$(B_s \to \mu^+\mu^-)$ is 5.8×10^{-8} (4.7×10^{-8}) [71] (we take Br$(B_s \to \mu^+\mu^-) < 10^{-6}$); (iv) $\delta a_\mu \in (-5.7, 47) \times 10^{-10}$ is taken as in [72] (a stricter limit on δa_μ will be discussed in the last section); (v) The following mass limits on light Higgs boson mass and on sparticle masses are imposed: $m_h > 100$ GeV, (the current data sets limits for the MSSM case of $m_h > 93$ GeV at 95% C.L. [63]) $m_{\tilde{\chi}_1^\pm} > 104.5$ GeV, $m_{\tilde{t}_1} > 101.5$ GeV, $m_{\tilde{\tau}_1} > 98.8$ GeV. For the calculations of the relic density of $\tilde{\chi}_1^0$, we use MicrOMEGAs [56] with sparticle and Higgs masses calculated by the RGE package SuSpect [54]. Evaluation of the branching ratio $b \to s\gamma$ has been carried out with both MicrOMEGAs and SusyBSG [58]. The models that pass the above constraints are exhibited in Fig.(3.1).

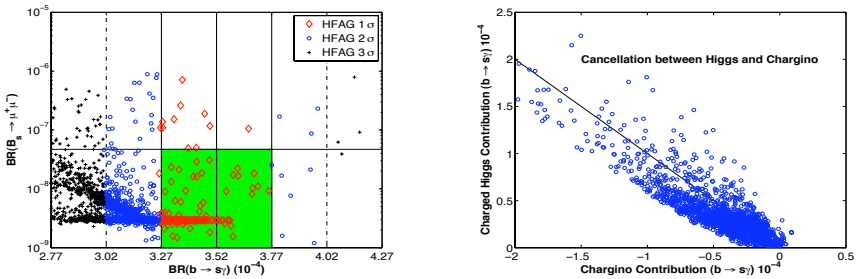

Figure 3.1: Left: Correlation of Br($B_s \to \mu^+\mu^-$) and Br($b \to s\gamma$) for models surviving the constraints. Right: Charged Higgs loop contribution vs the chargino loop contribution to the $b \to s\gamma$.

3.2 Cancellation of Charged Higgs and Chargino Loop Contributions to Br($b \to s\gamma$)

We discuss now in further detail the cancellation between the charged Higgs and the chargino loop contributions in the process $b \to s\gamma$ and the implications of this cancellation, which may point to a light charged Higgs mass. The effective interaction that controls the $b \to s\gamma$ decay is given by:

$$\mathcal{H}_{\rm eff} = -2\sqrt{2} G_F V_{ts}^* V_{tb} \sum_{i=1}^{8} C_i(Q) O_i(Q), \tag{3.1}$$

where V_{ts}, V_{tb} are the CKM matrix elements, $O_i(Q)$ are the effective dimension six operators and $C_i(Q)$ are the Wilson coefficients and Q is the renormalization group scale. The $b \to s\gamma$ receives contributions only from C_2, C_7, C_8 where the corresponding operators are:

$$
\begin{aligned}
O_2 &= (\bar{c}_L \gamma^\mu b_L)(\bar{s}_L \gamma_\mu c_L) \\
O_7 &= (e/16\pi^2) m_b (\bar{s}_L \sigma^{\mu\nu} b_R) F_{\mu\nu} \\
O_8 &= (g_s/16\pi^2) m_b (\bar{s}_L \sigma^{\mu\nu} T^a b_R) G^a_{\mu\nu}
\end{aligned} \tag{3.2}
$$

The dominant contribution arises from C_7, where $C_7(m_b)$ is given by:

$$
C_7^{(0)}(m_b) = \eta^{16/23} C_7(M_W) + \frac{8}{3}(\eta^{16/23} - \eta^{14/23}) C_8(M_W) + C \tag{3.3}
$$

where $\eta = \alpha_s(M_W)/\alpha_s(Q_b)$ and C ($\simeq .175$) arises from operator mixing. Now $C_{7,8}$ contain the Standard Model and new physics contributions so that:

$$
C_{7,8}(M_W) = C^W_{7,8}(M_W) + C^H_{7,8}(M_W) + C^\chi_{7,8}(M_W) \tag{3.4}
$$

Here $C^W_{7,8}$ is the standard model contribution arising from the W boson exchange, $C^H_{7,8}$ is the supersymmetric contribution from the charged Higgs exchange and $C^\chi_{7,8}$ is the contribution from the chargino exchange. In addition to the constraints on models arising from the $\mathrm{Br}(b \to s\gamma)$ experiment, there are also constraints from the $\mathrm{Br}(B_s \to \mu^+\mu^-)$ experiment. In the left panel of Fig. (3.1) we display the theoretical predictions in the $\mathrm{Br}(B_s \to \mu^+\mu^-)$–$\mathrm{Br}(b \to s\gamma)$ plane, where the 1σ, 2σ, 3σ corridors around the HFAG value of $\mathrm{Br}(b \to s\gamma)$ are also exhibited. The analysis of the left panel Fig. (3.1) exhibits that the parameter space gets reduced in a significant way as the $\mathrm{Br}(b \to s\gamma)$ constraint becomes more stringent. We now note that the sign of the chargino contribution $C^\chi_{7,8}$ has a very dramatic effect on the size of the supersymmetric contribution. A positive contribution would add constructively with the charged Higgs contribution $C^H_{7,8}$ while a negative contribution cancels partially the charged Higgs contribution reducing significantly the overall size. A numerical analysis shows that essentially for all the model points that lie in the 3σ corridor around the HFAG value the chargino contribution is negative and

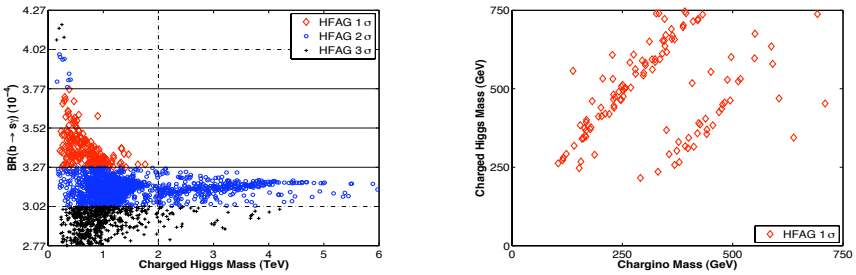

Figure 3.2: Left: Correlation of Br($B_s \to \mu^+\mu^-$) and Br($b \to s\gamma$) for models surviving the constraints. Right: Charged Higgs loop contribution vs the chargino loop contribution to the $b \to s\gamma$.

often large resulting in large cancellations. We exhibit this in the right panel of Fig.(3.1). One finds that a majority of the models are clustered around the standard model prediction of the $b \to s\gamma$. As discussed above this is a consequence of the cancellation between the charged Higgs and the chargino loop diagrams.

In the cancellations discussed above, the individual contributions from the charged Higgs loop and from the chargino loop are often much larger than the total SUSY contribution as exhibited in the right panel of Fig. (3.1). This implies that some of the sparticle spectrum must be light to allow for such large individual contributions in the branching ratio $b \to s\gamma$. The above also indicates that if the chargino is light, then correspondingly the charged Higgs must be correspondingly light to generate a large compensating contribution. So the cancellation phenomenon then strongly correlates the charged Higgs mass and the chargino mass in the region of large cancellations, i.e., in the region where the magnitude of the loop contributions from the chargino and from the charged Higgs are individually multiples of their sum.

An illustration of the correlation between the charged Higgs mass and

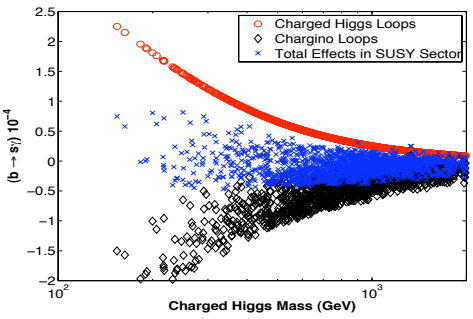

Figure 3.3: A display of the contributions from the charged Higgs loop, the chargino loop (and also other gaugino loops), and the total effect beyond the Standard Model.

$\mathrm{Br}(b \to s\gamma)$ is given in the left panel of Fig. (3.2) in $1\sigma, 2\sigma, 3\sigma$ corridors around the HFAG value. The analysis shows that a more stringent $\mathrm{Br}(b \to s\gamma)$ constraint typically leads to a lighter charged Higgs mass. Further, as stated earlier the cancellation phenomenon also correlates the chargino mass to the charged Higgs mass. This is illustrated the right panel of Fig. (3.2). Specifically, here one finds that for the model points within HFAG 1σ, a light charged Higgs mass often requires a light chargino to cancel the loop. So one expects to have light Higgs and a light chargino with comparable sizes. The cancellation between the charged Higgs contribution and the chargino contribution is also shown in Fig. (3.3) where the models with charged Higgs mass below 2 TeV are plotted. The charged Higgs contribution increases with decreasing charged Higgs mass, which forces the chargino contribution to increase in magnitude with decreasing charged Higgs mass in order that the total effect is consistent with the HFAG constraints. We note that in the Two Higgs Doublet Model (THDM), the charged Higgs mass is also constrained from below, since there is no gaugino contributions to cancel the large positive

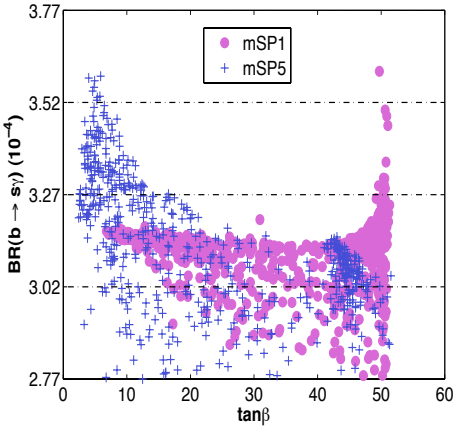

Figure 3.4: $\mathrm{Br}(b \to s\gamma)$ vs $\tan\beta$ for the mass patterns mSP1 and mSP5. The analysis of the figure shows that the 1σ $b \to s\gamma$ constraint selects models in distinct regions of $\tan\beta$: (i) a region of low $\tan\beta$ where the allowed models are mostly of type mSP5, and (ii) a region of large $\tan\beta$ where the allowed models are mostly of type mSP1.

contribution from the light charged Higgs. Thus, under the same constraints, the allowed charged Higgs mass can be much smaller in SUGRA models with a MSSM spectrum than in the THDM. We also note that the $\mathrm{Br}(B_s \to \mu^+\mu^-)$ constraint becomes important for the MSSM with large $\tan\beta$. The current experimental limit imposes a lower bound on the Higgs mass for models with large $\tan\beta$.

A display of the $\mathrm{Br}(b \to s\gamma)$ vs $\tan\beta$ for mSP1 and mSP5 models[1] is given in Fig. (3.4) and the models that pass the 1σ corridor cut on $\mathrm{Br}(b \to s\gamma)$ around the experimental value are shown. One finds that in the region of the 1σ HFAG corridor, the models from mSP1 where the lighter chargino is the NLSP have large $\tan\beta$ values around 50, while the models from mSP5 where the lighter stau is the NLSP has much smaller $\tan\beta$ values. We therefore collectively refer to models that reside in the $\tan\beta$ region where $\tan\beta < 40$ as low and high $\tan\beta$ models, "LH $\tan\beta$ models". We segregate these LH models from those in which $\tan\beta \geq 40$ denoting these as very high $\tan\beta$ models, "VH $\tan\beta$ models", for all the models that fall within the 1σ corridor around the

[1]mSPs are supergravity mass hierarchies as defined in earlier works [24], where (mSP1,mSP5) have a (chargino, stau) NLSP respectively.

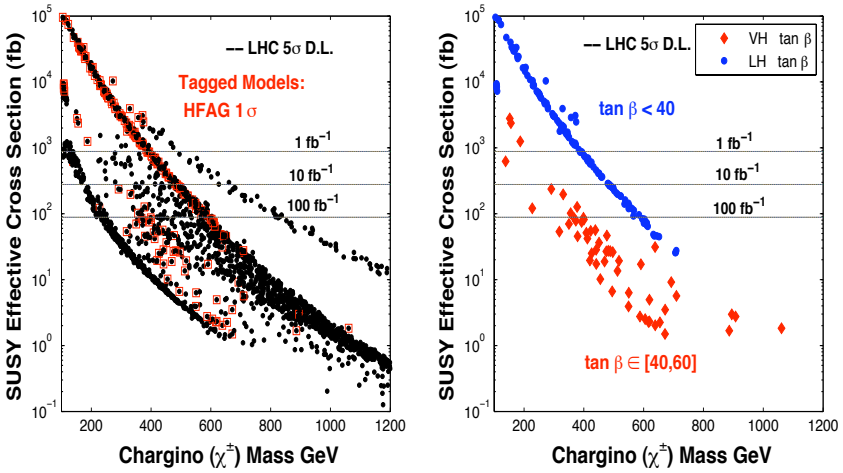

Figure 3.5: Total SUSY signatures at $\sqrt{s} = 14$ TeV analyzed with the SUSY detector cuts.

HFAG value. We do so for all the different mass hierarchical patterns with mSP1 and mSP5 serving as illustrative examples. Typically the "LH $\tan\beta$ models" are the ones in which the stau, the stop, or the gluino can be light, while the "VH $\tan\beta$ models" are the ones where the chargino, or the Higgs is the next heavier particle than the LSP. Some implications of the updated constraints on Higgs masses are also given in [64–66].

3.3 Production and Signatures of Sparticles

In the following, we focus our analysis on the models that are favored by the $b \to s\gamma$ constraint, namely, models that fall within a 1σ corridor around the HFAG value. We discuss here the signatures of the 2 to 2 SUSY processes. In the analysis we use SuSpect to create a SUSY Les Houches Accord (SLHA) [57] file which is then used as an input for PYTHIA [51] which computes the production cross sections and branching fractions, and for PGS [52] which simulates the LHC detector effects. The Level 1 (L1) trigger cuts based on the Compact Muon Solenoid detector specifications [59] are employed to analyze the LHC events. For our analysis of sparticles, we further impose the post trigger detector cuts as follows: We only select photons, electrons, and muons

that have transverse momentum $P_T > 10$ GeV and pseudorapidity $|\eta| < 2.4$, taus jets that have $P_T > 10$ GeV and $|\eta| < 2.0$, and other hadronic jets that have $P_T > 60$ GeV and $|\eta| < 3$. We also require a large missing energy, $\not{E}_T > 200$ GeV and at least two jets in an event to further suppress the Standard Model (SM) background. We will refer this set of cuts as "SUSY detector cuts" in the following analysis (for other recent works on signature analysis of SUGRA models see [25]).

We analyze the total number of events arising from the models in a 1σ corridor around the HFAG results out of the 3σ corridor using the SUSY detector cuts. The effective SUSY cross sections are then translated from the total number of events which are exhibited in Fig. (3.5). One finds that the models with low values of $\tan\beta$ have strong SUSY signals since these models tend to have a light sparticle spectrum, e.g., a light $\tilde{\tau}_1$, $\tilde{t}_1$ or even $\tilde{g}$. Most of the LH $\tan\beta$ models discussed above can be probed at the LHC at 100 fb^{-1} of integrated luminosity. It is found that the HFAG 1σ constraint places a limit on the chargino mass of about 800 GeV for detectable models. We note that different models with different mass hierarchical spectra can have distinct SUSY signatures. For instance, models that have a light $\tilde{\tau}_1$ are rich in lepton signals, while models with a light $\tilde{t}_1$ tend to produce a high multiplicity of jet signals. Thus the search strategies for new physics at the LHC for such models are quite different, and a well designed search technique for every specific model will surely further improve the discovery reach. Nevertheless, the models that have low values of $\tan\beta$ have strong SUSY production cross sections, and can be probed at the LHC. From the SUSY production analysis, one also finds that most of the VH $\tan\beta$ models have much smaller SUSY cross sections.

3.4 LHC Signatures in Higgs Production

We discuss here the signatures of the Higgs bosons in MSSM (the CP-even Higgs H^0, the CP-odd Higgs A^0, and the charged Higgs $H^\pm$) for the models that are within the 1σ corridor of the HFAG value. Specially, we are interested in the parameter region where the $\tan\beta$ value becomes very large. As discussed previously, the VH $\tan\beta$ models within the 1σ corridor of HFAG

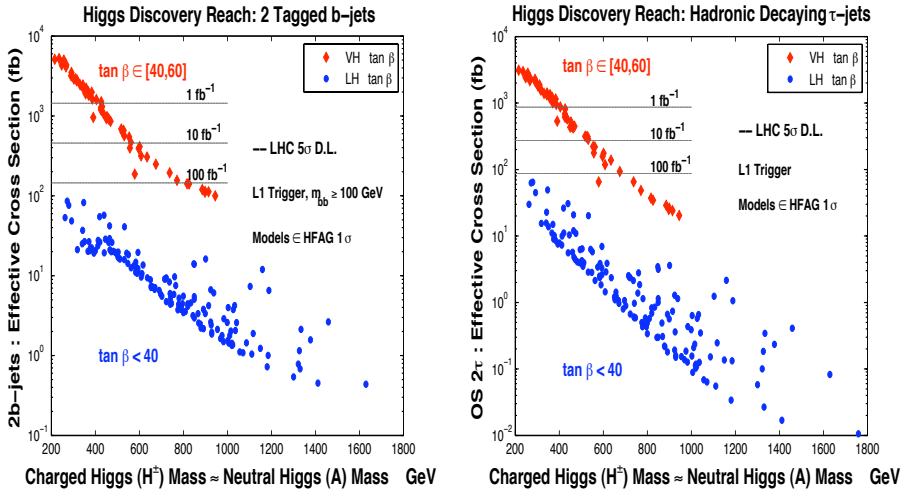

Figure 3.6: Total MSSM Higgs signatures at $\sqrt{s} = 14$ TeV.

have less promising SUSY signals. However, the Higgs production can be much enhanced at very high $\tan\beta$. The dominant processes that lead to the production of the MSSM Higgs bosons at the LHC for $\tan\beta \gg 1$ are the bottom quark annihilation process and the gluon fusion process [26] along with associated production processes with bottom quarks.

In our analysis, we focus on the hadronic τ and jet production with bottom quark tagging, since the $b\bar{b}$ and $\tau^+\tau^-$ modes are the dominant decays of the MSSM Higgs bosons at large $\tan\beta$. We analyze the opposite sign (OS) di-tau signature and the 2b-jets signature using the L1 trigger cuts. For the 2b jet signatures, we also require the reconstructed invariant mass of these two b-tagged jets to be larger than 100 GeV. An analysis of the signatures for these models reveals the 2τ jet and the $2b$ jet channels to be two of the optimal channels for the discovery of the Higgs bosons as shown in Fig. (3.6). It is found that the HFAG 1σ constraint places a limit on the charged Higgs mass about 1 TeV for the detectable models which can be probed with $\mathcal{L} = 100$ fb^{-1} or so at LHC. We note that for the region $\tan\beta < 40$, one needs much more luminosity to observe discoverable events from the Higgs production, and some of the models in this region may be even beyond the LHC reach in the Higgs production. Thus the VH $\tan\beta$ models are discoverable via Higgs production modes, while many of them have undetectable signals via sparticles

productions. Thus the more optimal channels to discover supersymmetry in these VH $\tan\beta$ models arise from Higgs production signals as they produce larger event rates than the event rates from SUSY production processes with R-parity odd particles. The associated production in which the Higgs bosons are produced along with one or two bottom quarks in the final states can be very useful for suppressing further the Standard Model background [28–32, 34, 35]. One example of the associated production with one additional bottom quark in the final state is given in Fig. (3.9). For the hadronic τ jets signature, we utilize both the 1-prong and the 3-prong hadronic τ-jets [36] in our analysis. We note that the leptonic decay modes of the τ lepton and a combined analysis of leptonic and hadronic decays may yield an even better discovery reach [37, 38, 60].

3.5 Complementarity of Signatures from Sparticle Decays and from Higgs Decays

Before discussing the issue of complementarity we discuss first the more stringent constraints arising from the recent revised analyses of $g_\mu - 2$ which seem to converge [80] towards a 3σ deviation from the Standard Model value. Fig.(3.7) illustrates a 2σ corridor around the central values of δa_μ and of the HFAG value of $\mathrm{Br}(b \to s\gamma)$. The analysis of Fig.(3.7) shows that the parameter space of allowed models is drastically reduced. A model point from the allowed set of models is discussed in further detail in the context of complementarity below.

Next we point out a complementarity that exists between two main types of processes in the production and decays of new particles expected at the LHC. The first of the main types consists of those production processes which have in their final decay products an even number of massive LSPs (each an R-parity odd particle). These arise from the production and subsequent decay of an even number of R parity odd particles (due to R parity conservation) such as pairs of squarks or gauginos or both at the LHC. These processes are characterized by a large missing energy since the final states have at least two or more LSPs, which for the models considered are the lightest neutralinos.

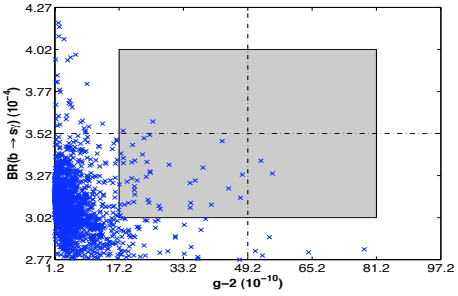

Figure 3.7: Combined analysis with $b \to s\gamma$ and $g_\mu - 2$ constraints. Shaded regions are the 2σ corridors from both constraints.

Thus here a larger missing transverse momentum is the smoking gun signature for the SUSY productions.

The second type of processes are those which do not contain pairs of LSPs and thus there is far less missing energy associated with these events. Such events are expected to arise from the production of the Higgs bosons where the dominant decay products are largely $b\bar{b}$ and $\tau^+\tau^-$. The signals arising from the Higgs decays typically suffer from a large QCD background, since the $\not{E}_T$ cut technique cannot be employed here which is efficient in suppressing the background for SUSY production. However, for models with very high $\tan\beta$, the Higgs production is enhanced and such model points can yield signals which can be discriminated from the QCD background. Thus we see that there is a complementarity between the signatures arising from the production and decay of the SUSY particles and from the Higgs particles, and this complementarity is exhibited in Fig.(3.8). Indeed for models with small $\tan\beta$, $\not{E}_T$ continues to be a dominant signal while for models with very high $\tan\beta$ and within 1σ corridor of HFAG value of $b \to s\gamma$ the Higgs production and decay into $b\bar{b}$ and $\tau^+\tau^-$ can provide signatures which can supersede the signatures from sparticle

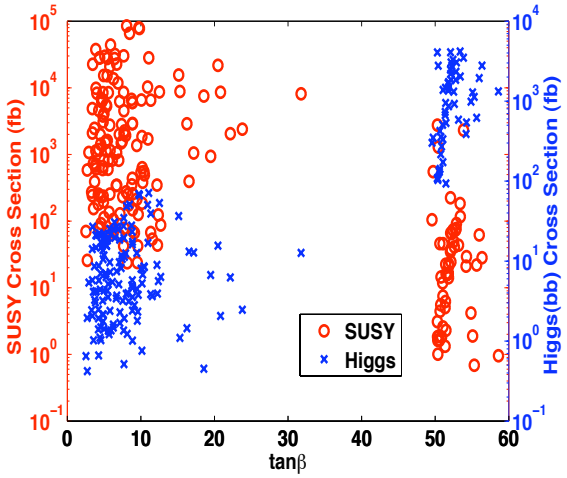

Figure 3.8: A plot of both SUSY signatures and MSSM Higgs signatures for the models that fall within the 1σ corridor around the HFAG value. The figure shows complementarity and inversion.

production for the discovery of supersymmetry at the LHC.

A more detailed signal analysis on SUSY production and on Higgs production is given in Fig.(3.9). In the left panel of Fig.(3.9), the model considered is the one where stau is the NLSP and it shows a strong SUSY production signal which is rich in lepton final states. The lightest sparticles in this model besides the LSP are $\tilde{\tau}$, $\tilde{\ell}_R$, so in the cascade decays of heavier gauginos, these sleptons can appear in the intermediate steps, for instance, $\tilde{\chi}_2^0$ decays predominantly via BR$(\tilde{\tau}\tau) \sim 70\%$ and BR$(\tilde{\ell}_R\ell) \sim 20\%$. The produced sleptons further decay into the LSP plus one lepton. Thus the reconstruction of the di-lepton events indicate the mass relations between the gauginos in the cascade decay chain due to the $\not{E}_T$ carried away by the LSP. In contrast, the invariant mass of the b-tagged jets from the Higgs production gives rise to a resonance which points to the actual value of the Higgs boson mass as exhibited by the right panel of Fig.(3.9). As stated in the caption of Fig. (3.9) the cuts used in the left panel are the SUSY detector cuts. The right panel of Fig.(3.9) is analyzed with the standard L1 trigger cuts in PGS. The background in the left panel of Fig.(3.9) is suppressed by using flavor subtraction in reconstructing the dilepton events. For the right panel, the background is suppressed by reconstructing the two

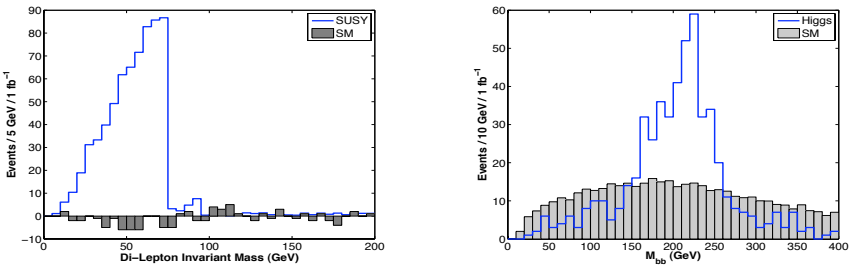

Figure 3.9: Invariant mass distributions for SUSY and Higgs productions for two different models: (m_0, $m_{1/2}$, A_0, $\tan\beta$, sign(μ))=(70.4, 243.2, 685.6, 11, 1) (left panel); (1533.8, 216.4, 1750.3, 53.8, 1) (right panel) where all masses are in GeV. Left: The opposite sign di-lepton with flavor subtraction ($e^+e^- + \mu^+\mu^- - e^+\mu^- - \mu^+e^-$), for the model that fall within 1σ for both $b \to s\gamma$ and $g_\mu - 2$ constraints. In this model, $M_{\tilde{\chi}_1^0} = 93$ GeV and $M_{\tilde{\chi}_2^0} = 168$ GeV. The ending edge of the distribution indicates the mass difference $(M_{\tilde{\chi}_2^0} - M_{\tilde{\chi}_1^0})$. Analysis is done with SUSY detector cuts. Shaded regions are the background $N_{\rm SM}$. Right: Reconstruction of the two hardest b-tagged jets in 3 b-jets events of Higgs productions for the model that satisfies the HFAG 1σ. The peak indicates the position of the Higgs boson mass. L1 trigger cuts are employed. Shaded regions are the background $\sqrt{N_{\rm SM}}$.

hardest b-tagged jets in the 3b events which can arise in the associated production modes of Higgs bosons. The associated production where the Higgs bosons are produced along with additional b-tagged jets is instrumental in suppressing the background.

Chapter 4

LHC Signals for Gravity-mediation Models

The MSSM itself has more than one hundred free parameters, hence it cannot be predictive. In addition, the MSSM spectrum contains 32 masses including all R-parity odd sparticles and the MSSM Higgs bosons. With Stirling's formula [$n! \sim \sqrt{2\pi n}(n/e)^n$], one would get more than $\mathcal{O}(10^{33})$ possibilities for the MSSM hierarchical patterns. To reduce this huge number of possibilities for the real phenomenological study, one is motivated to take the MSSM as a low-energy effective theory from some UV-complete theory, e.g., the supergravity-mediation theory as we have discussed in the previous chapter. Second, one should consider the experimental constraints on MSSM models, which will restrict our choice of parameters in the SUGRA models. In addition, one only needs to classify all MSSM models in terms of the mass hierarchies for several light sparticles from the collider signature point of view. Because the production of the light sparticles is relatively easy at the LHC, their signatures can be characteristic depending on their decay chains. A number of studies of SUGRA models have been carried out over the past 30 years, including pioneering studies by P. Nath and coworkers [20]. Our discussion here and below involves new results that we have published, with D. Feldman, Z. Liu, P. Nath, G. Peim and coauthors, in Refs. [49] [50]. Other recent work on this topic include: [24] [40] [41] [42] [44] [46].

We devote this chapter to a discussion of sparticle properties based upon the SUGRA-mediation models. We will start with mSUGRA models and analyze their collider signatures with various experimental constraints imposed. Then we will also discuss the LHC early discovery prospect for a class of non-universal SUGRA models (NUSUGRA)[1] in the gaugino sector. We will be particularly interested in models with low-mass gluinos[2] in contrast to the mSUGRA models.

4.1 mSUGRA Models

The mSUGRA models are the simplest to study since one only needs four soft SUSY parameters at the GUT scale $M_U \simeq 2 \times 10^{16}$ GeV, as indicated from the Appendix (B):

$$M_0 \qquad M_{1/2} \qquad A_0 \qquad \tan\beta \qquad \mathrm{sgn}(\mu) \tag{4.1}$$

Generically, the $(M_0, M_{1/2})$ set scales for the sfermion masses and the gaugino masses respectively. Usually scans over the parameter space are performed by taking a vanishing trilinear coupling, and/or by fixing the values of $\tan\beta$ while varying $(M_0, M_{1/2})$. In what follows, we shall take a large random scan over the 4-D mSUGRA parameter space within the following region:

$$\begin{aligned} &0 < M_0 < 4 \text{ TeV} \qquad 0 < M_{1/2} < 2 \text{ TeV} \\ &|A_0/M_0| < 10 \qquad 1 < \tan\beta < 60 \end{aligned} \tag{4.2}$$

Here we shall take models with $\mu > 0$ in particular. The other case of $\mu < 0$ is discussed on the Ref. [40]. This scan is done with the MicrOMEGAs version

[1] In general, "NUSUGRA" refers to any SUGRA-mediation models with more soft parameter inputs at the GUT scale. Throughout this thesis, we restrict our discussion to the non-universality in the gaugino sector only.

[2] By "low-mass gluinos", as discussed in the thesis, we mean gluinos with mass of several hundred GeV. These are still heavier than the lightest neutralino so that no color/charge breaking vacuum is present.

2.4 [56], whose default RGE code to obtain the sparticle spectrum is SuSpect 2.34 [54].

4.1.1 Model classification

By an extensive scan over the mSUGRA parameter space (4.2), one noticed that the possible next-to-lightest sparticles can have four possibilities in the mSUGRA scenario; indicating masses by the corresponding sparticle symbols, these possibilities are $\tilde{\chi}_1^\pm \sim \tilde{\chi}_2^0$, $\tilde{\tau}_1$, $\tilde{t}_1$, or $A^0 \sim H^0$. A more detailed classification is to find the four lightest sparticles in the MSSM spectrum in the following Table (4.1) [24].

Pattern Class	mSP	Mass Pattern
CP	mSP1	$\tilde{\chi}_1^0 < \tilde{\chi}_1^\pm < \tilde{\chi}_2^0 < \tilde{\chi}_3^0$
	mSP2	$\tilde{\chi}_1^0 < \tilde{\chi}_1^\pm < \tilde{\chi}_2^0 < A/H$
	mSP3	$\tilde{\chi}_1^0 < \tilde{\chi}_1^\pm < \tilde{\chi}_2^0 < \tilde{\tau}_1$
	mSP4	$\tilde{\chi}_1^0 < \tilde{\chi}_1^\pm < \tilde{\chi}_2^0 < \tilde{g}$
SUP	mSP5	$\tilde{\chi}_1^0 < \tilde{\tau}_1 < \tilde{l}_R < \tilde{\nu}_\tau$
	mSP6	$\tilde{\chi}_1^0 < \tilde{\tau}_1 < \tilde{\chi}_1^\pm < \tilde{\chi}_2^0$
	mSP7	$\tilde{\chi}_1^0 < \tilde{\tau}_1 < \tilde{l}_R < \tilde{\chi}_1^\pm$
	mSP8	$\tilde{\chi}_1^0 < \tilde{\tau}_1 < A/H$
	mSP9	$\tilde{\chi}_1^0 < \tilde{\tau}_1 < \tilde{l}_R < A/H$
	mSP10	$\tilde{\chi}_1^0 < \tilde{\tau}_1 < \tilde{t}_1 < \tilde{l}_R$
SOP	mSP11	$\tilde{\chi}_1^0 < \tilde{t}_1 < \tilde{\chi}_1^\pm < \tilde{\chi}_2^0$
	mSP12	$\tilde{\chi}_1^0 < \tilde{t}_1 < \tilde{\tau}_1 < \tilde{\chi}_1^\pm$
	mSP13	$\tilde{\chi}_1^0 < \tilde{t}_1 < \tilde{\tau}_1 < \tilde{l}_R$
HP	mSP14	$\tilde{\chi}_1^0 < A/H < H^\pm$
	mSP15	$\tilde{\chi}_1^0 < A/H < \tilde{\chi}_1^\pm$
	mSP16	$\tilde{\chi}_1^0 < A/H < \tilde{\tau}_1$

Table 4.1: Hierarchical mass patterns for the four lightest sparticles in mSUGRA for $\mu > 0$. The sparticle patterns are defined according to their NLSP's, including Chargino patterns (CP), Stau patterns (SUP), Stop patterns (SOP), and Higgs patterns (HP). The patterns marked in red are the dominant ones in each pattern class.

4.1.2 Experimental constraints

Now we list the relevant constraints from the collider experiments and astrophysical observations.

- The Wilkinson Microwave Anisotropy Probe (WMAP) seven-year data [87] gives $\Omega_{\rm DM}h^2 = 0.1109 \pm 0.0056$. Assuming that the relic abundance is solely due to the lightest supersymmetric particle (LSP) $\tilde{\chi}_1^0$, this constraints yields a narrow band of reasonable models. However, we shall only take a conservative upper bound as $\Omega_{\tilde{\chi}_1^0}h^2 < 0.13$ (corresponding to $\sim 3.4\sigma$ deviation) to take account of both experimental uncertainties and other possible dark matter contributions. Among all experimental constraints, this requirement from the dark matter relic density is the most stringent one, which is typically satisfied in less than 1% of models from a random scan. We will review the dark matter relic density in the context of SUGRA-mediation models in the following chapter.

- The $B_s \to \mu^+\mu^-$ will be significant for large $\tan\beta$ region, since the decay has a leading $\tan^6\beta$ dependence [15]. This limit has been updated to ${\rm Br}(B_s \to \mu^+\mu^-) < 5.8 \times 10^{-8}$ [71] by the CDF-II detector with $\sqrt{s} = 1.96$ TeV and 2 fb^{-1} of integrated luminosity.

- The sparticle loop exchange can make a contribution to the FCNC process of $b \to s\gamma$ also. The value of ${\rm Br}(B \to X_s\gamma)$ inferred from B decay data (as discussed by the Heavy Flavor Averaging Group, HFAG) [74] is above the NNLO evaluation of the Standard Model contribution [73]. Taking a 3σ corridor, we allow the models to have ${\rm Br}(b \to s\gamma) \in (2.77 - 4.27) \times 10^{-4}$.

- We shall impose lower bounds on masses of several light sparticles. The Standard Model Higgs boson is known to be excluded below ≈ 115 GeV by LEP data, and there is also an excluded interval of Higgs masses in the higher interval 158 GeV $< m_H <$ 175 GeV established by the CDF and D0 experiments at the Fermilab Tevatron [67]. The mass limit on the lightest MSSM Higgs is $m_h > 93$ GeV at 95% C. L. [63]. Other sparticle

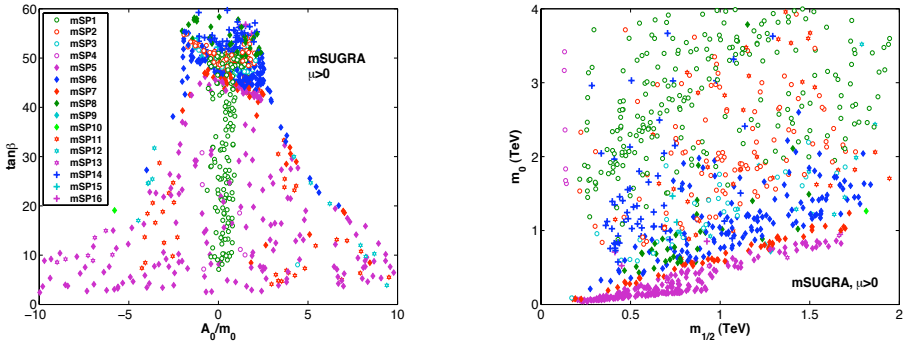

Figure 4.1: The dispersion of mSPs in mSUGRA ($\mu > 0$) in the $\tan\beta$ vs A_0/M_0 plane (left panel), and in the M_0 vs $M_{1/2}$ plane (right-panel).

mass lower bounds applied are: $m_{\tilde{\chi}_1^\pm} > 104.5$ GeV, $m_{\tilde{t}_1} > 101.5$ GeV, and $m_{\tilde{\tau}_1} > 98.8$ GeV.

4.1.3 Sparticle patterns

It is interesting to see if the patterns can be traced back to some specific regions of the parameter of soft-breaking. The analysis illustrating the origin of the patterns in the mSUGRA parameter space is given on Fig. (4.1).

Several observations can be made about the soft-parameter distributions. For example, most mSP1 models lie in the region of $|A_0/M_0| \lesssim 2$ and correspond to the Hyperbolic branch (HB)/ Focus Point (FP) regions [23]. Also, models with NLSP being the third generational sfermions $\tilde{\tau}_1$ (e.g., mSP5 and mSP6) or $\tilde{t}_1$ (e.g., mSP11) are located at regions with large $|A_0/M_0|$, which is due to the large off-diagonal mixing terms as seen from (2.41). On the right panel of Fig. (4.1), one can see that the models with NLSP being $\tilde{\tau}_1$ or $\tilde{t}_1$ are in the region with smaller M_0.

4.1.4 Updated LHC 7 TeV implication

The CMS [68] and ATLAS [69] [70] Collaborations have recently reported on the search for mSUGRA with 35 pb^{-1} of data and have put independent limits on the parameter space of the mSUGRA models. Both analyses were performed with fixed $A_0 = 0$ and $\tan\beta = 3$. The ATLAS analysis produces a reach more stringent than the one from the CMS, hence the ATLAS results will be taken as our constraint. Here we shall extend this study by examining other regions of the mSUGRA parameter space in A_0 and $\tan\beta$. This section contains results from [50], currently in press, coauthored with S. Akula, D. Feldman, M. Liu, Z. Liu, Prof. P. Nath, and G. Peim. Specifically, we found that a significant part of the parameter space excluded by CMS and ATLAS is essentially already excluded by the indirect constraints. We also found that models with gluino masses as low as 400 GeV but for $M_{\tilde{q}} \gg M_{\tilde{g}}$ remain unconstrained.

The ATLAS collaboration has released two analyses, one with 1 lepton [69] and the other with 0 lepton [70]. For the 1 lepton analysis, we shall list the pre-selection requirements:

- For any jet, $p_T > 20$ GeV and $|\eta| < 2.5$; electrons must have $p_T > 20$ GeV[3] and $|\eta| < 2.47$ and muons must have $p_T > 20$ GeV and $|\eta| < 2.4$. We further veto electrons in the electromagnetic calorimeter transition region $1.37 < |\eta| < 1.52$.

- An event is considered if it has a single lepton with $p_T > 20$ GeV and its three hardest jets have $p_T > 30$ GeV, with the leading jet having $p_T > 60$ GeV.

- The distance[4] between each jet with the lepton should satisfy $\Delta R(j_i, \ell) > 0.4$. An event is rejected if $\Delta\phi(j_i, \not{E}_T) > 0.2$ with $i = 1, 2, 3$.

Following the framework of the ATLAS Collaboration we have carried out a set of three parameter sweeps in the $M_0 - M_{1/2}$ plane taking $M_0 \leq 500$ GeV and

[3] In the 0 lepton ATLAS analysis, leptons are identified to have $p_T > 10$ GeV instead.
[4] The distance on the $\eta - \phi$ plane is defined as $\Delta R \equiv \sqrt{(\Delta\eta)^2 + (\Delta\phi)^2}$.

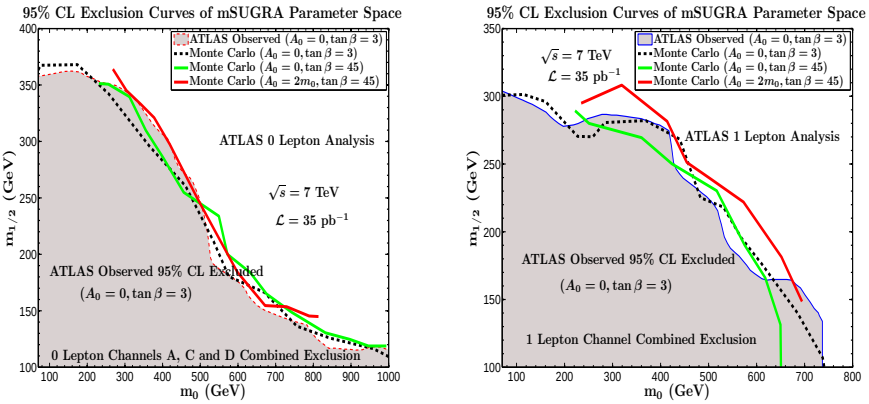

Figure 4.2: Left: Reach plot with $\mathcal{L}_{\rm tot} = 35$ pb^{-1} data using the ATLAS 1 lepton cuts with different $(A_0, \tan\beta)$: $(A_0, \tan\beta) = (0, 3)$ (dashed line); $(A_0, \tan\beta) = (0, 45)$ (solid green line); $(A_0, \tan\beta) = (2M_0, 45)$ (solid red line). For comparison we give the ATLAS observed limit $(A_0, \tan\beta) = (0, 3)$ (solid blue line). Right: Reach plot with $\mathcal{L}_{\rm tot} = 35$ pb^{-1} data using the ATLAS 0 lepton cuts. For comparison we give the ATLAS observed limit (red dashed line).

$M_0 \leq 1$ TeV. Each of the parameter sets has $(A_0, \tan\beta)$ being $(0, 3)$, $(0, 45)$ and $(2M_0, 45)$. Throughout the analysis we also take $\mu > 0$ and $m_t^{\rm pole} = 173.1$ GeV. A comparison of our reach to the reach done by the ATLAS Collaboration is shown in Fig (4.2).

In the analysis of the reach plots, other experimental constraints from collider, flavor and astrophysics were not imposed beyond those arising from the ATLAS analyses. Next we include these constraints in our analysis when all four mSUGRA parameters M_0, $M_{1/2}$, A_0, and $\tan\beta$ are varied. These constraints are the same as the constraints we listed in the subsection (4.1.2), where the Br$(b \to s\gamma)$ is taken within the 3σ corridor of $(2.77 - 4.27) \times 10^{-4}$. The effects of these sets of constraints are explicitly shown on Fig (4.3). As was pointed out in Ref [46] and also shown on Fig (4.3), the models with low mass gluinos (as low as even 420 GeV in mSUGRA) are allowed for the region with large M_0, where the relic density can be satisfied on the light CP even Higgs pole. Along the Higgs pole region, the electroweak symmetry breaking can also be natural, i.e., one has a small μ.

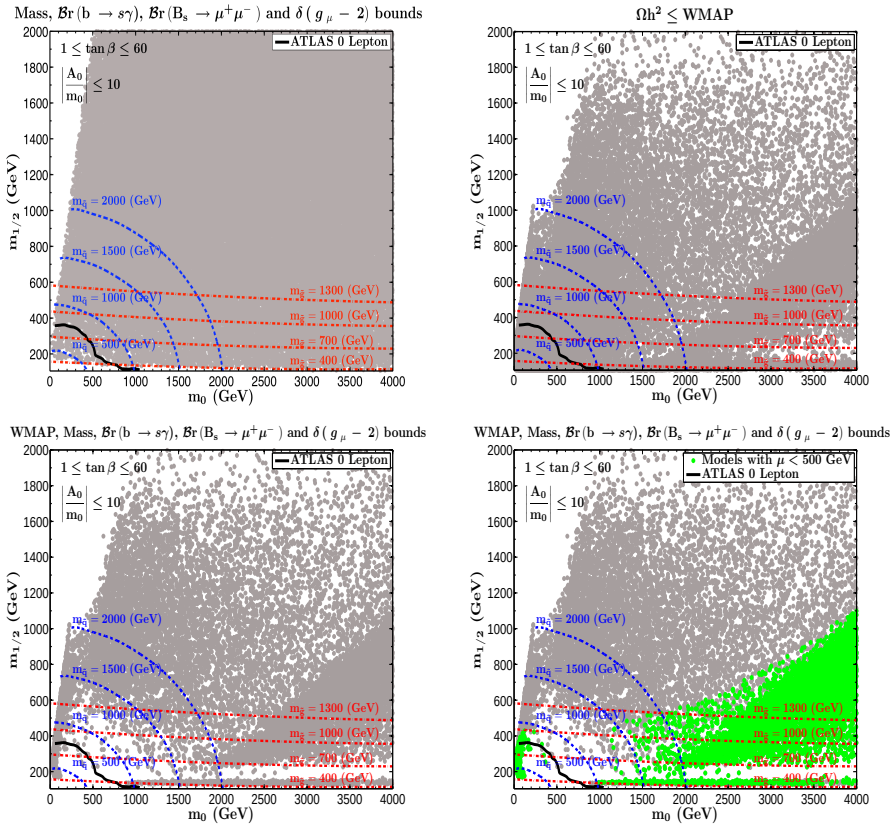

Figure 4.3: (color online) Upper left panel: An exhibition of the allowed models indicated by grey (dark) dots in the $m_0 - m_{1/2}$ plane when only flavor and collider constraints are imposed. The region excluded by ATLAS (as well as CMS) lies below the thick black curve in the left hand corner. Upper right panel: same as the left upper panel except that only an upper bound on relic density of $\Omega h^2 \leq 0.13$ is imposed. Lower left panel: Same as the upper left panel except that the relic density constraint as in the upper right panel is also applied. This panel exhibits that most of the parameter space excluded by ATLAS is already excluded by the collider/flavor and relic density constraints. The dark region below the ATLAS curve is the extra region excluded by ATLAS which was not previously excluded by the indirect constraints. Lower right panel: The analysis of this figure is similar to the lower left panel except that models with $|\mu| < 500$ GeV are exhibited in green.

4.2 Non-Universal SUGRA Models

In this section, we extend our discussion of sparticle mass spectra into NUSUGRA models. We include results that have been published in [49] [50]. As was clear from our discussion on the gaugino masses in the SUGRA-mediation models, the property of universality of the gaugino masses is a simplification. With such an assumption, one would get a well-known gaugino mass ratio in the M_Z scale (2.47). However, this assumption can certainly be generalized. Our discussion here will focus on models with arbitrary M_1, M_2, and M_3 inputs.

4.2.1 Low-mass gluino benchmark models

In particular, we are interested in the region of parameter space which will be promising in the LHC early run with $\sqrt{s} = 7$ TeV. The favorite models can be the ones with lighter gluinos other than the ratio predicted from the mSUGRA (2.47). An early study in the Ref [42] focus on the gluino as the NLSP (GNLSP) models. Here we extend our consideration such that gluino masses are within some accessible range in the LHC early run. A case of interest for LHC analysis is $M_3(M_U) \in (100, 300)$ GeV and this translates into gluino masses in the range of $(350, 750)$ GeV at the electroweak scale to be considered. Now we give a broad sample of benchmark models listed in Table (4.2), where the SUGRA model parameters are at the GUT scale M_U. The sparticle mass hierarchies corresponding to these models are given in Table (4.3). We shall mention that these models are subject to various dark matter constraints to be discussed in detail in chapter (5), including relic densities $\Omega_{\tilde{\chi}_1^0} h^2 \lesssim 0.13$, spin-independent WIMP-nucleon cross section subject to the most recent direct detection results, and indirect detection results by Fermi-LAT on the gamma ray line. These model should also satisfy the collider constraints mentioned in the context of mSUGRA. We shall discuss the dark matter implications for some of the light gluino models in the next chapter.

These benchmark models are intrinsically different in their nature, both in their sparticle spectra and their dark matter implication. A more detailed discussion of these benchmark models follows.

Label	$M_{\tilde{g}}$	m_0	M_1	M_2	M_3	A_0	$\tan\beta$
LG1	424	2000	130	130	130	-1000	8
LG2	715	60	300	300	300	-100	8
LG3	386	1400	800	528	132	3000	25
LG4	378	3785	836	508	98	-6713	20
LG5	385	2223	859	843	130	4680	48
LG6	391	1180	860	790	138	2692	42
LG7	442	2919	263	151	138	4206	18
LG8	417	1303	257	152	139	1433	18
LG9	696	1845	327	193	249	1898	13
LG10	365	1500	1600	1080	120	2100	15
LG11	433	605	302	176	161	1781	22
LG12	588	636	419	249	228	1568	37
LG13	684	335	391	466	279	-1036	3
LG14	618	48	289	310	256	-407	6
LG15	602	61	310	351	249	0	9
LG16	343	2200	450	235	100	300	5
LG17	425	3000	400	207	125	0	4

Table 4.2: A sample of low mass gluino models where additionally we take $\mu > 0$ and $m_{t(pole)} = 173.1$ GeV. The soft breaking parameters are given at the high scale of $M_U \simeq 2 \times 10^{16}$ GeV. Nonuniversalites in the gaugino sector $M_{a=1,2,3}$ are taken in 15 of the models. All masses in the table are in unit of GeV.

1. Low mass gluinos in mSUGRA: The possibility that a low mass gluino and heavy scalars can arise in the radiative breaking of the electroweak symmetry (REWSB) in SUGRA models was seen early on [22]. It was later realized that this phenomenon is more general, and the Hyperbolic Branch (HB) or the Focus Point (FP) region of radiative electroweak symmetry breaking (REWSB) was discovered where scalars are heavy and gauginos are light [23]. In the analysis of HB/FP models, it was found that the chargino is predominantly the NLSP over a very broad class of soft breaking models. However, a low mass gluino, around 400 GeV, can arise in minimal supergravity if the neutralinos annihilate near the Z-pole or near the Higgs poles [92]. Specifically a low mass gluino arises in mSUGRA in the sparticle mass landscape which was labeled as mSP4 in [24] where the first four sparticles have the mass

A sample of the sparticle landscape for low mass gluino SUGRA models

Label	Mass Pattern	$M_{\tilde{g}}$	Lightest $M_{\tilde{q}}$
LG1	$\tilde{\chi}_1^0 < \tilde{\chi}_1^\pm < \tilde{\chi}_2^0 < \tilde{g} < \tilde{\chi}_3^0 < \tilde{\chi}_4^0$	424	1985
LG2	$\tilde{\chi}_1^0 < \tilde{\tau}_1 < \tilde{\ell}_R < \tilde{\nu}_\tau < \tilde{\nu}_\ell < \tilde{\ell}_L$	715	635
LG3	$\tilde{\chi}_1^0 < \tilde{g} < \tilde{\chi}_1^\pm < \tilde{\chi}_2^0 < \tilde{t}_1 < \tilde{\chi}_3^0$	386	1411
LG4	$\tilde{\chi}_1^0 < \tilde{g} < \tilde{\chi}_1^\pm < \tilde{\chi}_2^0 < \tilde{t}_1 < \tilde{\chi}_3^0$	378	3751
LG5	$\tilde{\chi}_1^0 < \tilde{g} < \tilde{\chi}_1^\pm < \tilde{\chi}_2^0 < \tilde{t}_1 < \tilde{\tau}_1$	385	2217
LG6	$\tilde{\chi}_1^0 < \tilde{t}_1 < \tilde{g} < \tilde{\chi}_1^\pm < \tilde{\chi}_2^0 < \tilde{\chi}_3^0$	391	1202
LG7	$\tilde{\chi}_1^0 < \tilde{\chi}_1^\pm < \tilde{\chi}_2^0 < \tilde{g} < \tilde{\chi}_3^0 < \tilde{\chi}_4^0$	442	2888
LG8	$\tilde{\chi}_1^0 < \tilde{\chi}_1^\pm < \tilde{\chi}_2^0 < \tilde{g} < \tilde{\chi}_3^0 < \tilde{\chi}_4^0$	417	1314
LG9	$\tilde{\chi}_1^0 < \tilde{\chi}_1^\pm < \tilde{\chi}_2^0 < \tilde{\chi}_3^0 < \tilde{\chi}_4^0 < \tilde{\chi}_2^\pm$	696	1882
LG10	$\tilde{\chi}_1^0 < \tilde{\chi}_1^\pm < \tilde{\chi}_2^0 < \tilde{g} < \tilde{\chi}_3^0 < \tilde{t}_1$	365	1511
LG11	$\tilde{\chi}_1^0 < \tilde{\chi}_1^\pm \lesssim \tilde{\chi}_2^0 < \tilde{t}_1 < \tilde{g} < \tilde{b}_1$	433	690
LG12	$\tilde{\chi}_1^0 < \tilde{\chi}_1^\pm < \tilde{\chi}_2^0 < \tilde{\tau}_1 < \tilde{\chi}_3^0 < \tilde{\chi}_4^0$	588	790
LG13	$\tilde{\chi}_1^0 < \tilde{t}_1 < \tilde{\chi}_1^\pm < \tilde{\chi}_2^0 < \tilde{\tau}_1 < \tilde{\ell}_R$	684	677
LG14	$\tilde{\chi}_1^0 < \tilde{\tau}_1 < \tilde{\ell}_R < \tilde{\nu}_\tau < \tilde{\nu}_\ell < \tilde{\ell}_L$	618	550
LG15	$\tilde{\chi}_1^0 < \tilde{\tau}_1 < \tilde{\ell}_R < \tilde{\nu}_\tau < \tilde{\nu}_\ell < \tilde{\chi}_1^\pm$	602	536
LG16	$\tilde{\chi}_1^0 < \tilde{\chi}_1^\pm < \tilde{\chi}_2^0 < \tilde{g} < \tilde{\chi}_3^0 < \tilde{\chi}_2^\pm$	343	2178
LG17	$\tilde{\chi}_1^0 < \tilde{\chi}_1^\pm < \tilde{\chi}_2^0 < \tilde{g} < \tilde{\chi}_3^0 < \tilde{\chi}_2^\pm$	425	2966

Table 4.3: Sparticle mass hierarchies for the low mass gluino models. Listed are the first six lightest sparticles in the spectra. The lightest squark, shown in the fourth column, is taken from the first two generations. All masses are expressed in unit of GeV.

hierarchy as follows:

$$\text{Model LG1} : \tilde{\chi}_1^0 < \tilde{\chi}_1^\pm < \tilde{\chi}_2^0 < \tilde{g},\ M_{\tilde{g}} = 424 \text{ GeV}. \tag{4.3}$$

A very different situation holds for the model point LG2. While the gluino is still light in this model, lying in the sub-TeV region, it is actually the heaviest sparticle in the whole sparticle spectrum. Specifically the hierarchy is:

$$\text{Model LG2} : \tilde{\chi}_1^0 < \tilde{\tau}_1 < \tilde{\ell}_R < \tilde{\nu}_\tau < \ldots < \tilde{g},\ M_{\tilde{g}} = 715 \text{ GeV}. \tag{4.4}$$

The relic density in the model LG2 is satisfied via coannihilations with the stau

Low mass gluino models in minimal SUGRA

Label	M_h	$M_{\tilde{\chi}_1^0}$	$M_{\tilde{\chi}_1^\pm}$	$M_{\tilde{g}}$	Z_{11}	Z_{12}	Z_{13}	Z_{14}	$\sigma^{\rm SI}_{\tilde{\chi}_1^0 p}(\text{cm}^2)$
LG1	115	53	104	424	0.993	-0.051	0.103	-0.025	5.4×10^{-46}
LG2	111	118	220	715	0.990	-0.044	0.127	-0.051	5.2×10^{-45}

Table 4.4: mSUGRA models of a low mass gluino and a display of some of the lighter masses within the sparticle mass hierarchies. In model LG1 the neutralino, the chargino and the gluino are all light while the SUSY scalars are heavy. This model generates the relic density in the WMAP band via the annihilation of the neutralinos near the Higgs pole. However, in model LG2 the scalars are also light and the relic density lies in the WMAP band via coannihilations of the neutralinos with the stau and other light sleptons. All masses are in GeV.

and with the other sleptons. Since model LG2 has a lighter scalar sparticle spectrum, it has a larger spin-independent cross section than LG1 by a factor of about 10.

2. GNLSP models: Such models can lead to a low mass gluino that can be the NLSP, the NNLSP, etc. The case when the gluino is the NLSP requires special attention since here the relic density can be satisfied by the neutralino coannihilations with the gluino, as in the model LG3. This case was discussed at length in [42]. For the models LG3–LG5 discussed in Table. (4.2) the sparticle mass hierarchies are given by [42]:

$$\begin{aligned} &\text{Models (LG3, LG4, LG5)} : \tilde{\chi}_1^0 < \tilde{g} < \tilde{\chi}_1^\pm < \tilde{\chi}_2^0 < \tilde{t}_1 \\ &M_{\tilde{g}} = (386, 378, 385)\ \text{GeV} \end{aligned} \tag{4.5}$$

Since the gluino coannihilation in the GNLSP model is a relatively new entry among the ways dark matter originates in the early Universe, we summarize the main features of the relic density calculation here first, before discussing the relevant features of this class of models that enter in the LHC signature analysis. Thus, for a GNLSP the relic density depends strongly on coannihilation effects which are controlled by the Boltzmann factor [91]

Label	M_h	$M_{\tilde{\chi}_1^0}$	$M_{\tilde{\chi}_1^\pm}$	$M_{\tilde{g}}$	Z_{11}	Z_{12}	Z_{13}	Z_{14}	$\sigma^{\rm SI}_{\tilde{\chi}_1^0 p}(\text{cm}^2)$
LG3	112	340	429	386	0.997	-0.026	0.067	-0.029	6.3×10^{-46}
LG4	125	377	454	378	0.999	-0.006	0.021	-0.005	8.4×10^{-48}
LG5	117	365	660	385	0.999	-0.003	0.039	-0.012	2.1×10^{-46}

Table 4.5: A display of the lighter sparticle masses within the mass hierarchies, and other attributes of GNLSP models with low mass gluinos. The mass splitting between the gluino and neutralino is between $\sim (1-50)$ GeV for these models. Further details are given in the text. All masses are in GeV.

$$\gamma_i = \frac{n_i^{\rm eq}}{n^{\rm eq}} = \frac{g_i(1+\Delta_i)^{3/2}e^{-\Delta_i x}}{\sum_j g_j(1+\Delta_j)^{3/2}e^{-\Delta_j x}} \ , \tag{4.6}$$

where g_i are the degrees of freedom of χ_i, $x = m_1/T$, and $\Delta_i = (m_i - m_1)/m_1$, with m_1 defined as the LSP mass. Thus, for the analysis of the relic density, the effective annihilation cross section $\sigma_{\rm eff}$ can be written approximately as:

$$\sigma_{\rm eff} = \sum_{i,j} \gamma_i\gamma_j\sigma_{ij} \simeq \sigma_{\tilde{g}\tilde{g}}\gamma_{\tilde{g}}^2 + 2\sigma_{\tilde{g}\tilde{\chi}_1^0}\gamma_{\tilde{g}}\gamma_{\tilde{\chi}_1^0} + \sigma_{\tilde{\chi}_1^0\tilde{\chi}_1^0}\gamma_{\tilde{\chi}_1^0}^2 \simeq \sigma_{\tilde{g}\tilde{g}}\gamma_{\tilde{g}}^2 \ , \tag{4.7}$$

where we have used the fact that the gluino annihilation cross sections are usually much larger than the LSP annihilation even with inclusion of the Boltzmann factor and:

$$\sigma(\tilde{g}\tilde{g} \to q\bar{q}) = \mathcal{E}_q \frac{\pi\alpha_s^2\bar{\beta}}{16\beta s}(3-\beta^2)(3-\bar{\beta}^2) \ , \tag{4.8}$$

$$\sigma(\tilde{g}\tilde{g} \to gg) = \mathcal{E}_g \frac{3\pi\alpha_s^2}{16\beta^2 s}\left\{\log\frac{1+\beta}{1-\beta}\left[21-6\beta^2-3\beta^4\right] - 33\beta + 17\beta^3\right\} \tag{4.9}$$

where the non-perturbative corrections to the annihilation cross section can arise via multiple gluon exchange, giving rise to a Sommerfeld enhancement factor $\mathcal{E}$. These effects may be approximated by [27]:

$$\mathcal{E}_j = \frac{C_j \pi \alpha_s}{\beta}\left[1 - exp\left\{-\frac{C_j \pi \alpha_s}{\beta}\right\}\right]^{-1} , \tag{4.10}$$

where $C_{j=g} = 1/2 (C_{j=q} = 3/2)$ for $\tilde{g}\tilde{g} \to gg (\tilde{g}\tilde{g} \to q\bar{q})$. In the above $\beta = \sqrt{1 - 4m_{\tilde{g}}^2/s}$, and $\bar{\beta} = \sqrt{1 - 4m_q^2/s}$. Although the gluino annihilation cross section $\sigma_{\tilde{g}\tilde{g}}$ varies with gluino mass, the Boltzmann suppression factor $\gamma_{\tilde{g}}$ controls the contribution to the $\sigma_{\rm eff}$ so that the relic density of the bino-like neutralino is consistent with WMAP. We note that the effects of the Sommerfeld enhancement on the gluino cross sections can increase $\Delta_{\tilde{g}}$ by a small amount for a bino-like LSP $\sim (2-3)\%$ [33, 42]. Such an increase in the mass gap between the gluino and the neutralino can potentially enhance the discovery reach of this class of models at the LHC as the mass gap between the $\tilde{g}$ and $\tilde{\chi}_1^0$ plays a crucial role in the strength of the LHC signals [42] which we will discuss in details later. Three GNLSP models are exhibited in Table. (4.5). Some of their pertinent spectra and other attributes, including their spin-independent cross sections, are also given in Table. (4.5). It is seen from this table the neutralino is dominantly a bino. For each of these models gluino coannihilation dominates the relic density calculations. In the absence of additional hidden sector gauge groups (to be discussed in what follows), only LG3 lies in the WMAP band, while models LG4 and LG5 each have a reduced relic abundance and reduced mass gaps between $\tilde{g}$ and $\tilde{\chi}_1^0$.

3. GNNLSP models: Next we consider five models, LG6–LG10, in Table (4.2) where the gluino is light and in some cases it is the next to next to LSP (GNNLSP). Specifically the sparticle mass hierarchies are:

$$\begin{aligned}
&\text{Model LG6}: && \tilde{\chi}_1^0 < \tilde{t}_1 < \tilde{g} < \tilde{\chi}_1^{\pm} < \tilde{\chi}_2^0, && M_{\tilde{g}} = 391 \text{ GeV} ,\\
&\text{Model LG7}: && \tilde{\chi}_1^0 < \tilde{\chi}_1^{\pm} < \tilde{\chi}_2^0 < \tilde{g} < \tilde{\chi}_3^0, && M_{\tilde{g}} = 442 \text{ GeV} ,\\
&\text{Model LG8}: && \tilde{\chi}_1^0 < \tilde{\chi}_1^{\pm} < \tilde{\chi}_2^0 < \tilde{g} < \tilde{\chi}_3^0, && M_{\tilde{g}} = 417 \text{ GeV} ,\\
&\text{Model LG9}: && \tilde{\chi}_1^0 < \tilde{\chi}_1^{\pm} < \tilde{\chi}_2^0 < \tilde{\chi}_{3,4}^0 < \tilde{\chi}_2^{\pm} < \tilde{g}, && M_{\tilde{g}} = 696 \text{ GeV} ,\\
&\text{Model LG10}: && \tilde{\chi}_1^0 < \tilde{\chi}_1^{\pm} < \tilde{\chi}_2^0 < \tilde{g} < \tilde{\chi}_3^0 < \tilde{t}_1, && M_{\tilde{g}} = 365 \text{ GeV} .
\end{aligned} \tag{4.11}$$

Low mass gluinos including GNNLSP models

Label	M_h	$M_{\tilde{\chi}_1^0}$	$M_{\tilde{\chi}_1^\pm}$	$M_{\tilde{g}}$	Z_{11}	Z_{12}	Z_{13}	Z_{14}	$\sigma^{\rm SI}_{\tilde{\chi}_1^0 p}({\rm cm}^2)$
LG6	109	359	570	391	0.992	-0.020	0.109	-0.064	6.6×10^{-45}
LG7	119	108	120	442	0.998	-0.049	0.039	-0.006	2.4×10^{-47}
LG8	112	104	117	417	0.968	-0.202	0.143	-0.041	2.7×10^{-45}
LG9	115	135	152	696	0.985	-0.136	0.098	-0.030	7.8×10^{-46}
LG10	112	111	115	365	0.058	-0.075	0.721	-0.686	7.3×10^{-45}

Table 4.6: The spectrum of low mass sparticles including the GNNLSP models within the sparticle mass hierarchies, and other attributes of models in NUSUGRA with a low mass gluino. Model LG6 is a GNNLSP, and models LG7, LG8, and LG9 are effectively GNNLSP as the chargino and second heaviest neutralino are roughly mass degenerate. LG10 has a mass splitting between the chargino and the neutralino of $\sim$ 5 GeV and is effectively a GNNLSP model. All masses are in GeV.

Here the NLSP can be $\tilde{t}_1$ or $\tilde{\chi}_1^\pm$. The specific nature of the neutralino eigencontent makes these models significantly different from each other and from other light gluino models. This includes an interesting subclass of models where the LSP is dominantly Higgsino (LG10). Such a model class will be analyzed in the next chapter on both the PAMELA positron excess and the Fermi-LAT photon line constraint.

4. Low mass gluinos with light sfermions: we further discuss five models, LG11–LG15 where in addition to the low mass gluino one also has a light $\tilde{\tau}_1$, a light $\tilde{t}_1$ (due to the smaller GUT value of M_0) along with a light $\tilde{\chi}_1^\pm$. Models LG11–LG15 have compressed sparticle spectra with the heaviest sparticle mass around 850 GeV. Model LG11 has a highly reduced overall mass scale of the sparticles, with a low mass gluino and a light stop with the mass hierarchy

$$\text{Model LG11} : \tilde{\chi}_1^0 < \tilde{\chi}_1^\pm < \tilde{\chi}_2^0 < \tilde{t}_1 < \tilde{g},\ M_{\tilde{g}} = 433 \text{ GeV} , \tag{4.12}$$

with the remaining sparticles in the mass range (500-700) GeV. In each of these models the relic density can be satisfied via coannihilations with different superparticles, and, in particular, model LG13 proceeds via stop coannihilations. For LG12, the gluino mass lies in the middle of the sparticle mass

spectra, while for (LG13-LG15) the gluino mass is close to being the largest mass even though it is still relatively light, i.e., $M_{\tilde{g}} < 700$ GeV. Models LG11 and LG13 have rather low-lying light Higgs. However, the extraction of the Higgs mass from LEP data is model dependent, and we retain these models in the analysis pending further experimental data.

5. Low mass gluinos in extended SUGRA models and PAMELA data: Recently, the PAMELA collaboration [107] has included an analysis of statistical uncertainties in the positron fraction and presented its results on the absolute $\overline{p}$ flux. Models LG10, LG16, and LG17 in Table. (4.2) have low mass gluinos with many other desirable features. Specifically, they can explain the positron excess in the PAMELA satellite experiment. The detailed discussion for these models will be presented in the next chapter.

4.2.2 Signature analysis at the LHC with $\sqrt{s} = 7$ TeV

For this analysis, our emphasis is on the discovery of models which admit low mass gluinos in early runs at the LHC consistent with dark matter interpretations for a neutralino LSP.

Standard Model background: The discovery of new physics requires an accurate determination of the Standard Model background. The recent works of [44] have given an analysis of such backgrounds including $2 \to n$ processes at $\sqrt{s} = 7$ TeV appropriate for pp collisions at the LHC. We use for our analysis the simulated SM background of [44] which was generated with MadGraph 4.4 [55] for parton level processes, Pythia 6.4 [51] for hadronization and PGS-4 [52] for detector simulation. An MLM matching algorithm with a k_T jet clustering scheme was used to prevent double counting of final states. Further, the b-tagging efficiency in PGS-4 is based on the Technical Design Reports of ATLAS (see [44]), which is similar to the efficiency of CMS, with the mis-tagging rate of b-jet unmodified from the default in PGS-4. In addition Tauola is called for tau decays. The processes that are included in the SM background are: (QCD $2, 3, 4$ jets), ($t\bar{t} + 0, 1, 2$ jets), ($b\bar{b} + 0, 1, 2$ jets), ($Z/\gamma\left(\to l\bar{l}, \nu\bar{\nu}\right)+0, 1, 2, 3$ jets), ($W^{\pm}\left(\to l\nu\right)+0, 1, 2, 3$ jets), ($Z/\gamma\left(\to \ell\bar{\ell}, \nu\bar{\nu}\right)+ t\bar{t}+0, 1, 2$ jets), ($Z/\gamma\left(\to l\bar{l}, \nu\bar{\nu}\right)+b\bar{b}+0, 1, 2$ jets), ($W^{\pm}\left(\to l\nu\right)+b\bar{b}+0, 1, 2$ jets),

$(W^{\pm}(\to l\nu) + t\bar{t} + 0,1,2$ jets), $(W^{\pm}(\to l\nu) + t\bar{b}\,(\bar{t}b) + 0,1,2$ jets), $(t\bar{t}t\bar{t}$, $t\bar{t}b\bar{b}$, $b\bar{b}b\bar{b})$, $(W^{\pm}(\to l\nu) + W^{\pm}(\to l\nu))$, $(W^{\pm}(\to l\nu) + Z(\to\ all))$, $(Z(\to\ all) + Z(\to\ all))$, $(\gamma + 1,2,3$ jets). A more detailed discussion of the Standard Model background can be found in the [44] which includes a list of cross section, number of events and luminosity for each process.

SUSY signal generation and optimization of cuts: For these benchmark models with light gluinos, we emphasize the discovery possibility in early runs at the LHC with $\sqrt{s} = 7$ TeV. These models are expected to be significant in their SUSY productions. A large number of cuts on the events are investigated which includes: p_T of jets and leptons, the jet transverse sphericity S_T, and missing energy $\not{E}_T$. Accordingly, we shall optimize the cuts to enhance the significance of signal over the background $S/\sqrt{B}$. In each event, we order objects by their p_T's, i.e., the hardest jet would be denoted as j_1 and so on. We shall define several kinematic variables mentioned in the above list. They are the jet transverse sphericity S_T, the effective mass m_{eff}, and the H_T:

$$S_T \equiv 1 - \left(1 - 4\left(\frac{\sum_i p_x^2(j_i)\sum_i p_y^2(j_i)}{\sum_i p_x^2(j_i) + \sum_i p_y^2(j_i)} - \frac{(\sum_i p_x(j_i)\cdot p_y(j_i))^2}{\sum_i p_x^2(j_i) + \sum_i p_y^2(j_i)}\right)\right)^{1/2} \tag{4.13}$$

$$m_{\text{eff}} \equiv \sum_{i=1}^{4} p_T(j_i) + \not{E}_T \tag{4.14}$$

$$H_T \equiv \sum_{i=1}^{4} p_T(x_i) + \not{E}_T \tag{4.15}$$

where x_i stand for any visible objects. In this analysis we define a signal that produces S events to be discoverable for a particular signature cut if $S \geq \max\{5\sqrt{B}, 10\}$, where B stands for the number of SM background events. The optimal cuts were found by varying the bounds on observables. First, a broad optimization was carried out where the varied observables include $\not{E}_T$ (100 GeV to 800 GeV in steps of 50 GeV), S_T of all visible objets (0.15 to 0.25 in steps of 0.05), number of jets (2 to 6 in integer steps), number of b-jets (0 to 3 in integer steps), as well as the p_T of the hardest jet (10 GeV to 500 GeV in steps of 10 GeV) and the second hardest jet (10 GeV to 250 GeV in steps

of 10 GeV). For the particular cuts which deal with opposite sign same flavor (OSSF) leptons, a Z-veto is applied, i.e., the 76 GeV $\leq m_{\bar{\ell}\ell} \leq$ 105 GeV region is excluded. A subset of cuts found using the procedure above are listed below. In choosing these cuts we have taken into account of the uncertainty of how well $\not{E}_T$ can be determined in the early runs. For this reason we have taken lower values of $\not{E}_T$ as low as 100 GeV. Better optimization can occur with larger values of $\not{E}_T$. However, this requires a greater degree of confidence on how well $\not{E}_T$ is determined in the early runs.

C1: $\not{E}_T \geq 100$ GeV

C2: $S_T \geq 0.2$, $\not{E}_T \geq 100$ GeV

C3: $S_T \geq 0.2$, $\not{E}_T \geq 100$ GeV, $n(\ell) = 0$, $p_T(j_1) \geq 150$ GeV, $p_T(j_2, j_3, j_4) \geq 40$ GeV

C4: $S_T \geq 0.2$, $\not{E}_T \geq 250$ GeV, $n(\ell) = 0$, $p_T(j_1) \geq 250$ GeV, $p_T(j_2, j_3, j_4) \geq 40$ GeV

C5: $S_T \geq 0.2$, $\not{E}_T \geq 150$ GeV, $n(\ell) = 0$, $p_T(j_1) \geq 150$ GeV, $p_T(j_2, j_3, j_4) \geq 40$ GeV

C6: $S_T \geq 0.2$, $\not{E}_T \geq 250$ GeV, $n(\ell) = 0$, $p_T(j_1) \geq 100$ GeV, $p_T(j_2) \geq 40$ GeV

C7: $S_T \geq 0.2$, $\not{E}_T \geq 200$ GeV, $n(\ell) = 0$, $p_T(j_1) \geq 30$ GeV

C8: $S_T \geq 0.2$, $\not{E}_T \geq 200$ GeV, $n(j) \geq 2$, $n(\ell) \geq 2$

C9: $S_T \geq 0.2$, $\not{E}_T \geq 200$ GeV, $n(b\text{-jets}) = 1$

C10: $S_T \geq 0.2$, $\not{E}_T \geq 100$ GeV, $n(\ell) = 0$, $n(b\text{-jets}) \geq 1$

C11: $S_T \geq 0.2$, $\not{E}_T \geq 100$ GeV, $n(\ell) = 0$, $n(b\text{-jets}) \geq 2$

C12: $S_T \geq 0.2$, $\not{E}_T \geq 100$ GeV, $n(j) \geq 4$

C13: $S_T \geq 0.2$, $\not{E}_T \geq 100$ GeV, $n(j) \geq 4$, $p_T(j_1) \geq 100$ GeV, $m_{\text{eff}} \geq 400$ GeV

C14: $S_T \geq 0.2$, $\not{E}_T \geq 100$ GeV, $n(j) \geq 4$, $p_T(j_1) \geq 100$ GeV, $m_{\text{eff}} \geq 550$ GeV

C15: $S_T \geq 0.2$, $\not{E}_T \geq 100$ GeV, $n(j) + n(\ell) \geq 4$, $p_T(j_1) \geq 100$ GeV, $H_T \geq 400$ GeV

C16: $S_T \geq 0.2$, $\not{E}_T \geq 100$ GeV, $n(j) + n(\ell) \geq 4$, $p_T(j_1) \geq 100$ GeV, $H_T \geq 550$ GeV

C17: $S_T \geq 0.2$, $\not{E}_T \geq 100$ GeV, Z-veto, $n(\ell_a^+) = 1$, $n(\ell_b^-) = 1$, $p_T(\ell_2) \geq 20$ GeV, $p_T(j_1) \geq 100$ GeV, $p_T(j_2) \geq 40$ GeV ,[5]

C18: $S_T \geq 0.2$, $\not{E}_T \geq 100$ GeV, Z-veto, $n(\ell_a^+) = 1$, $n(\ell_b^-) = 1$, $p_T(\ell_2) \geq 20$ GeV, $p_T(j_2) \geq 40$ GeV

C19: $S_T \geq 0.2$, $\not{E}_T \geq 100$ GeV, $\not{E}_T \geq 0.2 m_{\text{eff}}$, $n(j) \geq 4$, $p_T(j_1) \geq 100$ GeV,

C20: $\not{E}_T \geq 100$ GeV, $n(\ell) = 3$, $p_T(j_1) \geq 150$ GeV, $n(j) \geq 2$

C21: $\not{E}_T \geq 150$ GeV, $n(\ell) = 3$, $p_T(j_2) \geq 40$ GeV

Signature analysis: Our analysis is carried out to determine the potential for discovery of the dark matter motivated models LG1, . . . , LG17, for 0.5 fb^{-1}, 1 fb^{-1}, 2 fb^{-1} and 5 fb^{-1} (with a focus on 1 fb^{-1}) of integrated luminosity with 7 TeV center of mass energy. These models exhibit generic features of a very broad class of SUSY models.

We now discussion Fig. (4.4) a bit more generally. The potential for discovering the models of Table. (4.2) at 1 fb^{-1} of integrated luminosity is given in Table. (4.7). A subset of the results in Table. (4.7) are given in Fig. (4.4). Thus, Table. (4.7) displays each model's significance, $S/\sqrt{B}$, for the 21 cuts listed above. One finds that a particular model, LG$_k$, often has several signatures that lead to large excesses of signal over background, i.e. $S/\sqrt{B} > 5$, and the set of signatures in which the model becomes visible varies significantly from one model to the next. Additionally, in studying the tri-leptonic channels, C20 and C21, we see that consistently only 6 models among those listed in Table (4.2) are discoverable (LG1, LG2, LG10, LG11, LG14, LG15) and the majority of the other models show less then 10 events in the tri-leptonic channels.

[5]In the specification of the cuts C17 and C18, the subscripts a and b indicate that they may be different flavors, but a Z-veto is applied only to OSSF.

LHC significance over channels for 1 fb^{-1} of integrated luminosity

	C1	C2	C3	C4	C5	C6	C7	C8	C9	C10	C11	C12	C13	C14	C15	C16	C17	C18	C19	C20	C21
LG1	6	9	18	6	19	4	5	3	7	10	8	13	17	20	16	19	2	2	17	3	2
LG2	3	4	4	13	7	14	9	10	5	2	2	4	5	8	6	8	1	1	4	9	10
LG3	4	3	1	3	2	8	7	0	2	3	1	4	3	2	2	2	0	0	1	0	0
LG4	4	2	0	1	1	5	7	0	1	0	0	1	1	1	1	1	0	0	0	0	0
LG5	4	2	0	1	1	5	6	0	1	1	0	2	1	1	1	1	0	0	0	0	0
LG6	4	3	1	3	2	8	8	0	1	1	0	3	2	2	2	2	0	0	1	0	0
LG7	6	9	17	9	23	9	9	2	12	12	11	13	17	20	16	19	0	0	17	0	0
LG8	7	10	18	9	24	9	10	2	11	13	10	15	20	21	19	21	0	1	18	1	1
LG9	0	0	1	2	1	1	1	1	1	0	0	0	1	1	1	1	0	0	1	0	0
LG10	18	24	18	13	25	29	31	4	21	23	16	30	33	28	31	27	0	0	19	1	4
LG11	12	19	31	24	39	17	15	16	24	33	42	27	34	38	32	36	2	5	34	9	5
LG12	2	4	10	16	16	8	6	3	8	6	7	6	8	11	7	10	0	1	10	2	2
LG13	6	5	8	25	14	17	13	0	11	6	5	7	7	9	7	9	0	0	7	0	0
LG14	8	10	10	24	17	31	19	25	17	6	5	11	15	20	15	20	4	5	12	20	20
LG15	9	11	16	38	26	34	22	22	19	8	7	13	18	24	18	25	5	5	16	20	18
LG16	19	28	15	11	18	11	14	0	11	27	15	37	27	16	25	15	0	0	17	0	0
LG17	7	10	13	7	19	10	11	0	11	11	8	14	17	16	16	15	0	0	14	0	0

Table 4.7: A display of the signal significance $S/\sqrt{B}$ in each discovery channel for the models in Table. (4.2) for 1 fb^{-1} of integrated luminosity at the LHC. For a signal to be discoverable we require $S \geq \max\left\{5\sqrt{B}, 10\right\}$.

LHC reach for (0.5, 1, 2, 5) fb^{-1} of integrated luminosity

	C1	C2	C3	C4	C5	C6	C7	C8	C9	C10	C11	C12	C13	C14	C15	C16	C17	C18	C19	C20	C21
LG1	1.0	0.5	0.5	1.0	0.5	2.0	1.0	5.0	0.5	0.5	0.5	0.5	0.5	0.5	0.5	0.5			0.5	5.0	
LG2	5.0	2.0	2.0	0.5	1.0	0.5	0.5	0.5	1.0			2.0	1.0	0.5	1.0	0.5			2.0	2.0	1.0
LG3	2.0	5.0		5.0	5.0	0.5	1.0			5.0		2.0	5.0		5.0						
LG4	2.0					2.0	1.0														
LG5	5.0					2.0	1.0														
LG6	2.0	5.0		5.0		0.5	0.5					5.0									
LG7	1.0	0.5	0.5	0.5	0.5	0.5	0.5		0.5	0.5	0.5	0.5	0.5	0.5	0.5	0.5			0.5		
LG8	1.0	0.5	0.5	0.5	0.5	0.5	0.5		0.5	0.5	0.5	0.5	0.5	0.5	0.5	0.5			0.5		
LG9				5.0																	
LG10	0.5	0.5	0.5	0.5	0.5	0.5	0.5	2.0	0.5	0.5	0.5	0.5	0.5	0.5	0.5	0.5			0.5		5.0
LG11	0.5	0.5	0.5	0.5	0.5	0.5	0.5	0.5	0.5	0.5	0.5	0.5	0.5	0.5	0.5	0.5	5.0	2.0	0.5	2.0	2.0
LG12	5.0	2.0	0.5	0.5	0.5	0.5	1.0	5.0	0.5	1.0	1.0	1.0	0.5	0.5	0.5	0.5			0.5		
LG13	1.0	1.0	0.5	0.5	0.5	0.5	0.5		0.5	1.0	2.0	1.0	0.5	0.5	1.0	0.5			0.5		
LG14	0.5	0.5	0.5	0.5	0.5	0.5	0.5	0.5	0.5	1.0	2.0	0.5	0.5	0.5	0.5	0.5	2.0	1.0	0.5	0.5	0.5
LG15	0.5	0.5	0.5	0.5	0.5	0.5	0.5	0.5	0.5	0.5	1.0	0.5	0.5	0.5	0.5	0.5	2.0	1.0	0.5	0.5	1.0
LG16	0.5	0.5	0.5	0.5	0.5	0.5	0.5		0.5	0.5	0.5	0.5	0.5	0.5	0.5	0.5			0.5		
LG17	1.0	0.5	0.5	0.5	0.5	0.5	0.5		0.5	0.5	0.5	0.5	0.5	0.5	0.5	0.5			0.5		

Table 4.8: The values in the table are the integrated luminosity in units of fb^{-1} when the model is first discoverable in that channel. The table shows that many of the low mass gluino models will become visible with an integrated luminosity of 0.5 fb^{-1}, and all models become visible with an integrated luminosity of 2 fb^{-1} except the model LG9 which requires an integrated luminosity of 5 fb^{-1} to be discovered.

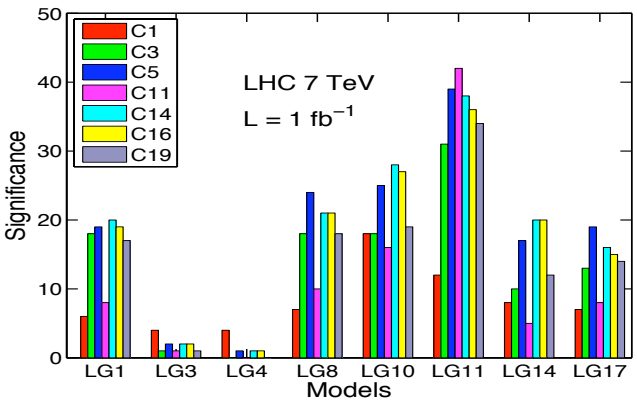

Figure 4.4: A summary of significance $S/\sqrt{B}$ for various signature channels/cuts for a subset of low gluino (LG) models. The data is simulated under $\mathcal{L}_{\rm tot} = 1fb^{-1}$ at the LHC for $\sqrt{s} = 7$ TeV.

The overall production cross section of superparticles is determined mainly by the production of squarks and gluinos. For the gluino production modes at the LHC, the cross section is determined by the gluino mass. However, for models with low mass gluinos, like those that appear in Table. (4.2), the detectable signals at the LHC are strongly influenced by the other low-lying sparticles, i.e., the superparticles that are lighter than the gluino. In Fig.(4.5), an analysis of the jet multiplicity and the transverse momentum of the leading jets is given for LG3, LG4, LG11, LG13, and LG14. The distributions for jet multiplicity and jet momentum look quite different from model to model. For instance, the model LG11 has a gluino mass of 433 GeV, and several of its superparticles are lighter than the gluino, including the lighter stop and gauginos. This leads to lengthy cascade decay chains which produce multiple jets. Further, the mass differences between the sparticles in LG11 are relatively large which give rise to large momentum of the SM final states including jets. In contrast, models LG3 and LG4 tend to produce events with less jet multiplicity and smaller transverse momentum, which is due to the fact that these models having a gluino as the NLSP; i.e., these models are GNLSPs. For these GNLSP models the masses of the gluino and the LSP are correlated in the gluino coannihilation mechanism such that the mass gap is relatively small.

Specifically, LG3 has $M_{\tilde{g}} - M_{\tilde{\chi}_1^0} \sim 50$ GeV and the gluino production is, overwhelmingly, the dominant production mode. For this model, the gluinos decay directly to the LSP + 2 jets, i.e., $\mathrm{Br}(\tilde{g} \to (b\bar{b}\tilde{\chi}_1^0, q\bar{q}\tilde{\chi}_1^0)) \sim (20, 80)\%$ where q stands for first two generation quarks. We note in passing that generally one needs to take into account the radiative decay of the gluino, $\tilde{g} \to g\tilde{\chi}_1^0$. Such a case occurs, for example, in LG4, and the decay $\tilde{g} \to g\tilde{\chi}_1^0$ dominates the branching ratio. The relatively small mass splitting in model LG3 between the gluino and the LSP (as well as the extreme case of LG4) makes this model class harder to discover due to the softer jets and low jet multiplicity, compared to other models. (For recent work on relatively small gluino-LSP splittings see [39, 40, 42] and [43, 45].) This feature is illustrated further in Table. (4.7) and Table. (4.8). We note that in such cases where the mass gap between gluino and the LSP is extremely small, the effects of the initial state radiation (ISR)

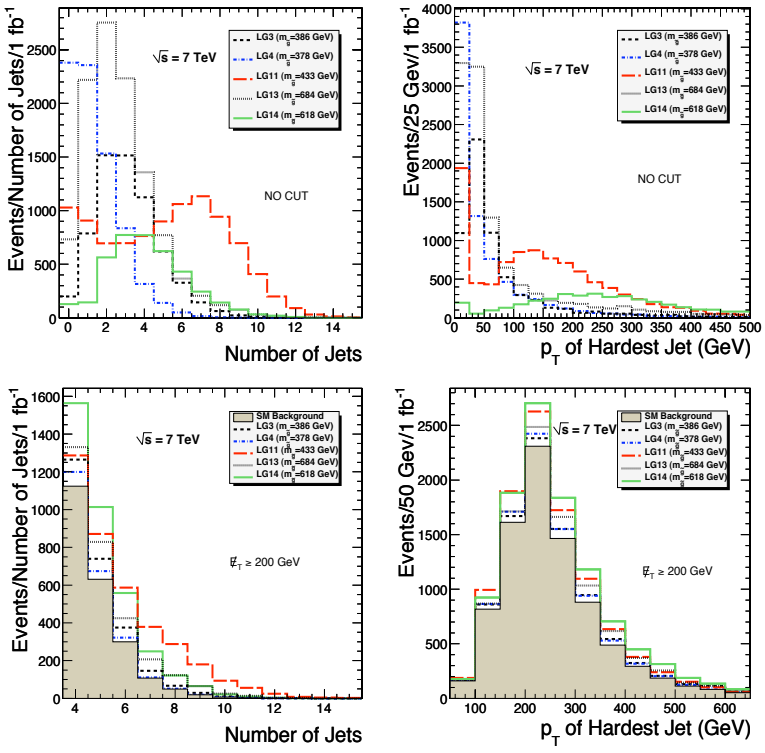

Figure 4.5: (Color online) Top Left: Distribution of the number of jets without cuts. Top Right: Distribution of the p_T of the hardest jet also without cuts. Bottom Left: Distribution of the number of SUSY events (plus SM background) vs. the number of jets after a cut of $\not{E}_T \geq 200$ GeV. Bottom Right: Distribution of the number of SUSY events (plus SM background) vs. the p_T of the hardest jet after a cut of $\not{E}_T \geq 200$ GeV.

can be substantial for the collider signatures. We also note that although it can be challenging to discover events from gluino production for the GNLSP models, (depending on the degree of the mass degeneracy), one should keep in mind that some other subdominant SUSY production modes could be detectable and become the leading signals for such models. For example, in model LG3, the stop is relatively light and decays entirely into a chargino and bottom quark, i.e., $\mathrm{Br}(\tilde{t}_1 \to \tilde{\chi}_1^{\pm} b) \sim 100\%$, and the chargino subsequently decays entirely into a neutralino and a W boson, i.e., $\mathrm{Br}(\tilde{\chi}_1^{\pm} \to \tilde{\chi}_1^0 W^+) \sim 100\%$. Hence, this GNLSP model class may be able to produce discoverable leptonic

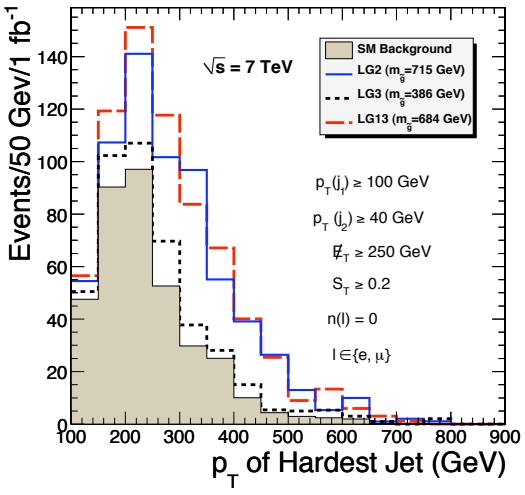

Figure 4.6: SUSY plus Standard Model background events vs $p_T(j_1)$ at 1 fb^{-1} for the signature cut $p_T(j_1) \geq 100$ GeV, $p_T(j_2) \geq 40$ GeV, $\not{E}_T \geq 250$ GeV, $S_T \geq 0.2$ and $n(\ell) = 0$ for LG2, LG3, LG13. The figure illustrates the softness of the jets in model LG3, a GNLSP model, relative to the models LG2 and LG13.

events through these decay chains with upgraded center of mass energy and luminosity.

Further, these features of the GNLSP models can explicitly be seen by studying the top panels of Fig. (4.5) and by observing the relative broadness (or width) of the p_T distribution of models LG11 and LG14 relative to LG3 and LG4. In addition, LG13, a stop NLSP model, is also peaked at low jet p_T much like LG3 and LG4. The stop mass for model LG13 is near 200 GeV and the stop-LSP mass splitting is small ($\lesssim 30$ GeV). Thus, this model produces stops at a large rate, which decay (via an off-shell loop-induced and FCNC decay) into a charm quark and LSP ($\tilde{t}_1 \to c\tilde{\chi}_1^0$) with a $\sim 75\%$ branching ratio. However, the softness of jets in LG13 mimics the softness of jets in LG4 in part due to the phase space, which explains the peaking of the distributions at low p_T. The restricted phase space from the small mass splittings is also why the effective mass distribution for stop NLSPs is narrow (see [40]) relative to other cases.

In Fig. (4.6) we highlight the GNLSP model LG3, which satisfies the double-sided relic density band, along with the light stau and stop models, LG2 and LG13, which also satisfy the WMAP bound via scalar coannihilations. Thus, Fig. (4.6) shows jet p_T, signal plus background, for the models LG2, LG3, and LG13 compared to the Standard Model background alone. As discussed earlier the model LG3 arises from gluino coannihilations and has a relatively small mass splitting between the gluino and the LSP neutralino. This is to be contrasted with the model LG2, which satisfies the WMAP relic density band via stau coannihilations, or the model LG13, which also satisfies the WMAP relic density band via stop coannihilations. Because of the compressed spectra of LG2 and LG13, there are more jets arising from the combinations of both low mass gluino and the low mass squark production relative to the dominant gluino production found in the GNLSP model LG3. This effect is exhibited in the figure. For model LG2, as the scalars are quite light, and even lighter than the 715 GeV gluino, the cross section for the production of squarks as well as the mixed squark gluino production cross sections are about an order of magnitude larger than the $\tilde{g}\tilde{g}$ production. Here the gluino two body decay modes are spread out rather uniformly with no dominant channel. Instead the first two generation squark decay modes are short with large branchings. In particular, one has for the first two generation squarks, $\mathrm{Br}(\tilde{q}_R \to \tilde{\chi}_1^0 q) \sim 100\%$ and $\mathrm{Br}(\tilde{q}_L \to \tilde{\chi}_2^0 q) \sim 32\%$ as well as $\mathrm{Br}((\tilde{q}_{d_L}, \tilde{q}_{u_L}) \to \tilde{\chi}_1^{(-,+)}(q_u, q_d)) \sim (60-65)\%$ for each decay. Thus, the two body decays of the first two generation squarks provide the large signal in model LG2 even though the gluino is quite light. In addition, for LG2, the direct production of chargino pairs as well as chargino and neutralino production is competitive with the squark production, leading to leptonic decays and large lepton multiplicities. The discovery potential of the models is also exhibited in Fig. (4.4), where one finds that the significance of LG3 and LG4 is much less than for LG11.

In Fig. (4.7) (left-panel) we show the potential for early discovery for the PAMELA compliant models (LG10, LG16, LG17) listed in Table. (4.2) at $\sqrt{s} = 7$ TeV and at an integrated luminosity of 1 fb^{-1}. The displayed models have a rather large gluino production. Since the gluino, the light chargino,

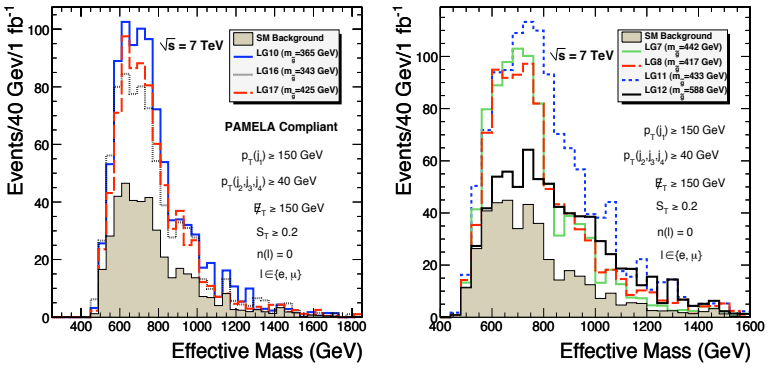

Figure 4.7: Left: SUSY plus SM background events vs $m_{\rm eff}$ at 1 fb^{-1} of integrated luminosity for the signature cut $p_T\,(j_1) \geq 150$ GeV, $p_T\,(j_2, j_3, j_4) \geq 40$ GeV, $\not{E}_T \geq 150$ GeV, $S_T \geq 0.2$ and $n(\ell) = 0$ for the PAMELA compliant models. As discussed in the text LG10 is a Higgsino LSP model and LG16 and LG17 are models with a mixed-wino LSP. Right: The same as the left panel except for a subset of the GNNLSP models (with chargino and neutralino degenerate), i.e., LG7, LG8, along with the compressed models LG11, LG12, which in addition to a low mass gluino, also have a light stau and a light stop and have a compressed mass spectrum for the first two generation squarks and sleptons.

and the second heaviest neutralino are the lightest SUSY particles beyond the LSP, and the squarks are rather heavy for these models, the sparticle production at the LHC will be dominated by $\tilde{g}\tilde{g}$, $\tilde{\chi}_2^0\tilde{\chi}_1^\pm$ and $\chi_1^+\chi_1^-$ production. For example, models (LG10, LG16, and LG17) have a total SUSY cross section of $\sim (12, 15, 5)$ pb at leading order and the gluino production is at the level of $\sim (9, 14, 4)$ pb, respectively. The chargino neutralino production makes up most of the remaining part of the cross section. The leading decays of the gluino are $\tilde{g} \to \tilde{\chi}_1^\pm + \bar{q}q'$ and $\tilde{g} \to \tilde{\chi}_2^0/\tilde{\chi}_1^0 + q\bar{q}$. These decays are subsequently followed by $\tilde{\chi}_2^0 \to \tilde{\chi}_1^0 + \bar{f}f$ and $\tilde{\chi}_1^\pm \to \tilde{\chi}_1^0 + \bar{f}f'$ where f, f' are the standard model quarks and leptons. In particular, the lightness of the gluino in the three models (LG10, LG16,and LG17) gives rise to multi-jets which produce a strong signal over the background. Hence, these models are good candidates for early discovery. Further, if a model of the type LG10, LG16, or LG17 is verified at the LHC, it would also provide a consistent explanation of the PAMELA

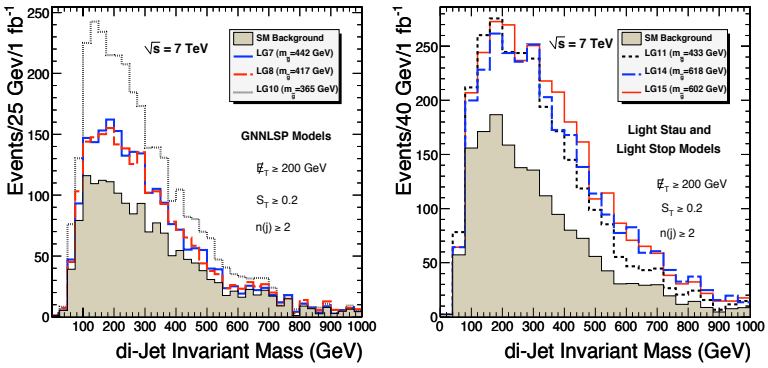

Figure 4.8: Left: SUSY plus SM background events vs the di-jet invariant mass (m_{jj}) at 1 fb^{-1} of integrated luminosity for signature cut $\not\!\!E_T \geq 200$ GeV, $S_T \geq 0.2$ and $n(j) \geq 2$ for the models LG7, LG8, LG10. Right: Same as the left plot except that the analysis is for models LG11, LG14, LG15. The left panel shows the light gluino models which are effectively GNNLSP models, while the right panel shows the models with a compressed mass spectrum for the scalars and for the light gluinos. As such the right panel shows distributions which are significantly broader from the squark production and decays.

anomaly. However, to fully demonstrate the validity of the models, additional luminosity would be needed to extract information about the neutralino mass. We do not give a detailed methodology for accomplishing this, but as argued in [96] it may be possible to extract information about the neutralino and the chargino states in the gluino decay products.

In Fig. (4.8), we show a comparison of di-jet invariant mass distributions for the GNNLSP models compared to models where the gluino is positioned higher in the mass hierarchy. One sees the GNNLSP models (LG7, LG8, and LG10) have a relatively narrow di-jet invariant mass which arises from these models being dominated by the three-body decays resulting from $\tilde{\chi}_2^0\tilde{\chi}_1^{\pm}$, $\tilde{\chi}_1^+\tilde{\chi}_1^-$, and $\tilde{g}\tilde{g}$ production. Further, the distributions for the models LG8 and LG10 become depleted (or more narrow) relative to the light stau and light stop models from the three-body decays which result in softer jets. These subsequent decays produce an increase in the multi-jet signal compared to the SM background. However, the light stau and light stop models LG11,

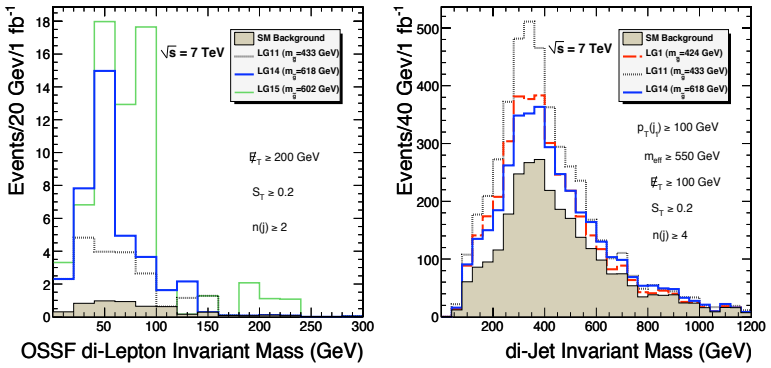

Figure 4.9: Left: SUSY plus background events for models LG11, LG14, LG15 vs the OSSF di-lepton invariant mass ($m_{\ell^+\ell^-}$) at 1 fb^{-1} for signature cut $\not{E}_T \geq 200$ GeV, $S_T \geq 0.2$ and $n(j) \geq 2$ with 2 leptons of any sign and flavor. Right: SUSY plus background events for models LG1, LG11, LG14 vs the di-jet invariant mass (m_{jj}) at 1 fb^{-1} of integrated luminosity for signature cut $\not{E}_T \geq 100$ GeV, $S_T \geq 0.2$, $p_T(j_1) \geq 100$ GeV, $m_{\text{eff}} \geq 550$ GeV and $n(j) \geq 4$. Here the peak in the distribution is a consequence of the m_{eff} cut.

LG14, and LG15 have a relatively broader distribution, which arises from the compression of their sparticle spectrum. For these models, all the sparticle masses are below 700 GeV. Further, LG14 and LG15, where the mass spectra are compressed, the gluino is in the 31$^{\text{st}}$ position of the mass hierarchy. The compressed spectra causes a large sampling of sparticle production, which results in a production of many jets with a more diverse range of momentum.

The right panel of Fig. (4.9) shows the number of SUSY signature events plus the SM background in 40 GeV energy bins at 1 fb^{-1} of integrated luminosity vs the di-jet invariant mass for models LG1, LG11, and LG14. As exhibited in this figure, these models have a significantly larger di-jet invariant mass compared to the Standard Model. As discussed earlier LG11 has a relatively large sparticle mass splittings in the scalar sector relative to the LSP mass as well as lengthy cascade decay chains that produce multiple final state jets with large momentum. Further, the right panel of Fig. (4.9) helps illustrate the effectiveness of the m_{eff} cut. Comparing the values of C13 to C14 in Table. (4.7), one sees that the significance for models LG1, LG11,

and LG14 increases as $m_{\rm eff}$ increases. For the case when $m_{\rm eff} \geq 400$ GeV (C13) we get $S/\sqrt{B} = (17, 34, 15)$ and when $m_{\rm eff} \geq 550$ GeV (C14) we get $S/\sqrt{B} = (20, 38, 20)$, respectively, for (LG1 ,LG11, LG14). However, models LG3, LG10, and LG16 have a reverse effect, i.e., $S/\sqrt{B} = (3, 23, 27)$ for $m_{\rm eff} \geq 400$ GeV (C13) and $S/\sqrt{B} = (2, 15, 15)$ for $m_{\rm eff} \geq 550$ GeV (C14) for (LG3, LG10, LG16), respectively. These effects arise since models LG3, LG10, and LG16 have lower jet multiplicity, less missing energy, and fewer cascades than the models shown in the right panel of Fig. (4.9). For instance, the model LG16 cross section is dominated by $\tilde{g}\tilde{g}$ production with the $\tilde{g}$ dominantly decaying into $\tilde{\chi}_1^0$ or $\tilde{\chi}_1^\pm$. This results in low jet multiplicity and lower missing energy compared to models LG1, LG11, and LG14.

Mass Reconstruction: We now discuss the potential to do mass reconstruction for some of the models with the early data. In the left panel of Fig. (4.9) we display the number of SUSY signature events plus background events in 20 GeV energy bins at 1 fb^{-1} of integrated luminosity vs the OSSF di-lepton invariant mass for models LG11, LG14, and LG15. The plot also displays the cuts used as well as the standard model background alone for comparison. In large portions of the figure, the SUSY signals plus the background distribution stands significantly above the background. The leptonic events are mostly produced from the gaugino cascade decays through low-lying sleptons. If the OSSF di-leptons arise from the same decay chain $\tilde{\chi}_2^0 \to \tilde{\ell}^\pm \ell^\mp \to \tilde{\chi}_1^0 \ell^\pm \ell^\mp$, the invariant mass from the reconstruction of the di-leptons obeys the following mass relations for on-shell sleptons:

$$M_{\ell^+\ell^-} \leq M_{\tilde{\chi}_2^0} \sqrt{1 - \frac{M_{\tilde{\ell}}^2}{M_{\tilde{\chi}_2^0}^2}} \sqrt{1 - \frac{M_{\tilde{\chi}_1^0}^2}{M_{\tilde{\ell}}^2}} \ . \tag{4.16}$$

In particular, for model LG15 the three sleptons, $(\tilde{\tau}_1, \tilde{e}_R, \tilde{\mu}_R)$ with the latter two being degenerate, contribute to the OSSF di-lepton events with the di-lepton invariant mass lying between $\tilde{\chi}_1^0$ and $\tilde{\chi}_2^0$. Using the sparticle masses from LG15, i.e., $(M_{\tilde{\chi}_1^0}, M_{\tilde{\ell}_R}, M_{\tilde{\chi}_2^0}) = (121, 137, 240)$ GeV, one can use Eq. (4.16) to obtain $M_{\ell^+\ell^-} \lesssim 92$ GeV from the $\tilde{e}_R/\tilde{\mu}_R$ decay modes. The $\tilde{\chi}_2^0$ decays into $\tilde{\chi}_1^0$

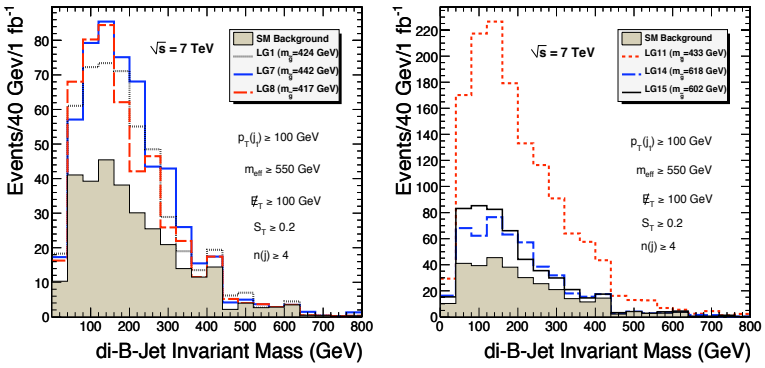

Figure 4.10: Left: SUSY plus Standard Model background events vs the b-tagged di-jet invariant mass (m_{bb}) at 1 fb^{-1} of integrated luminosity for signature cut $\not{E}_T \geq 100$ GeV, $S_T \geq 0.2$, $p_T(j_1) \geq 100$ GeV, $m_{\rm eff} \geq 550$ GeV and $n(j) \geq 4$ for the models LG1, LG7, LG8. Right: Same as the left panel except that the analysis is for models LG11, LG14, LG15. As discussed in the text, there is a hint of kinematical endpoints forming for some of the models in the di-b-jet invariant mass plots exhibited above.

via Br($\tilde{\chi}_2^0 \to \tilde{\ell}_R^{\pm}\ell^{\mp}$) $\simeq 28\%$, and then the right-handed slepton decays entirely into a lepton and $\tilde{\chi}_1^0$, i.e., Br($\tilde{\ell}_R^{\pm} \to \tilde{\chi}_1^0\ell^{\pm}$) $\simeq 100\%$. The decay of the light stau follows similarly through Br($\tilde{\chi}_2^0 \to \tilde{\tau}_1^{\pm}\tau^{\mp}$) $\simeq 33\%$, and then the stau decays entirely into $\tilde{\chi}_1^0$ and a τ, i.e., Br($\tilde{\tau}_1^{\pm} \to \tilde{\chi}_1^0\tau^{\pm}$) $\simeq 100\%$. The tau produced from the $\tilde{\chi}_2^0$ decay has a subsequent leptonic tau decay with branching ratio of Br($\tau \to \ell\nu_\ell\nu_\tau$) $\simeq 35\%$. We do not attempt to reconstruct taus here, and we note that there are also further mixings arising from chargino decays which require flavor subtraction and other techniques to isolate lepton pairs coming from the same cascade decay. Further, due to the low statistics at the early runs of the LHC data, we do not perform a more detailed mass reconstruction in our analysis here. As discussed above, and as can be seen in Fig. (4.9), the mixings arising from other processes are rather small and the edge in the di-lepton invariant mass agrees well with the prediction of Eq. (4.16).

We now discuss the reconstruction of the b-tagged di-jet invariant mass peak. In the left panel of Fig. (4.10) we give an analysis of the number of SUSY event vs the b-tagged di-jet invariant mass (m_{bb}) at 1 fb^{-1} for the

models LG1, LG7, and LG8 for the cuts displayed as well as a comparison to the Standard Model background. One finds that the three models are distinguishable above the background. For these models, the majority of the b-tagged di-jet events come from the gluino off-shell decay $\tilde{g} \to \tilde{\chi}_2^0 + b\bar{b}$, which leads to an upper bound of the kinematic endpoint $M_{bb} \leq M_{\tilde{g}} - M_{\tilde{\chi}_2^0}$ that is estimated to be in the range $(300 - 322)$ GeV. In the left panel of Fig. (4.10), one sees a hint of an endpoint forming in this region. However, for these models, the kinematic endpoint is not yet discernible; more luminosity would be needed, and further, additional uncertainties arise in the interpretation of the invariant mass endpoint due to additional cascade processes. A similar analysis can be given for models LG11, LG14, and LG15 in the right panel of Fig. (4.10). The source of the jets for the three models differ from those of the left panel of Fig. (4.10) due to their spectra. Further, LG11 produces a significantly larger number of jet events compared to those for LG14 and LG15 due to its light color particles, i.e., the gluino and the stop, dominantly decaying to b jet final states. In addition, some of the b jets in the models from Fig. (4.10) come from the light CP even Higgs. For example, in model LG15 $\mathrm{Br}(\tilde{\chi}_2^0 \to \tilde{\chi}_1^0 h) \sim 30\%$ and $\mathrm{Br}(h \to b\bar{b}) \sim 80\%$. Thus with increased statistics one may be able to partially reconstruct events coming from the Higgs decay in this model and other models as well.

More generally in Table. (4.8) we summarize the result of our analysis for the full set of integrated luminosities 0.5 fb^{-1}, 1 fb^{-1}, 2 fb^{-1}, and 5 fb^{-1}. The entries in the boxes in this table indicate the integrated luminosity at which a model listed in the first column will become visible in a specific signature channel listed in the top row. Thus, the entries in Table. (4.8) show that a good number of the models in Table. (4.2) will become visible at 0.5 fb^{-1} of integrated luminosity, and all of the models given in Table. (4.2) will become visible (in at least one channel) at 5 fb^{-1} of integrated luminosity. Indeed, as discussed above, one observes that the relative mass splitting and the relative position of the gluino within the sparticle mass hierarchies strongly influences the discovery capability of the LG models. Several channels in some cases are needed to establish a signal, and the variance amongst channels for different models is apparent.

Chapter 5

Dark Matter in Supersymmetric Models with Gravity Mediation

Dark matter is a significant component of the total mass of the Universe, yet it is not addressed by the Standard Model itself. In this chapter, we will study the dark matter phenomena in supersymmetric models with gravity mediation. This scenario for supersymmetry breaking has been intensively studied over more than twenty years. One obvious reason is that the lightest sparticle (LSP) is always the neutralino with typical mass $\sim$ 100 GeV. Its lightness and protection from decay by R-parity assures its stability. We will start with a brief introduction about the dark matter evidence and some of candidates from particle physics. Afterwards, we will move to the recent discussion of the possible dark matter detection in the framework of NUSUGRA, where the dark matter detection techniques will be briefly reviewed. Our original research in this area has been published in the following two papers: N. Chen, D. Feldman, Z. Liu, P. Nath, and G. Peim, "Higgsino dark matter model consistent with galactic cosmic ray data and possibility of discovery at LHC-7", Phys. Rev. D **83**, 023506 (2011), Ref. [48]; and "Low-mass gluino within the sparticle landscape, implications for dark matter, and early discovery prospects at LHC-7", Phys. Rev. D**83**, 035005 (2011), Ref. [49].

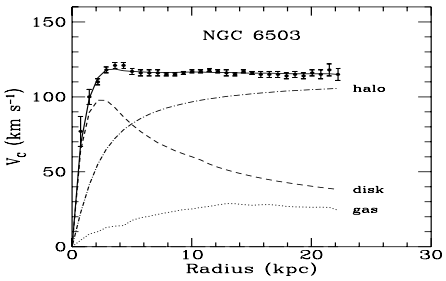

Figure 5.1: Rotation curve of NGC 6503 [90]

5.1 Dark Matter Evidence, Relic Density, And Candidates

5.1.1 Evidence from different scales

As noted before, the first evidence for dark matter was reported by Zwicky in the 1930's on the basis of his observation of the motion of galaxies in the Coma cluster, and his finding that this motion was considerably greater than could be accounted for by the visible matter and resultant gravitation acting on these galaxies in the cluster.

Within galaxies, on the scale of 10-20 kpc, strong evidence for dark matter comes from the observation of galactic velocity rotation curves. A curve of this type usually exhibits a flat behavior at large distance from the galactic center. A typical example is shown on the Fig. (5.1). By Newtonian dynamics, the circular velocity should be:

$$v(r) = \sqrt{\frac{G_N M(r)}{r}} \tag{5.1}$$

with the mass being $M(r) = 4\pi \int \rho(r) r^2 dr$. $\rho(r)$ is the mass density and should fall as $1/\sqrt{r}$ beyond the optical disc. However, the observed $v(r) = \text{const}$ implies a possible halo with $M(r) \propto r$ and $\rho(r) \propto 1/r^2$.

In addition to evidence of dark matter from galactic rotation curves, it is crucial to know the total amount of dark matter in the Universe. This in-

formation can be extracted from the analysis of the Cosmic Microwave Background Radiation (CMBR) [86]. Such background radiation is due to the propagation of photons in the early Universe. The CMBR is observed to be isotropic and homogenous at the level of $\delta T/T \simeq 10^{-5}$. In recent years, the best constraints on the relic abundances of baryons and matter in the Universe are obtained from the Wilkinson Microwave Anisotropy Probe (WMAP) data [87]. Their seven-year data shows the relic density of baryon, matter and cold dark matter as: $\Omega_{\rm B}h^2 = 0.02260 \pm 0.00053$, $\Omega_{\rm M}h^2 = 0.1334^{+0.0056}_{-0.0055}$, and $\Omega_{\rm CDM}h^2 = 0.1123 \pm 0.0035$. Here, for each contribution of type i, one defines the dimensionless ratio $\Omega_i h^2 \equiv \rho_i/\rho_c$, where $\rho_c \equiv 3H_0^2/8\pi G_N$ is the critical density for closure[1], with H_0 Hubble constant[2] in the present epoch, and G_N is the Newton gravitational constant. The data clearly indicates that the dark matter should be non-baryonic.

5.1.2 Dark matter relic density

We shall briefly discuss the evaluation of the relic abundance $\Omega_\chi h^2 \equiv \rho_\chi/\rho_c$ (Here and below, we use the notation χ for the dark matter in general. In most cases, we focus on the case where χ is the neutralino in the MSSM.). One uses the Boltzmann equation for one particular species of dark matter particle number density n:

$$\frac{dn}{dt} + 3Hn = -\langle\sigma v\rangle(n^2 - n_{eq}^2) \tag{5.2}$$

If there were no dark matter annihilation, the total dark matter particle number would be a constant. This means $n \propto R^{-3}$, hence $\dot{n} = -3Hn$. In reality, one should also take the $\overline{\chi}\chi$ annihilation into account, which is described on the RHS of Eq. (5.2). The $\langle\sigma v\rangle$ is the thermal averaged annihilation cross section times the relative velocity v between $\overline{\chi}$ and χ. The n_{eq} stands for the

[1]The $\rho > \rho_c$, $\rho = \rho_c$, and $\rho < \rho_c$ correspond to the closed, flat and open universe.

[2]In practice, one usually uses the dimensionless Hubble parameter $h \equiv H_0/(100$ km/s/Mpc).

number density of the dark matter species while in thermal equilibrium[3]. For heavy states like the $\tilde{\chi}_1^0$ in our discussion, $v \ll 1$. Eq. (5.2) cannot be analytically solved, one can at best get the approximated estimation about the relic density as:

$$\Omega_\chi h^2 \approx \frac{3 \times 10^{-27} \mathrm{cm}^3 \mathrm{s}^{-1}}{\langle \sigma v \rangle} \tag{5.3}$$

If one or more particles have masses close to the relic particle, which is often the case in various SUGRA-mediation parameter regions, the standard calculation of relic density should be modified. Assuming N particles χ_i with masses M_i and intrinsic degrees of freedom g_i $(1 \leq i \leq N)$, we shall modify Eq. (5.2) into:

$$\frac{dn}{dt} + 3Hn = -\sum_{i,j=1}^{N} \langle \sigma_{ij} v_{ij} \rangle (n_i n_j - n_i^{eq} n_j^{eq}) \tag{5.4}$$

where $n \equiv \sum_i n_i$ is the number density of the relic particles. Besides, σ_{ij} is the total annihilation cross section for the $\chi_i \chi_j$ into the Standard Model particles, and v_{ij} is the relative velocity defined as:

$$v_{ij} = \frac{\sqrt{(\vec{p}_i \cdot \vec{p}_j)^2 - M_i^2 M_j^2}}{E_i E_j} \tag{5.5}$$

Therefore, the effective annihilation rate of the dark matter particles becomes much faster with a modified effective annihilation rate:

$$\langle \sigma_{\mathrm{eff}} v \rangle = \sum_{ij} \langle \sigma_{ij} v_{ij} \rangle \frac{n_i^{\mathrm{eq}} n_j^{\mathrm{eq}}}{(n^{\mathrm{eq}})^2} \tag{5.6}$$

[3]The equilibrium number density is approximately to be a Boltzmann distribution: $n_{eq} \approx g_\chi (\frac{M_\chi T}{2\pi})^{-3/2} \exp(-M_\chi/T)$, where g_χ is the intrinsic degrees of freedom of the dark matter particle χ.

Such co-annihilation effects [91] have been included in the numerical computations of relic densities, e.g., the MicrOMEGAS computer program [56].

5.1.3 Candidates

Many candidates for the non-baryonic dark matter have been studied, with masses span a wide range from sub-eV scale to $\mathcal{O}(100$ TeV). We will briefly discuss some typical candidates here.

The Standard Model, as augmented to include massive neutrinos, does have a candidate that could contribute to the dark matter, namely neutrinos. An estimate of the relic density contribution from the neutrino reads:

$$\Omega_\nu h^2 \;=\; \sum_{i=1}^{3} \frac{m_{\nu_i}}{93 \text{ eV}} \tag{5.7}$$

If one uses as an upper limit the neutrino mass bound from the non-observation of neutrinoless double β decay, $m_\nu < 2.05$ eV, then one infers that $\Omega_\nu h^2 \lesssim 0.02$. Hence, obviously, massive neutrinos in the (augmented) Standard Model cannot be the dominant part of the dark matter. However, there are also the possibilities of sterile (i.e., electroweak-singlet) neutrinos or fourth-generation neutrinos with masses at least greater than $M_Z/2$.

Supersymmetric models have provided varieties of sparticles to be the dark matter candidates. In general, the dark matter in a supersymmetric model that is R-parity odd and neutral in color and charge is the lightest supersymmetric particle (LSP). The most widely studied example of an LSP is the lightest neutralino in the gravity-mediation model. In the framework of MSSM, the neutralino is a mixture of bino ($\tilde{B}$), wino ($\tilde{W}$) and two higgsino states ($\tilde{H}_{1,2}$). Generically, with soft masses around several hundred GeV for these states, one gets the neutralino mass $\sim \mathcal{O}(100$ GeV). Using the rough information we know here, one can estimate that the annihilation cross section of the neutralino goes like $\langle \sigma v \rangle \sim \alpha^2/\Lambda^2$ with $\alpha \sim 0.01$ and $\Lambda \sim 100$ GeV. Using the estimate from (5.3), one gets $\Omega_\chi h^2 \simeq 2.5 \times 10^{-2}$, which is not very far away from the WMAP data we mentioned before. Therefore, this so-called

WIMP miracle strongly suggests that the WIMP could very well saturate the measured cold dark matter relic density. In the NMSSM a further gauge singlet state (called *singlino*) will enter, and this could also play a role in dark matter.

Many other efforts to build models of dark matter are being pursued at present, e.g. [95] among many others. It is an open question what the real source of dark matter is; however, the SUSY LSP remains one of the most appealing candidates.

5.2 Dark Matter in mSUGRA

In this section, we briefly mention the DM in the mSUGRA models. The LSPs in the mSUGRA must be bino-like, as from the simple gaugino mass relation (2.47). As we mentioned in the previous chapter, the relic density constraint we imposed $\Omega_{\tilde{\chi}_1^0}h^2 < 0.13$ is the most stringent one among all. In general, viable mSUGRA models satisfying the relic density constraints should have an adequately large $\langle\sigma v\rangle$ (5.3). Three well-known scenarios[4] are possible for a viable relic density:

- The stau or stop co-annihilation [91] is important when $\tilde{\tau}_1$ or $\tilde{t}_1$ are the NLSP.
- The enhancement of $\langle\sigma v\rangle$ could also happen when the LSP sits on the h-pole $m_\chi = m_h/2$ [5] or the MSSM Higgs pole $m_\chi = m_H/2$. [92] .
- The "Focus Point" SUSY models [23] with multi-TeV sfermions not only have the appeal to suppress the FCNC amplitudes, but also appear consistent with the relic density constraints.

5.3 Dark Matter in NUSUGRA

In this section, we discuss the dark matter implication in the framework of the gaugino NUSUGRA models. The key observation is that the most rele-

[4]For decoding various DM scenarios at the LHC, see Ref. [41].

[5]It was possible to have the LSP on the Z-pole, i.e., $m_\chi = M_Z/2$. This has been eliminated from the lower bounds on the chargino mass.

vant sparticles in the discussion of dark matter are the LSP and sometimes also the NLSP when co-annihilation becomes important. For the NUSUGRA models, their LSP eigen-contents can be different from the bino-like case in the mSUGRA; they can be wino-like or Higgsino-like instead. These models could enhance the $\tilde{\chi}_1^0\tilde{\chi}_1^0$ annihilation cross sections via the Z or (MSSM) Higgs channels. Further more, the gluino is not always the heaviest among all gauginos. In a special case when $\tilde{g}$ becomes the NLSP [42], there can strong gluino co-annihilation with the LSP. Hence there are more annihilation channels open in the NUSUGRA models for reasonable relic densities.

5.3.1 Direct detection constraints

Besides the dark matter relic density constraint from the WMAP data, one important constraint is from the direct detection experiments, where one measures the recoil energy produced by a dark matter particle scattering off a nucleus in the detector. The velocity of DM particles near the Earth is expected to be of the same order as the orbital velocity of the Sun and solar system around the galaxy, which is $v \approx .001c$. For typical masses of WIMP $m_\chi \approx 100$ GeV and of nuclei $m_N \approx 100$ GeV, the maximum recoil energy is:

$$E_{\text{rec.}} \sim \frac{(m_\chi v_\chi)^2}{2m_N} \approx 100 \text{ keV} \tag{5.8}$$

In general, the WIMP-nucleon elastic amplitudes are divided into spin-independent (SI) interaction or spin-dependent (SD) interaction. In particular, the cross section for the SI interaction[6] gets enhanced by nuclei with large nucleon numbers A.

Many experiments searching for direct detection of dark matter have been performed or are being performed. A few of these include Edelweiss [100],

[6]For a point-like nuclei, one gets the cross section for a WIMP scattering as: $\sigma_0^{\text{SI}} = \frac{4\mu_\chi^2}{\pi}(\lambda_p Z + \lambda_n(A-Z))^2$, with $\mu_\chi \equiv m_\chi m_N/(m_\chi + m_N)$ being the WIMP-nucleus reduced mass. The cross section adds coherently so that there is a strong enhancement $\propto A^2$ for large nuclei when $\lambda_p \approx \lambda_n$. For real WIMP-nucleon amplitudes, the nucleon structure must be taken into account. Details of this computation are reviewed on the Ref. [88].

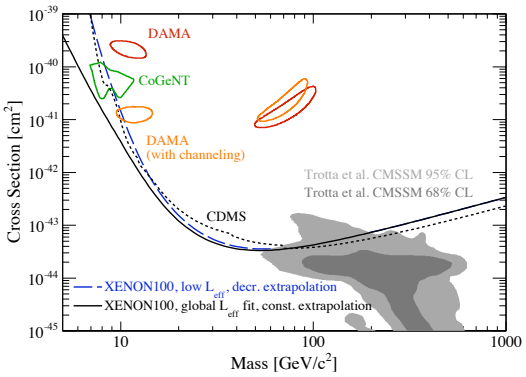

Figure 5.2: 90% confidence limit on the SI elastic WIMP-nucleon cross section together with the best limit from CDMS [103] (dotted) and Xenon100 2010 data [105] (solid and dashed).

DAMA [101], CDMS [102], and Xenon [104]. Of these, only DAMA has definitely claimed to have observed a dark matter signal. We should particularly mention the first results of the SI direct detection from the Xenon 100 [105], which is given on the Fig (5.2). For our later discussion on the LSP DM in the context of gravity-mediation models, we would focus on the region with $m_\chi \sim 100$ GeV. Therefore, the WIMP-nucleon SI interaction should have $\sigma_{\rm SI} \lesssim 5 \times 10^{-44}$ cm^2 in such a region[7]. Notice also the CoGeNT and DAMA detections are focusing on the region with DM masses ~ 10 GeV. They were designed for models with lower masses. As we mentioned earlier, a typical example is from the NMSSM model. Their results are not particularly relevant to our following discussions.

5.3.2 Indirect detection constraints

There are also a number of efforts to detect dark matter indirectly, via its annihilation or decays into Standard Model particles in the galactic halo. The dark matter annihilation rate depends on the dark matter density: $\Gamma \propto \rho^2_{\rm DM}$. Therefore, one promising place to look for such a signal is the galactic center

[7]During the preparation of this thesis, we got to learn the updated dark matter results from 100 live days of Xenon100 data [106]. With the 2σ exclusion band of the updated data, we found that the models LG2, LG6, LG8, and LG10 as displayed in Table (4.2) have very well been excluded.

with large DM densities. Two recent experiments are the PAMELA experiment [107] and the Fermi-LAT (large-area telescope) experiment [108]. Of these, PAMELA has reported observing high energy positrons that may be in excess of known astrophysical sources (although it has also been suggested that conventional astrophysical source can account for the PAMELA data). The Fermi-LAT mission has reported finding no significant excess in its search for monochromatic photons with energies $E_\gamma \in (30 - 200)$ GeV range.

In general, the observed flux of dark matter annihilation products reads:

$$\Phi_i(\psi, E) = \frac{\langle \sigma v \rangle}{4\pi m_\chi^2} \frac{dN_i}{dE} \int_{\text{line}} ds \rho^2(r(s, \psi)) \tag{5.9}$$

Here $\langle \sigma v \rangle$ is the thermal averaged annihilation cross section, and dN_i/dE is the energy distribution of Standard Model particle i produced in one reaction. The $\rho(r)$ is the dark matter halo distribution function. Several useful spherically symmetric halo profiles are listed in Table. (5.1).

Halo parameters for three common profiles

Halo model	α	β	γ	a (kpc)
Isothermal	2	2	0	4
NFW	1	3	1	20
Moore	1.5	3	1.5	28

Table 5.1: The halo distribution function is parameterized by $\rho(r) = \rho_\odot F(r)$, with $F(r) = (\frac{r_\odot}{r})^\gamma \left(\frac{1+(r_\odot/a)^\alpha}{1+(r/a)^\alpha}\right)^{\frac{\beta-\gamma}{\alpha}}$. Here, $\rho_\odot$ and $r_\odot$ are the solar location and the distance of the Sun to the galactic center. There is also another totally different parameterization for the halo called the "Einasto profile". Its distribution function is $F(r) = \exp[-\frac{2}{\alpha}((\frac{r}{r_\odot})^\alpha - 1)]$, with the default value for α is 0.17.

The PAMELA experiments [107] measured both e^+ and $\overline{p}$ [8]. The antiproton-to-proton flux ratio is well measured with energy up to 100 GeV and shows no

[8]The propagation of the charged particles from the dark matter annihilation is affected by the galactic magnetic field, synchrotron radiation and inverse Compton scattering. The detailed discussion of their propagation can be found on Ref [97] [98] [99].

anomalous behavior. As remarked above, PAMELA reports a possible excessive positron flux with energies up to ~ 100 GeV in the cosmic radiation. If one takes the point of view that conventional astrophysical sources cannot account for this, then it is suggestive of classes of DM with $\mathcal{O}(100)$ GeV masses, subject to the constraint that they do not produce $\bar{p}$'s also. We will mention one such possibility in the context of NUSUGRA soon.

Another possible and distinctive signal for the indirect detection is a narrow γ-ray line from dark matter particle annihilating or decaying into γX, where X can be another photon, a Z boson, or a Higgs boson. Dark matter particles of mass m_χ annihilating (in pair) into γX produce monochromatic γ-rays of energy $E_\gamma = m_\chi(1 - \frac{m_X^2}{4m_\chi^2})$. Therefore, one would expect a strong line feature, or a strong line-like feature as a sharp cut-off in the γ-ray spectrum. The most recent results set γ-ray line upper limits from 30 GeV to 200 GeV obtained from 11 months of Fermi-LAT data from $20 - 300$ GeV energy region. The γ-ray line flux upper limits are in the range of $0.6 - 4.5 \times 10^{-9}$ cm^{-2}s^{-1}, and their corresponding DM annihilation cross sections can be found on Ref. [108].

Prior to our work, wino-like LSP models [96] were suggested to be promising for the PAMELA data since they can have strong annihilation of neutralinos into W^+W^- and/or ZZ. However, this type of models are disfavored by the null results of the Fermi-LAT searches for the gamma ray lines as shown on Fig (5.3).

5.3.3 Higgsino-like LSP scenario

Here we present several SUSY models with a Higgsino LSP which can accommodate various dark matter constraints: relic abundance, the positron excess from PAMELA, the anti-proton flux, as well as the Fermi-LAT gamma ray line data. The benchmark models are (P1-P3)[9] listed in Table. (5.2). In Table. (5.3), we give the theoretical predictions of the Higgsino LSP models for the γZ and $\gamma\gamma$ modes and the exhibit the current upper limits from the Fermi-LAT search. However, these models give fairly small contributions to

[9]These benchmarks are similar to the benchmark models (LG10, LG16, LG17) defined in the Table (4.2) from the previous chapter.

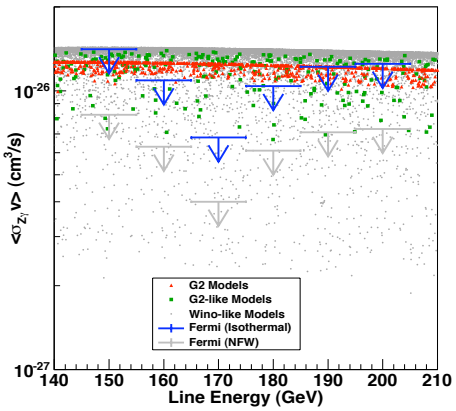

Figure 5.3: The $\langle\sigma v\rangle_{Z\gamma}$ for wino-like models as from Ref. [96]. The upper bounds are the Fermi-LAT data with either an NFW or an isothermal halo profile.

the relic densities, which are generally smaller than the relic density upper bounds from the electroweak neutrinos as we evaluated above. One way to enhance the relic density is via an extended Abelian gauge symmetry from the hidden sector, which is called the *Stueckelberg mechanism*. In such mechanism, one is allowed to include kinematic mixings between the hypercharge gauge multiplet (λ_Y, Y_μ, D_Y) and the hidden gauge multiplet of $\mathrm{U}(1)_X$ (λ_X, X_μ, D_X). The effective Lagrangian containing the mixing terms is:

$$-\frac{1}{2}(\partial_\mu\sigma + M_Y Y_\mu + M_X X_\mu)^2 + [\psi(M_X\lambda_X + M_Y\lambda_Y) + h.c.] \quad (5.10)$$

with the axionic field σ arising from a chiral multiplet $S = (\rho + i\sigma, \psi, F_S)$. The ψ and λ_X produce two Majorana spinors, which are hidden sector neutralinos mixing with the MSSM neutralinos. Such analysis can be extended to a $\mathrm{U}(1)_X^n$ gauge symmetry in the hidden sector, which yields $2n$ additional Majorana fields. Therefore, the LSP can co-annihilate with the hidden sector Majorana fields, which yields the following enhancement factor for the density of relic neutralinos relative to that in the MSSM:

Model	m_0	M_1	M_2	M_3	A_0	$\tan\beta$	μ'	$M_1^{'}$	$M_2^{'}$	$M_3^{'}$	Ωh^2
P1	1033	1600	1051	120	2058	13	195	683	836	259	6×10^{-3}
P2	1150	1600	1080	160	2080	15	152	684	859	347	4×10^{-3}
P3	950	1425	1820	748	1925	25	109	617	1453	1589	2×10^{-3}
WB	2000	400	210	200	300	5	562	170	163	441	2×10^{-3}

Table 5.2: Parameters which produce an LSP which are mostly Higgsino (P1-P3), or mixed wino-bino, WB. Here $m_0(A_0)$ is the universal scalar mass (trilinear coupling), M_1, M_2, M_3 are the gaugino masses at the GUT scale for the gauge groups $U(1)_Y, SU(2)_L, SU(3)_c$ and $\tan\beta$ is the ratio of the two Higgs vacuum expectation values in the MSSM. The parameters that enter the neutralino mass matrix at scale $Q=\sqrt{M_{\tilde{t}_1}M_{\tilde{t}_2}}$ are $(\mu', M_1^{'}, M_2^{'}, M_3^{'})$, where μ' is the Higgs mixing parameter. The models have also been run through both SuSpect [54] and SOFTSUSY [53] via micrOMEGAs [56]. Here $m_{\rm top}^{\rm pole}$=173.1 GeV.

E_γ	Einasto	NFW	Isothermal	Model	$\langle\sigma v\rangle_{\gamma Z,[\gamma\gamma]}^{\rm theory}$
180[190]	4.4[2.3]	6.1[3.2]	10.4[5.5]	P1	0.24[0.08]
130[150]	5.3[2.5]	7.3[3.5]	12.6[6.0]	P2	0.23[0.09]
90[110]	4.3[0.7]	6.0[1.0]	10.3[1.7]	P3	0.18[0.09]
150[160]	5.9[2.0]	8.2[2.7]	14.1[4.7]	WB	7.00[1.29]

Table 5.3: Cross sections $\langle\sigma v\rangle_{\gamma Z}$ and $\langle\sigma v\rangle_{\gamma\gamma}$ upper limits (10^{-27}cm^3/s) [108] for three halo profiles (Einasto, Navarro-Frenk-White (NFW), and Isothermal) along with predictions for (P1-P3) and WB. The mostly Higgsino models (P1-P3) are unconstrained by any profile while the mixed wino-bino model, WB, is on the edge.

$$\Omega_{\tilde{\chi}_1^0}h^2 \simeq f_E \times \Omega_{\tilde{\chi}_1^0}^{\rm MSSM}h^2 \qquad f_E=(1+2n)^2 \tag{5.11}$$

Roughly for models we listed in Table (5.2), one can reasonably enhance the relic densities close to the WMAP value with $n\simeq 5$.

Next, we discuss the positron excess prediction in the Higgsino-like model. In Higgsino and wino models, the high energy positron flux can arise from WW and ZZ production from the neutralino annihilation in the halo with approximate cross sections at leading order [88]:

$$\langle\sigma v\rangle(\chi\chi \to VV) \simeq \frac{g^4}{C_V 2\pi M_\chi^2}\frac{(1-x_V)^{3/2}}{(2-x_V)^2}, \tag{5.12}$$

where $V = (W, Z)$, $x_V = M_V^2/M_\chi^2$, $C_W = 16$ (1) for Higgsino (wino) models and the ZZ production is only significant for Higgsino models where $C_Z = 32\cos^4(\theta_W)$. For the models (P1-P3) the LSP is mostly a Higgsino with only a very small portion being gaugino. Here the cross sections that enter in the positron excess are size $\langle\sigma v\rangle(\chi\chi \to WW, ZZ)_{\rm Higgsino} \lesssim 4\times 10^{-25}{\rm cm}^3/{\rm s}$.

The positron flux from the Higgsino dark matter can be decribed semi-analytically (for general discussion for positron propagation and fluxes in the halo, see Ref. [93]). The flux enters as a solution to the diffusion loss equation, which is solved in a region with a cylindrical boundary. The particle physics determines the $\langle\sigma v\rangle_{\rm halo}$ and the energy distributions dN_i/dE. The astrophysics determines the dark matter profile and the energy loss in the flux from the presence of magnatic fields and from scattering off galactic photons. A boost factor B which parametrizes the possible local inhomogeneities of the dark matter distribution can be present, which is as low as $\sim (2-3)$ in our consideration. The antiproton flux follows reather analogously, and the general dicussion follows the Ref [94].

The full analysis of the positron flux is exhibited in the left panel of Fig. (5.4) where we show fits to the PAMELA positron fraction. For comparison we also show the essentially pure wino case, which will generally lead to an overproduction of photons however. In the right panel of Fig. (5.4), we give a comparison of the $\overline{p}$ flux with the recent data from PAMELA [107]. It is seen that the theoretical prediction of the $\overline{p}$ flux is in good accord with the data.

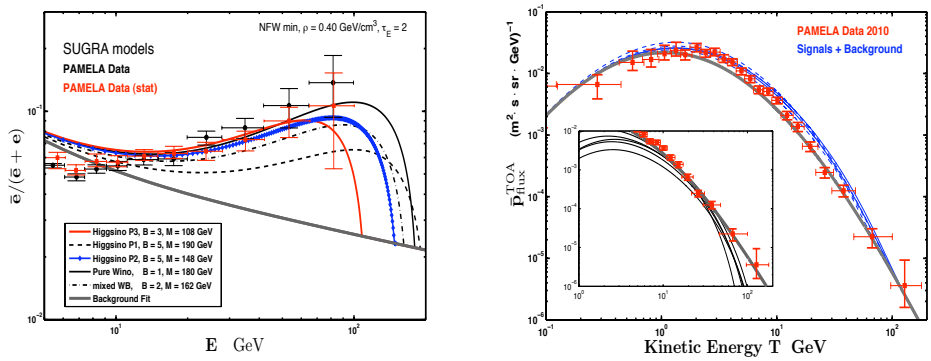

Figure 5.4: . Left: PAMELA positron excess and the Higgsino models (P1-P3). The wino dominated model is also shown for comparison along with a mixed wino-bino model (WB). Right: The PAMELA $\bar{p}$ flux and the predictions are seen to be compatible with the data. Equal dark matter densities and boosts are taken in both panels.

Chapter 6

Dynamical Electroweak Symmetry Breaking

In this chapter, we discuss another type of beyond Standard Model physics, namely the dynamical electroweak symmetry breaking models.

6.1 Motivation and Technicolor Model

6.1.1 New strong dynamics

Even without Higgs mechanism, the electroweak symmetry is already broken by the bilinear quark condensation in quantum chromodynamics (QCD) [109, 110]: $\langle \overline{q}q \rangle = \Lambda^3_{\text{QCD}} \simeq 4\pi f_\pi^3$, with $\Lambda_{\text{QCD}} \simeq 200$ MeV and the pion decay constant $f_\pi \simeq 93$ MeV. This quantity transforms with weak $T_3 = 1/2$ and $|\Delta Y| = 1$. If the quark condensation were the only source for EWSB, one would get a W boson mass like:

$$M_W = \frac{g f_\pi}{2} \sim 30 \text{ MeV} \tag{6.1}$$

Since this is much smaller than the observed value, $M_W \simeq 80.4$ GeV, QCD makes only a very small contribution to the actual EWSB in nature. However, this immediately suggests that maybe there exists another kind of strong

gauge theory somewhat similar to QCD, but with its dynamical scale around the electroweak scale $\Lambda_{\rm TC} \simeq 250$ GeV. The new gauge theory is required to be vectorial and asymptotically free like QCD. This hypothetical new strong gauge theory is called *technicolor* (or TC for short) [109]. One may construct TC models with a TC gauge group of the form $\mathrm{SU}(N_{\rm TC})$. One should have at least two Dirac technifermions so that these can be assigned to transform as the upper and lower components of a left-handed $\mathrm{SU}(2)_L$ doublet and corresponding right-handed $\mathrm{SU}(2)_L$ singlets. The dynamical scale of technicolor is obtained by rescaling relation as:

$$\Lambda_{\rm TC} \simeq \sqrt{\frac{3}{N_{\rm TC}}}\,\frac{F_{\rm TC}}{f_\pi}\Lambda_{\rm QCD} \tag{6.2}$$

At scale slightly above $\Lambda_{\rm TC}$, the operative gauge symmetry is

$$\mathrm{SU}(N_{\rm TC}) \times \mathrm{SU}(3)_c \times \mathrm{SU}(2)_L \times \mathrm{U}(1)_Y \tag{6.3}$$

In order to give masses to quarks and leptons, which are TC-singlets, it is necessary to embed the TC theory in a larger theory, called extended technicolor (ETC), which contains fields that communicate the EWSB in the TC sector to these Standard-Model fermions [111]. Some recent reviews of TC/ETC theories include Refs. [112]-[115].

6.1.2 One-doublet model

A minimal TC model contains a weak doublet of (color-singlet) technifermions in the fundamental representation of the TC gauge group,

$$Q_L^\tau = \begin{pmatrix} U^\tau \\ D^\tau \end{pmatrix}_{0,L} \qquad U_{1,R}^\tau \qquad D_{-1,R}^\tau \tag{6.4}$$

where $\tau = 1, ..., N_{\rm TC}$ is the technicolor index. For generic $N_{\rm TC}$, the formation of the technifermion condensates $\langle \overline{U}U \rangle$ and $\langle \overline{D}D \rangle$ breaks the $\mathrm{SU}(2)_L \times \mathrm{SU}(2)_R$ chiral symmetry of the model to $\mathrm{SU}(2)_V$, yielding three Nambu-Goldstone bosons (NGBs), which are absorbed by the $W^{\pm}$ and Z, giving them masses and longitudinal components. This is thus dynamical electroweak symmetry breaking. In contrast to the Standard Model Higgs sector, one did not have to artificially set the sign of any quadratic term in a Higgs potential to get this breaking; it follows automatically from the property that the TC theory is asymptotically free, so that the TC gauge coupling increases as the reference energy scale decreases and eventually becomes large enough (at the scale $\Lambda_{\rm TC}$) to produce these technifermion condensates. The W mass in this model is given by the expression $M_W^2 = \frac{1}{4} g^2 F_{TC}^2$, which implies that $F_{TC} = v \simeq 250$ GeV. Because the technifermion condensates transform as weak $T_3 = 1/2$ and $|\Delta Y| = 1$ operators, it follows that, to leading order, the $\rho = [M_W/(M_Z \cos\theta_W)]^2$ parameter is unity, in agreement with experiment.

6.1.3 One-family model

A different TC model that can be more conveniently embedded in an ETC model has a set of technifermions that transform according to the fundamental representation of the TC gauge group and form one family under the Standard Model gauge group. These can be written as

$$\begin{array}{lll} Q_L^{\tau,a} = \begin{pmatrix} U^{\tau,a} \\ D^{\tau,a} \end{pmatrix}_{1/3,L} & U_{4/3,R}^{\tau,a} & D_{-2/3,R}^{\tau,a} \\ \begin{pmatrix} N^{\tau} \\ E^{\tau} \end{pmatrix}_{-1,L} & E_{-2,R}^{\tau} & \end{array} \tag{6.5}$$

where $\tau = 1, ..., N_{\rm TC}$ and $a = 1, 2, 3$. The formation of technifermion condensates $\langle \overline{F}F \rangle$, where $F = U,\ D,\ N,\ E$, produces the EWSB. The resultant part, yielding 63 (P)NGBs. Three of these are absorbed to produce the W and Z masses. We have $M_W^2 = \frac{1}{4} g^2 (N_c + 1) F_{\rm TC}^2$, so that $F_{\rm TC} \simeq 130$ GeV. The ρ

parameter is unity at tree level, so $M_Z = M_W/\cos\theta_W$. In addition to these three, the model also has a number of other (P)NGBs. There are also other techni-hadrons, including techni-vector and axial-vector mesons. In modern TC models, one often takes the minimal TC gauge symmetry to be $\mathrm{SU}(2)_{\mathrm{TC}}$. This choice minimizes the TC contributions to electroweak corrrections, such as corrections to the Z and W propagators (encloded in the S parameter [117]) and can also lead to an approximate infrared fixed point (IRFP) in the TC theory. In turn, the latter property produces a large but slowly running ("walking") TC gauge coupling, which enhances quark and charged lepton masses.

TC/ETC models are subject to a number of stringent constraints from measurements of and limits on flavor-changing neutral current interactions (FCNCs), precision electroweak corrections, and limits on techni-hadrons. These models are very ambitious; for example, a truly successful TC/ETC model would answer longstanding questions such as explaining mass ratios like m_e/m_μ, m_μ/m_τ, m_u/m_d, m_u/m_c, and other quark mass ratios including m_b/m_t. Not surprisingly, there is no fully realistic TC/ETC model at present. Recent LHC results from the ATLAS and CMS experiments have set lower limits of order 1.5 TeV on a color-octet technivector meson [118, 119].

6.2 Extended Technicolor Model

6.2.1 Model setup

Now we discuss an ETC model. The ETC gauge symmetry is usually taken to be:

$$\mathcal{G}_{\mathrm{ETC}} = SU(N_{\mathrm{ETC}}) \qquad N_{\mathrm{ETC}} = N_{\mathrm{TC}} + N_{\mathrm{gen}} \tag{6.6}$$

where the ETC theory gauges the SM generational indices, of which there are $N_{\mathrm{gen}} = 3$. This means that the first N_{gen} components of a fundamental representation of the ETC theory are for the SM fermions, and the remaining

$N_{\rm TC}$ components are the TC fermions. For the observed Standard Model fermion generations of $N_{\rm gen}=3$ and the minimal choice of the $N_{\rm TC}=2$, one typically takes an $SU(5)_{\rm ETC}$ gauge theory. Therefore, the set of ETC fermions here follows from Eq. (6.5), with the τ index generalized to $i=1,...,5$ for the fundamental representation of SU(5). To explain the hierarchy structure of the Standard Model families, the ETC gauge symmetry should break in three steps: $\mathrm{SU}(5)_{\rm ETC} \xrightarrow{\Lambda_1} \mathrm{SU}(4)_{\rm ETC} \xrightarrow{\Lambda_2} \mathrm{SU}(3)_{\rm ETC} \xrightarrow{\Lambda_3} \mathrm{SU}(2)_{\rm TC}$. The Λ_i represents the scale for each symmetry-breaking. The sequential symmetry breaking in the ETC models is produced by certain ETC fermion condensates. In general, the determination of which condensation channels occur is based on the most attractive channel (MAC) criterion. Consider the channel $\mathcal{R}_1 \times \mathcal{R}_2 \to \mathcal{R}_0$. Then the MAC is the channel that maximizes the quantity $\Delta C_2 = C_2(\mathcal{R}_1) + C_2(\mathcal{R}_2) - C_2(\mathcal{R}_0)$. The model is designed so that these channels break the ETC gauge symmetry in the desired sequential manner.

The Standard Model fermion masses are related to the TC condensate through the ETC gauge boson exchange. An estimate of the dynamical masses (actually, the diagonal elements of the SM fermion mass matrices) is

$$M_{ii} \simeq (\frac{g_{\rm ETC}}{\sqrt{2}})^2 \frac{\eta \langle \overline{F} F \rangle}{M_i^2} \tag{6.7}$$

where $\langle \overline{F} F \rangle$ stands for the TC fermion condensation, and $M_i \sim g_{\rm ETC} \Lambda_i$ is the mass of the ETC gauge bosons which get their masses at scale Λ_i. The quantity η is an renormalization group (RG) factor which reads:

$$\eta = \exp[\int \frac{d\mu}{\mu} \gamma(\alpha_{\rm TC}(\mu))] \tag{6.8}$$

with γ being the anomalous dimension for the bilinear operator $\overline{F}F$. For a TC theory with walking behavior $\gamma \simeq 1$ between $\Lambda_{\rm TC}$ and the lowest ETC scale Λ_3, one has $\eta \simeq \Lambda_3/\Lambda_{\rm TC}$. It follows that

$$M_{ii} \simeq \frac{8\pi}{3}\frac{\Lambda_{\rm TC}^2 \Lambda_3}{\Lambda_i^2} \tag{6.9}$$

Choosing the ETC scales to be $(\Lambda_1, \Lambda_2, \Lambda_3) \simeq (10^3, 50, 4)$ TeV and using that $\Lambda_{\rm TC} = 250$ GeV, this procedure can yield roughly reasonable values of SM fermion masses, although it does not have enough ingredients to fit these masses precisely. Explaining light neutrino masses has been a further challenge, but a mechanism for doing this has been given in [121] [123]. Some related works include [120]-[126].

6.3 Standard Model Gauge Symmetry Unification in Technicolor

We mentioned in the introduction that the SM gauge couplings are well measured at the M_Z scale, but the Standard Model does not explain their values. Grand unified theories (GUTs) can do this. Such GUTs include those with the gauge groups SU(5) and SO(10). However, nonsupersymmetric GUTs are excluded by their lack of gauge coupling unification as well as their prediction of excessive proton decay. (Of course, their Higgs sectors are also unstable to large radiative corrections; i.e., even before being ruled out experimentally, they had a hierarchy problem.) The MSSM has the appeal of gauge coupling unification as well as stabilization of the Higgs sector. Here we shall study the partial and/or complete unification of gauge symmetries in theories with dynamical symmetry breaking. The results here are based on the paper [127], which continued the earlier study of Christensen and Shrock, [122]. A related work is [128].

6.4 Unification of SM and TC gauge symmetries

An interesting question concerns the extent to which one might unify the Standard Model gauge symmetry with the TC/ETC gauge symmetry, and embed these in a simple group. Since the ETC theory encodes the number N_{gen} of SM fermion generations, if such a unification were successful, it would predict this number. This would thus be an even more ambitious unification than the previous GUT theories, which put in the value of N_{gen} as a free parameter. In one approach we shall look for a simple gauge group $\mathcal{G}$ such that $\mathcal{G} \supset \mathcal{G}_{\rm TC} \times \mathcal{G}_{\rm SM}$. At an appropriate scale, $\mathcal{G}$ should break to $\mathcal{G}_{\rm TC} \times \mathcal{G}_{\rm SM}$. An alternate approach is to consider $\mathcal{G} \supset \mathcal{G}_{\rm SC} \times \mathcal{G}_{\rm GUT}$ with $\mathcal{G}_{\rm SC} \supseteq \mathcal{G}_{\rm TC}$ containing the TC interaction and $\mathcal{G}_{\rm GUT} \supset \mathcal{G}_{\rm SM}$ being the GUT symmetry. It is natural to take the unified symmetry to be $\mathcal{G} = {\rm SU}(N)$ with $N = N_{\rm SC} + 5$, i.e., the $\mathcal{G}_{\rm GUT} = {\rm SU}(5)$ is chosen as the symmetry containing the SM-nonsinglet fermions.

6.4.1 General structure of unification models

We consider a general approach in which some Standard Model fermion generations may arise directly from the representations of the unified group $\mathcal{G}$, while the remaining ones arise indirectly, from sequential symmetry breaking of a subgroup of $\mathcal{G}$ at ETC-type scales. Let us denote N_{gh} and $N_{g\ell}$ as the numbers of standard-model fermion generations arising from these two sources, respectively, where the subscripts gh and $g\ell$ refer to generations from the representation content of the high-scale symmetry group and from the lower-scale breaking. The sum of these satisfies:

$$N_{\rm gen} = 3 = N_{gh} + N_{g\ell} \ . \tag{6.10}$$

At this stage the number $N_{g\ell}$ is only formal; that is, we construct a model so that, *a priori*, it can have the possibility that a subgroup of $\mathcal{G}$ such as

$\mathcal{G}_{SC}$ might break in such a manner as to peel off $N_{g\ell}$ Standard Model fermion generations. However, we must examine for each model whether this breaking actually occurs; this will be discussed further below.

We next sketch our procedure for analyzing the models; for further details, the reader is referred to Ref. [122]. The fermion representations are determined by the structure of the fundamental representation, which we take to be:

$$\psi_R = \begin{pmatrix} (N^c)^\tau \\ d^a \\ -e^c \\ \nu_e^c \end{pmatrix}_R \tag{6.11}$$

where d, e, and ν are generic symbols for the fermions with these quantum numbers. Thus, the indices on ψ_R are ordered so that the indices in the SC (strongly coupled) set, which we shall denote τ, take on the values $\tau = 1, ...N_{\rm SC}$ and then the remaining five indices are those of the 5_R of $\mathrm{SU}(5)_{\rm GUT}$, including the color index a on d^a. The components of N_R^c transform according to the fundamental representation of $\mathrm{SU}(N_{\rm SC})$, are singlets under $\mathrm{SU}(3)_c$ and $\mathrm{SU}(2)_w$, and have zero weak hypercharge and hence also zero electric charge. This structure is concordant with the direct product of $\mathcal{G}_{\rm SC} \times \mathcal{G}_{\rm GUT}$ and the corresponding commutativity property $[\mathcal{G}_{\rm SC}, \mathcal{G}_{\rm GUT}] = 0$ and hence $[\mathcal{G}_{\rm TC}, \mathcal{G}_{\rm GUT}] = 0$. (Recent discussions of models with higher-dimensional representations of $\mathcal{G}_{\rm TC}$ include [129].)

We next specify the fermion representations of $\mathcal{G} = \mathrm{SU}(N)$. In the following, we shall usually write the fermion fields as left-handed. In order to avoid fermion representations of $\mathrm{SU}(3)_c$ and $\mathrm{SU}(2)_w$ other than those experimentally observed, namely singlets and fundamental or conjugate fundamental representations, we restrict the fermions to transform as k-fold totally antisymmetrized products of the fundamental or conjugate fundamental representation of $\mathrm{SU}(N)$; these are denoted as $[k]_N$ and $[\bar{k}]_N = \overline{[k]}_N$. A set of (left-handed) fermions $\{f\}$ transforming under $\mathcal{G}$ is thus given by:

$$\{f\} = \sum_{k=1}^{N-1} n_k \, [k]_N \tag{6.12}$$

where n_k denotes the multiplicity (number of copies) of each representation $[k]_N$. We use a compact vector notation $\mathbf{n} \equiv (n_1, ..., n_{N-1})_N$. If $k = N - \ell$ is greater than the integral part of $N/2$, we shall work with $[\bar{\ell}]_N$ rather than $[k]_N$; these are equivalent with respect to SU(N).

An acceptable model should satisfy the following requirements: (i) the contributions from various fermions to the total SU(N) gauge anomaly must cancel each other, yielding zero gauge anomaly; (ii) the resultant TC-singlet, SM-nonsinglet left-handed fermions must comprise a well-defined set of generations, i.e., must consist of $N_{gen.} = 3$ copies of $[(1, \bar{5})_L + (1, 10)_L]$, where the first number in parentheses signifies that these are singlets under G_{TC} and the second number denotes the dimension of the $\mathrm{SU}(5)_{\mathrm{GUT}}$ representation; and (iii) in order to account for neutrino masses, one needs to have TC-singlet, electroweak-singlet neutrinos to produce Majorana neutrino mass terms that can drive an appropriate seesaw [121, 123]. Here these are also singlets under $\mathrm{SU}(5)_{\mathrm{GUT}}$.

As another requirement, (v), the ETC gauge bosons should have appropriate masses, in the range from a few TeV to 10^3 TeV, so as to produce acceptable Standard Model fermion masses. This requirement cannot be satisfied if $\mathcal{G}$ breaks directly to the direct product group $\mathcal{G}_{\mathrm{TC}} \times \mathcal{G}_{\mathrm{SM}}$ at the unification scale M_{GU}. The requirement could be satisfied if the breaking of $\mathcal{G}$ at M_{GU} would leave an invariant subgroup $\mathrm{SU}(2)_w \times \mathcal{G}_{SCC}$, where

$$\mathrm{SU}(N_{SCC}) \supset \mathrm{SU}(N_{SC}) \times \mathrm{SU}(3)_c \tag{6.13}$$

with

$$N_{SCC} = N_{SC} + N_c = N_{SC} + 3 \; . \tag{6.14}$$

Here SCC stands for the SC group together with the color group. As the energy scale decreases, this intermediate symmetry $\mathcal{G}_{\rm SCC}$ should break at ETC scales, eventually yielding the residual exact symmetry group $\mathrm{SU}(2)_{TC}\times\mathrm{SU}(3)_c$. This could occur naturally if the SCC gauge interaction is chiral and asymptotically free; as the energy scale decreases and the SCC gauge coupling increases, it could thus trigger the formation of a fermion condensate which would self-break $\mathcal{G}_{\rm SCC}$. This type of process in which a strongly coupled chiral gauge interaction self-breaks via formation of a fermion condensate has been termed "tumbling" [116]. Further requirements are that (vi) if $N_{\rm SC} > N_{\rm TC}$, there should be a mechanism to break $\mathrm{SU}(N_{SC})$ to $\mathrm{SU}(N_{TC})$; (vii) the TC interaction should be vectorial and asymptotically free, so that the TC gauge coupling gets large as the energy scale decreases to the TeV scale, triggering the formation of a technifermion condensate for EWSB; and (viii) the residual $\mathrm{SU}(3)_c$ color group should be asymptotically free.

Let us define a $(N-1)$-dimensional vector whose components are the values of the anomaly $A([k]_N)$ with respect to $\mathrm{SU}(N)$, $\mathbf{a} = (A([1]_N), ..., A([N-1]_N))$. Then the constraint that there be no $\mathcal{G}$ gauge anomaly is the condition

$$\mathbf{n}\cdot\mathbf{a} = 0\ . \tag{6.15}$$

This is a diophantine equation for the components of the vector of multiplicities $\mathbf{n}$, subject to the constraint that the components n_k are non-negative integers (as well as additional constraints discussed below).

It is convenient to display the transformation property of a fermion representation of $\mathcal{G}$ with respect to the subgroups $\mathcal{G}_{\rm SC}$ and $\mathrm{SU}(5)_{\rm GUT}$ by the notation $(\mathcal{R}_{\rm SC}, \mathcal{R}_{\rm GUT})$. The number of (left-handed) fermions that transform as singlets under $\mathcal{G}_{\rm SC}$ and $\bar{5}$'s of $\mathrm{SU}(5)_{\rm GUT}$ is

$$N_{(1,\bar{5})} = n_{_{N_{SC}+4}} + n_4 \tag{6.16}$$

and the number of (left-handed) fermions that transform as singlets under $\mathcal{G}_{\rm SC}$ and 10's of $\mathrm{SU}(5)_{\rm GUT}$ is

$$N_{(1,10)} = n_2 + n_{_{N_{SC}+2}}\ . \tag{6.17}$$

Hence, the requirement that the left-handed SC-singlet, SM-nonsinglet fermions comprise equal numbers of $(1, \bar{5})$ and (1,10)'s implies the condition

$$n_{N_{SC}+4} + n_4 = n_2 + n_{N_{SC}+2} \ . \tag{6.18}$$

The number of Standard Model fermion generations N_{gh} produced by the representations of $\mathcal{G}$ is given by either side of this equation;

$$N_{gh} = n_2 + n_{N_{SC}+2} \ . \tag{6.19}$$

The remaining $N_{g\ell}$ generations of Standard Model fermions arise via the breaking of $\mathcal{G}_{\rm SC}$. Electroweak-singlet neutrinos, arise, in general, from two sources: (i) $[N_{\rm SC}]_N$, when all of the $N_{\rm SC}$ indices take values in SU($N_{\rm SC}$); and (ii) $[5]_N$, when all of the indices take values in SU(5)$_{\rm GUT}$. In the special case $N_{\rm SC} = 5$, these each contribute. Hence,

$$N_{(1,1)} = n_{N_{\rm SC}} + n_5 \ . \tag{6.20}$$

Electroweak-singlet neutrinos arise from fermions that are singlets under both $\mathcal{G}_{\rm SC}$ and SU(5)$_{\rm GUT}$; there are $N_{(1,1)} = n_{N_{\rm SC}} + n_5$ of these.

With the envisioned sequential breaking of $\mathcal{G}_{\rm SCC}$ and $\mathcal{G}_{\rm SC}$ that would produce the $N_{g\ell}$ SM fermion generations, one has $N_{g\ell} = N_{SCC} - (N_{TC} + N_c)$ and

$$N_{g\ell} = N_{SC} - N_{TC} \ . \tag{6.21}$$

The requirement that there be no (left-handed) fermions transforming as singlets under SU(N_{SC}) and in an exotic manner, as 5's or $\overline{10}$'s of SU(5)$_{GU}$ is satisfied if

$$n_1 = 0, \quad n_{N_{SC}+1} = 0 \tag{6.22}$$

and

$$n_3 = 0, \quad n_{N_{SC}+3} = 0 \tag{6.23}$$

respectively. In the following, we list our discussion of two GUT models with $\mathcal{G} = \mathrm{SU}(11)$ and $\mathcal{G} = \mathrm{SU}(12)$ respectively. The cases with $\mathcal{G} = \mathrm{SU}(N)$ for $N = 7,\ 8,\ 9,\ 10$ had already been studied in Ref. [122, 127].

6.4.2 $N_{\mathrm{SC}} = 6$, $\mathcal{G} = \mathrm{SU}(11)$

Here we consider the case where $N_{SC} = 6$, so that $N = N_{SC} + 5 = 11$ and $\mathbf{n} = (n_1, ..., n_{10})_{11}$. With $N_{gh} + N_{g\ell} = N_{gen.} = 3$ and $N_{SC} - N_{TC} = N_{g\ell}$, one has, *a priori*, four possibilities for the manner in which the Standard Model fermion generations arise, as specified by $(N_{gh}, N_{g\ell}, N_{TC})$, namely (3,0,6), (2,1,5), (1,2,4), and (0,3,3). However, only the cases with $N_{gh} = 0$ and $N_{gh} = 2$ are actually allowed by the various constraints. This SU(11) model was not studied in Ref. [122] because it does not allow one to use the preferred, minimal value, $N_{TC} = 2$. This latter value is preferred in order to minimize technicolor corrections to precisely measured electroweak quantities and because it makes possible a mechanism to produce light neutrino masses [121, 123, 125]. However, if one takes into account the fact that quasi-conformal behavior in the technicolor theory can reduce the technicolor corrections to the Z and W boson propagators, the effect of the larger value of N_{TC} might not be too serious. The conditions (6.22) and (6.23) that the theory should not contain any 5_L or $\overline{10}_L$ yield

$$n_1 = n_3 = n_7 = n_9 = 0\ , \tag{6.24}$$

and Eq. (6.18) is

$$N_{gh} = n_2 + n_8 = n_4 + n_{10}\ . \tag{6.25}$$

The condition of zero gauge anomaly, Eq. (6.15), is

$$7(n_2 + 4n_4 + 2n_5 - 2n_6) - 20n_8 - n_{10} = 0 \ . \tag{6.26}$$

For a given value of $N_{gh} = 3 - N_{g\ell}$, these are three nondegenerate linear equations for the six quantities n_2, n_4, n_5, n_6, n_8, and n_{10}. The solution entails the relation

$$n_5 = n_6 + \frac{1}{14}(27n_8 + 29n_{10}) - \frac{5}{2}N_{gh} \ . \tag{6.27}$$

A necessary condition for an acceptable solution is thus that

$$27n_8 + 29n_{10} - 35N_{gh} = 0 \mod 14 \ . \tag{6.28}$$

Let r be a non-negative integer. We find two classes of such solutions: (i) $N_{gh} = 0$, $n_8 = n_{10} = r$ and hence, from Eq. (6.27), $n_5 = n_6 + 4r$; (ii) $N_{gh} = 2$, $n_8 = n_{10} = r$, and hence $n_5 = n_6 + 4r - 5$.

We first consider solutions of class (i). These have $N_{g\ell} = 3$ and $N_{TC} = 3$. Now $N_{gh} = n_2 + n_8 = n_4 + n_{10} = 0$, which implies that $r = 0$, $n_2 = n_8 = n_4 = n_{10} = 0$, and $n_5 = n_6 = s$, where s is some positive integer. The resultant vector $\mathbf{n}$ is

$$\text{class } (i): \quad \mathbf{n} = (0, 0, 0, 0, s, s, 0, 0, 0, 0) \ . \tag{6.29}$$

The minimal choice would be $s = 1$, but for generality, we shall keep s arbitrary. Since $[6]_{11} \approx [\bar{5}]_{11}$, this SU(11) theory has left-handed chiral fermion content

$$s\{[5]_{11} + [\bar{5}]_{11}\} \tag{6.30}$$

and thus is vectorial. Consequently, the fermion content with respect to the subgroups $\mathrm{SU}(9)_{\mathrm{SCC}}$ and $\mathrm{SU}(6)_{\mathrm{SC}}$ is also vectorial. With respect to the subgroup

$$\mathrm{SU}(2)_w \times \mathrm{SU}(9)_{SCC} \ , \tag{6.31}$$

the $[5]_{11}$ representation transforms as

$$[5]_{11} = (1, [\bar{4}]_9) + (2, [4]_9) + (1, [3]_9) \ , \tag{6.32}$$

where we use the $[k]_9$ notation for the representations of $\mathrm{SU}(9)_{\mathrm{SCC}}$ and the well-known dimensions to label the representations of $\mathrm{SU}(2)_w$. The total fermion content with respect to the subgroup (6.31) is comprised of s copies of Eq. (6.32) and its conjugate.

With respect to the subgroup

$$\mathrm{SU}(6)_{\mathrm{SC}} \times \mathrm{SU}(5)_{\mathrm{GUT}} \ , \tag{6.33}$$

the $[5]_{11}$ representation transforms as

$$\begin{aligned} [5]_{11} &= (1,1) + ([1]_6, \bar{5}) + ([2]_6, \overline{10}) + ([3]_6, 10) \\ &+ ([\bar{2}]_6, 5) + ([\bar{1}]_6, 1) \ , \end{aligned} \tag{6.34}$$

where, aside from the overall singlet (1,1), we use the $[k]_6$ notation for the representations of $\mathrm{SU}(6)_{\mathrm{SC}}$ and the well-known dimensions to label the representations of $\mathrm{SU}(5)_{\mathrm{GUT}}$. The fermion content of this model with respect to the subgroup (6.33) is the sum of s copies of eq. (6.34) and its conjugate.

We recall the requirement that the SCC and SC interactions should be asymptotically free. For a given gauge group $\mathcal{G}_j$ with gauge coupling g_j and $\alpha_j = g_j^2/(4\pi)$, the evolution of the gauge couplings as a function of the momentum scale μ is given by the beta function $\beta_j = d\alpha_j/dt = -b_0^{G_j}\alpha_j^2/(2\pi) + \mathcal{O}(\alpha_j^3)$, where $t = \ln \mu$. We find that the $\mathrm{SU}(9)_{\mathrm{SCC}}$ and $\mathrm{SU}(6)_{SC}$ gauge interactions are non-asymptotically free, which disfavors models of class (i).

We next consider models of class (ii). These have $N_{g\ell} = 1$ and $N_{\mathrm{TC}} = 5$. The relations $N_{gh} = n_2 + n_8 = n_4 + n_{10} = 2$, together with the assignment $n_8 = n_{10} = r$ imply that

$$n_2 = n_4 = 2 - r \ . \tag{6.35}$$

We thus have three subclasses of solutions, namely (ii.a) $r = 2$, whence $n_2 = n_4 = 0$ and $n_5 = n_6 + 3$; (ii.b) $r = 1$, whence $n_2 = n_4 = 1$ and $n_5 = n_6 - 1$; and (ii.c) $r = 0$, whence $n_2 = n_4 = 2$ and $n_5 = n_6 - 5$. Minimal choices in each of these three subclasses have the following $\mathbf{n}$ vectors:

$$(iia): \quad \mathbf{n} = (0, 0, 0, 0, 3, 0, 0, 2, 0, 2) \tag{6.36}$$

$$(iib): \quad \mathbf{n} = (0, 1, 0, 1, 0, 1, 0, 1, 0, 1) \tag{6.37}$$

$$(iic): \quad \mathbf{n} = (0, 2, 0, 2, 0, 5, 0, 0, 0, 0) \ . \tag{6.38}$$

The fermions of set (iia) transform, with respect to the subgroup (6.31), according to

$$3[5]_{11} = 3\{(1, [\bar{4}]_9) + (2, [4]_9) + (1, [3]_9)\} \tag{6.39}$$

$$2[\bar{3}]_{11} = 2\{(1, [\bar{3}]_9) + (2, [\bar{2}]_9) + (1, [\bar{1}]_9)\} \tag{6.40}$$

$$2[\bar{1}]_{11} = 2\{(1, [\bar{1}]_9) + (2, 1)\} \ . \tag{6.41}$$

With the $\mathrm{SU}(2)_w$ couplings small, the nonsinglet $\mathrm{SU}(9)_{\mathrm{SCC}}$ fermion content is thus

$$\{f\} = 4[\bar{1}]_9 + 4[\bar{2}]_9 + 3[3]_9 + 2[\bar{3}]_9 + 6[4]_9 + 3[\bar{4}]_9 \ . \tag{6.42}$$

Hence, the $\mathrm{SU}(9)_{\mathrm{SCC}}$ sector is a chiral gauge theory. If the $\mathrm{SU}(9)_{\mathrm{SCC}}$ gauge interaction were asymptotically free and hence increased as the energy scale decreased below M_{GU}, one could proceed to the next step and analyze self-breaking condensate formation in the theory. However, we find that the $\mathrm{SU}(9)_{\mathrm{SCC}}$ interaction is non-asymptotically free.

With respect to the subgroup (6.33), the (left-handed chiral) fermions of

the set (iia) decompose according to

$$\begin{aligned} 3[5]_{11} &= 3\{(1,1) + ([1]_6, \bar{5}) + ([2]_6, \overline{10}) + ([3]_6, 10) \\ &+ ([\bar{2}]_6, 5) + ([\bar{1}]_6, 1)\} \end{aligned} \tag{6.43}$$

$$\begin{aligned} 2[8]_{11} \approx 2[\bar{3}]_{11} &= 2\{(1,10) + ([\bar{1}]_6, \overline{10}) + \\ &+ ([\bar{2}]_6, \bar{5}) + ([\bar{3}]_6, 1)\} \end{aligned} \tag{6.44}$$

and

$$2[10]_{11} \approx 2[\bar{1}]_{11} = 2\{([\bar{1}]_6, 1)) + (1, \bar{5})\} \ . \tag{6.45}$$

With the $\mathrm{SU}(5)_{\mathrm{GUT}}$ couplings small, the nonsinglet left-handed fermions transform according to the following $\mathrm{SU}(6)_{\mathrm{SC}}$ representations:

$$\{f\} = 15[1]_6 + 25[\bar{1}]_6 + 30[2]_6 + 25[\bar{2}]_6 + 32[3]_6 \tag{6.46}$$

where we have used the fact that $[3]_6$ is equivalent to $[\bar{3}]_6$. Hence, the $\mathrm{SU}(6)_{\mathrm{SC}}$ gauge interaction is chiral. However, we find that the $\mathrm{SU}(6)_{\mathrm{SC}}$ gauge interaction is not asymptotically free. Because of the lack of asymptotic freedom of the $\mathrm{SU}(9)_{\mathrm{SCC}}$ and $\mathrm{SU}(6)_{\mathrm{SC}}$ gauge sectors, this class of models (iia) is disfavored.

We next consider the subclass (iib). The fact that an $\mathrm{SU}(N)$ gauge theory with odd $N \geq 5$ and left-handed fermion content given by $n_i = 0$ for $i = 1, 3, ..., N-2$ and $n_i = 1$, $i = 2, 4, ..., N-1$ is anomaly-free was shown in [130]. With respect to the subgroup (6.31), the fermions for this class decompose according to

$$[2]_{11} = (1, [2]_9) + (2, [1]_9) + (1, 1) \tag{6.47}$$

$$[4]_{11} = (1, [4]_9) + (2, [3]_9) + (1, [2]_9) \tag{6.48}$$

$$[6]_{11} \approx [\bar{5}]_{11} = (1,[4]_9) + (2,[\bar{4}]_9) + (1,[\bar{3}]_9) \tag{6.49}$$

$$[8]_{11} \approx [\bar{3}]_{11} = (1,[\bar{3}]_9) + (2,[\bar{2}]_9) + (1,[\bar{1}]_9) \tag{6.50}$$

$$[10]_{11} \approx [\bar{1}]_{11} = (1,[\bar{1}]_9) + (2,1)\ . \tag{6.51}$$

With the $SU(2)_w$ couplings small, the nonsinglet $SU(9)_{SCC}$ fermion sector is then

$$\begin{aligned} \{f\} &= 2\{[1]_9 + [\bar{1}]_9 + [2]_9 + [\bar{2}]_9 + \\ &\quad [3]_9 + [\bar{3}]_9 + [4]_9 + [\bar{4}]_9\}\ . \end{aligned} \tag{6.52}$$

Hence, although the SU(11) gauge interaction is chiral, the $SU(9)_{\rm SCC}$ gauge interaction is vectorial. Even if the $SU(9)_{\rm SCC}$ interaction were asymptotically free, this vectorial property would disfavor this class of models because it would not self-break. We find that the $SU(9)_{\rm SCC}$ interaction is actually not asymptotically free.

With respect to the subgroup (6.33), the fermion decompose according to

$$[2]_{11} = (1,10) + ([1]_6,5) + ([2]_6,1) \tag{6.53}$$

$$\begin{aligned} [4]_{11} &= (1,\bar{5}) + ([1]_6,\overline{10}) + ([2]_6,10) + \\ &+ ([3]_6,5) + ([\bar{2}]_5,1) \end{aligned} \tag{6.54}$$

and

$$\begin{aligned} [6]_{11} &\approx [\bar{5}]_{11} = (1,1) + ([\bar{1}]_6,5) + ([\bar{2}]_6,10) + \\ &+ ([\bar{3}]_6,\overline{10}) + ([2]_6,\bar{5}) + ([1]_6,1)\ . \end{aligned} \tag{6.55}$$

with the decompositions of $[8]_{11} \approx [\bar{3}]_{11}$ and $[10]_{11} \approx [\bar{1}]_{11}$ given above. With the $SU(5)_{GU}$ couplings small, the nonsinglet fermion content under $SU(6)_{SC}$ is

$$16\{[1]_6 + [\bar{1}]_6 + [2]_6 + [\bar{2}]_6 + [3]_6\} \ . \tag{6.56}$$

As before, we find that the $SU(6)_{SC}$ gauge interaction for this set of fermions is not asymptotically free. This disfavors this class of models. We have analyzed the class (iic) in a similar manner and find that it is disfavored for the same reason, lack of asymptotic freedom.

6.4.3 $N_{SC} = 7$, $\mathcal{G} = SU(12)$

We have also studied the case where $N_{SC} = 7$, so that $N = N_{SC} + 5 = 12$ and $\mathbf{n} = (n_1, ..., n_{11})_{12}$. With $N_{gh} + N_{g\ell} = N_{gen.} = 3$ and $N_{SC} - N_{TC} = N_{g\ell}$, one has, *a priori*, four possibilities for the manner in which the SM fermion generations arise, as specified by $(N_{gh}, N_{g\ell}, N_{TC})$, namely (3,0,7), (2,1,6), (1,2,5), and (0,3,4). The conditions (6.22) and (6.23) that the theory should not contain any 5_L or $\overline{10}_L$ yield

$$n_1 = n_3 = n_8 = n_{10} = 0 \ , \tag{6.57}$$

and Eq. (6.18) is

$$N_{gh} = n_2 + n_9 = n_4 + n_{11} \ . \tag{6.58}$$

The condition of zero gauge anomaly, Eq. (6.15), is

$$8n_2 + 48n_4 + 42(n_5 - n_7) - 27n_9 - n_{11} = 0 \ . \tag{6.59}$$

For a given value of $N_{gh} = 3 - N_{g\ell}$, these are three linear equations for the seven quantities n_2, n_4, n_5, n_6, n_7, n_9, and n_{11}. The solution implies the relations

$$n_4 = \frac{1}{7}\Big[6(-n_5 + n_7) + 5n_9 - N_{gh}\Big] \tag{6.60}$$

and

$$n_{11} = \frac{1}{7}\Big[6(n_5 - n_7) - 5n_9 + 8N_{gh}\Big] \ . \tag{6.61}$$

If $N_{gh} = 0$, then $n_4 = -n_{11}$, so the only allowed values are $n_4 = n_{11} = 0$. It follows that $n_2 = n_9 = 0$ also, and, substituting these values into eqs. (6.60) and (6.61), one obtains $n_5 = n_7$. Thus, this class of solutions, which we denote as (i), has an **n** vector equal to

$$\mathbf{n} = (0, 0, 0, 0, s, t, s, 0, 0, 0, 0) \ , \tag{6.62}$$

where s and t are non-negative integers. Since $[6]_{12} \approx [\bar{6}]_{12}$ and $[5]_{12} \approx [\bar{7}]_{12}$, this SU(12) theory is vectorial, and hence so are resultant $\mathrm{SU}(10)_{\mathrm{SCC}}$ and $\mathrm{SU}(5)_{\mathrm{SC}}$ theories. Hence, even if the SCC and SC interactions were asymptotically free (which they are not), these sectors would not self-break via condensate formation as would be necessary in order to extract the TC theory and the Standard Model fermion generations. In order to minimize the number of fermions in an effort to maintain asymptotic freedom, we consider the two minimal classes (cases), (ia) $s = 0$, $t = 1$; and (ib) $s = 1$, $t = 0$. As mentioned, we find that the $\mathrm{SU}(10_{SCC})$ sector is not asymptotically free for either the cases (ia) or (ib).

Among other solutions, we focus on one that minimize the fermion content in an effort to preserve asymptotic freedom. We find cases with minimal **n** vectors for $N_{gh} = 3$. Among these, the minimal one has

$$(ii): \quad \mathbf{n} = (0, 1, 0, 1, 0, 0, 0, 0, 2, 0, 2) \ . \tag{6.63}$$

We find that this yields a chiral $\mathrm{SU}(10)_{\mathrm{SCC}}$ gauge interaction, as desired, but the $\mathrm{SU}(10)_{\mathrm{SCC}}$ sector is again not asymptotically free. We have found similar non-asymptotically free SCC sectors for other solutions for this $N_g = 3$ case, and also for cases with $N_g = 1, 2$. Our results suggest that non-asymptotically free SCC and SC sectors appear to be a generic problem with models having unification groups SU(N) with $N \geq 11$.

N	$N_{\rm SC}$	$N_{\rm TC}$	N_{gl}	N_{gh}	**n**	SCC	$N_{(1,1)}$
11	6	5	1	2	(0000300202)	iia, CGT, NAF	3
11	6	5	1	2	(0101010101)	iib, VGT, NAF	1
11	6	5	1	2	(0202050000)	iic, CGT, NAF	5
11	6	3	3	0	(0000110000)	i, VGT, NAF	2
12	7	4	3	0	(00000100000)	ia, VGT, NAF	0
12	7	4	3	0	(00001010000)	ib, VGT, NAF	2
12	7	7	0	3	(01010000202)	ii, CGT, NAF	0

Table 6.1: Solutions to models with $\mathcal{G}_{\rm SC}$ and $\mathcal{G}_{\rm SM}$ unified into a simple gauge group $\mathcal{G} = {\rm SU}(N)$ from [127]. Here $\mathcal{G}_{\rm SC} = {\rm SU}(N_{\rm SC})$ and $\mathcal{G}_{\rm SC} \supseteq \mathcal{G}_{\rm TC}$. The "SCC" notation list the properties of the ${\rm SU}(N_{\rm SC})$ and the ${\rm SU}(3)_c$. The notation VGT and CGT stand for vectorial or chiral gauge theory respectively; AF and NAF stand for asymptotically free theories or non asymptotically free theories respectively. The **n** notation follows the (6.12). The $N_{(1,1)}$ is the number of EW-singlet neutrinos.

Chapter 7

Outlook

This thesis has reported new results on phenomenological implications for two scenarios for physics beyond the Standard Model, namely supersymmetric models with supergravity mediation and models with dynamical electroweak symmetry breaking. Experiments at the LHC are giving important information constraining both of these scenarios. The experimental analysis has been carried out with focus on the mSUGRA models. Within this scenario, our results suggest that models with lighter MSSM Higgs should also be considered seriously, which would need completely different searching strategies compared to the large $\not{E}_T$ plus jets signals. Of course, the NUSUGRA models have more sparticle hierarchies, which lead to more possibilities to the LHC signals. As we have analyzed, one type of such models are those with light gluinos in the spectrum, which can be soon discovered or ruled out in the LHC run in Year 2011 and 2012 with $\sqrt{s} = 7$ TeV. In our extended study of SUGRA models, we have also noticed the possibility of explaining the anomalous positron signals from PAMELA search for dark matter. Several direct and indirect dark matter detection null results yield constraints on the SUGRA models, and their improved results in the near future will be directly related to the current SUGRA model searches.

We are already in the exciting LHC era. Above all, we shall have a complete understanding of electroweak symmetry breaking from the LHC data. Yet there should be more ultraviolet completion work to understand other

puzzles beyond Standard Model, e.g., the fermion mass hierarchies, the neutrino masses and mixing, the dark matter candidates, and so on. Experimental results from LHC and the dark matter searches would be important guidelines for the future work.

Bibliography

[1] Julius Wess and Jonathan Bagger, *Supersymmetry and Supergravity*, Princeton University Press.

[2] Peter van Nieuwenhuizen and Peter West, *Principles of Supersymmetry and Supergravity*, lecture notes.

[3] Manuel Drees, Rohini M. Godbole, Probir Roy, *Theory And Phenomenology of Sparticles, An account of four-dimensional* $\mathcal{N} = 1$ *supersymmetry in High Energy Physics*, World Scientific Publishing Co. Pte. Ltd.

[4] Peter W. Higgs, Phys. Rev. Lett. **13**: 508-509, 1964.

[5] Benjamin W. Lee, C. Quigg, H. B. Thacker, Phys. Rev. D **16**: 1519, 1977.

[6] H. Georgi and S. Glashow, Phys. Rev. Lett. **32**, 438 (1974).

[7] P. Langacker, Phys. Repts. **72**, 185 (1981).

[8] M. Fukugita and T. Yanagida, *Physics of Neutrinos and Applications to Astrophysics*.

[9] Ed. Witten, Nucl. Phys. B **188**: 513, 1981.

[10] Ed. Witten, Nucl. Phys. B **202**: 253, 1982.

[11] Stephen P. Martin, *A Supersymmetry Primer*, In *Kane, G.L. (ed.): Perspectives on supersymmetry II* 1-153, [arXiv: hep-ph/9709356].

[12] S. P. Martin and M. T. Vaughn, Phys. Rev. D **50** (1994) 2282, [arXiv: hep-ph/9311340].

[13] S. P. Martin, Phys. Rev. D **79**: 095019, 2009, [arXiv: 0903.3568 [hep-ph]].

[14] J. E. Kim and H. P. Nilles, Phys. Lett. B **138**, 150 (1984).

[15] S. Rai Choudhury, Naveen Gaur, Phys. Lett. B **451**, 86-92 (1999); [arXiv: hep-ph/9810307].

[16] J. S. Hagelin, S. Kelly, and T. Tanaka, Nucl. Phys. B **415** (1994) 293, [arXiv: hep-ph/9304218]. D. W. Sutter, [arXiv: hep-ph/9704390].

[17] G. F. Giudice, R. Rattazzi, Phys. Rept. 332: 419-499, 1999, [arXiv: hep-ph/9801271].

[18] M. Dine, A. E. Nelson, Phys. Rev. **D 48** (1993) 1277, [arXiv: hep-ph/9303230]; M. Dine, A. E. Nelson, Y. Shirman, Phys. Rev. **D 51** (1995) 1362, [arXiv: hep-ph/9408384]; M. Dine, A. E. Nelson, Y. Nir, Y. Shirman, Phys. Rev. **D 53** (1996) 2658, [arXiv: hep-ph/9507378].

[19] Patrick Meade, Nathan Seiberg, David Shih, Prog. Theor. Phys. Suppl. **177**: 143-158, 2009, [arXiv: 0801.3278 [hep-ph]].

[20] A. H. Chamseddine, R. Arnowitt, and Pran Nath, Phys. Rev. Lett. **49**: 970, 1982; Nucl. Phys. B **227**, 121 (1983).

[21] Lawrence J. Hall, Joseph D. Lykken, Steven Weinberg, Phys. Rev. D **27**: 2359-2378, 1983.

[22] Richard L. Arnowitt and Pran Nath, Phys. Rev. D **46**: 3981-3986,1992.

[23] K. L. Chan, U. Chattopadhyay, and P. Nath, Phys. Rev. D **58**, 096004 (1998) [arXiv: hep-ph/9710473]; J. L. Feng, K. T. Matchev, and T. Moroi, Phys. Rev. Lett. **84**, 2322-2325 (2000) [arXiv: hep-ph/9908309]; H. Baer, C. Balazs, A. Belyaev, T. Krupovnickas and X. Tata, JHEP **0306**, 054 (2003) [arXiv: hep-ph/0304303].

[24] Daniel Feldman, Zuowei Liu, and Pran Nath, Phys. Rev. Lett. **99**: 251802, 2007, [arXiv: 0707.1873 [hep-ph]].

[25] R. Arnowitt *et al.*, Phys. Lett. B **649**, 73 (2007); U. Chattopadhyay, D. Das, A. Datta and S. Poddar, Phys. Rev. D **76**, 055008 (2007), [arXiv:0705.0921 [hep-ph]]; H. Baer, A. Mustafayev, E. K. Park and X. Tata, JHEP **0805**, 058 (2008), [arXiv:0802.3384 [hep-ph]]; D. Feldman, Z. Liu and P. Nath, Phys. Rev. D **78**, 083523 (2008), [arXiv:0808.1595 [hep-ph]]; S. Bhattacharya, U. Chattopadhyay, D. Choudhury, D. Das and B. Mukhopadhyaya, [arXiv:0907.3428 [hep-ph]]; H. Baer, V. Barger, A. Lessa and X. Tata, [arXiv:0907.1922 [hep-ph]].

[26] A. Djouadi, M. Spira and P. M. Zerwas, Phys. Lett. B **264**, 440 (1991); M. Spira, A. Djouadi, D. Graudenz and P. M. Zerwas, Nucl. Phys. B **453** (1995) 17, [arXiv:hep-ph/9504378].

[27] H. Baer, K. m. Cheung and J. F. Gunion, Phys. Rev. D **59**, 075002 (1999), [arXiv:hep-ph/9806361]; S. Raby and K. Tobe, Nucl. Phys. B **539**, 3 (1999), [arXiv:hep-ph/9807281].

[28] C. Balazs, J. L. Diaz-Cruz, H. J. He, T. M. P. Tait and C. P. Yuan, Phys. Rev. D **59**, 055016 (1999), arXiv:hep-ph/9807349].

[29] D. J. Miller, S. Moretti, D. P. Roy and W. J. Stirling, Phys. Rev. D **61**, 055011 (2000), [arXiv:hep-ph/9906230].

[30] J. M. Campbell, R. K. Ellis, F. Maltoni and S. Willenbrock, Phys. Rev. D **67**, 095002 (2003), [arXiv:hep-ph/0204093].

[31] F. Maltoni, Z. Sullivan and S. Willenbrock, Phys. Rev. D **67**, 093005 (2003), [arXiv:hep-ph/0301033].

[32] R. V. Harlander and W. B. Kilgore, Phys. Rev. D **68**, 013001 (2003), [arXiv:hep-ph/0304035].

[33] S. Profumo, Phys. Rev. D **72**, 103521 (2005), [arXiv:astro-ph/0508628]; S. Profumo, C. Yaguna, Phys. Rev. D **69**, 115009 (2004), [arXiv:hep-ph/0402208].

[34] M. S. Carena, S. Heinemeyer, C. E. M. Wagner and G. Weiglein, Eur. Phys. J. C **45**, 797 (2006), [arXiv:hep-ph/0511023].

[35] A. Belyaev, A. Blum, R. S. Chivukula and E. H. Simmons, Phys. Rev. D **72**, 055022 (2005), [arXiv:hep-ph/0506086]; U. Aglietti *et al.*, [arXiv:hep-ph/0612172].

[36] M. Guchait, R. Kinnunen and D. P. Roy, Eur. Phys. J. C **52**, 665 (2007), [arXiv:hep-ph/0608324].

[37] S. Dawson, D. Dicus, C. Kao and R. Malhotra, Phys. Rev. Lett. **92**, 241801 (2004), [arXiv:hep-ph/0402172].

[38] C. Kao, D. A. Dicus, R. Malhotra and Y. Wang, Phys. Rev. D **77**, 095002 (2008), [arXiv:0711.0232 [hep-ph]].

[39] D. Feldman, Z. Liu and P. Nath, Phys. Lett. B **662**, 190 (2008), [arXiv:0711.4591 [hep-ph]].

[40] Daniel Feldman, Zuowei Liu, and Pran Nath, JHEP 0804: 054, 2008, [arXiv: 0802.4085 [hep-ph]].

[41] Daniel Feldman, Zuowei Liu, and Pran Nath, Phys. Rev. D **78**: 083523, 2008, [arXiv: 0808.1595 [hep-ph]].

[42] Daniel Feldman, Zuowei Liu, and Pran Nath, Phys. Rev. D **80**: 015007, 2009, [arXiv: 0905.1148 [hep-ph]].

[43] D. S. M. Alves, E. Izaguirre and J. G. Wacker, [arXiv:1008.0407 [hep-ph]].

[44] B. Altunkaynak, M. Holmes, P. Nath, B. D. Nelson and G. Peim, Phys. Rev. D **82**:115001,2010, [arXiv: 1008.3423 [hep-ph]].

[45] L. Covi, M. Olechowski, S. Pokorski, K. Turzynski and J. D. Wells, JHEP **1101**: 033, 2011, [arXiv:1009.3801 [hep-ph]].

[46] Daniel Feldman, Katherine Freese, Pran Nath, Brent D. Nelson, and Gregory Peim, [arXiv: 1102.2548 [hep-ph]].

[47] Ning Chen, Daniel Feldman, Zuowei Liu, and Pran Nath, Phys. Lett. B **685**: 174-181, 2010.

[48] Ning Chen, Daniel Feldman, Zuowei Liu, Pran Nath, and Gregory Peim, Phys. Rev. D **83**: 023506, 2011, [arXiv: 1010.0939 [hep-ph]].

[49] Ning Chen, Daniel Feldman, Zuowei Liu, Pran Nath, and Gregory Peim, Phys. Rev. D **83**: 035005, 2011, [arXiv: 1011.1246 [hep-ph]].

[50] Sujeet Akula, Ning Chen, Daniel Feldman, Mengxi Liu, Zuowei Liu, Pran Nath, and Gregory Peim, Phys. Lett. B, in press [arXiv: 1103.1197 [hep-ph]].

[51] http://home.thep.lu.se/ torbjorn/Pythia.html

[52] http://www.physics.ucdavis.edu/ conway/research/software/pgs/pgs.html

[53] B. C. Allanach, Comput. Phys. Commun. **143**: 305-331, 2002, [arXiv: hep-ph/0104145].

[54] Abdelhak Djouadi, Jean-Lioc Kneur, Gilbert Moultaka, Comput. Phys. Commun. **176**: 426-455, 2007, [arXiv: hep-ph/0211331].

[55] Johan Alwall *et al.* JHEP 0709: **028**, 2007, [arXiv: 0706.2334 [hep-ph]].

[56] G. Belanger, F. Boudjema, A. Pukhov, A. Semenov, Comput. Phys. Commun. **180**: 747-767, 2009, [arXiv: 0803.2360 [hep-ph]]. G. Belanger, F. Boudjema, P. Brun, A. Pukhov, S. Rosier-Lees, P. Salati, A. Semenov, Comput. Phys. Commun. **182**: 842-856, 2011, [arXiv: 1004.1092 [hep-ph]].

[57] Peter Z. Skands *et al.*, JHEP 0407: 036, 2004. [arXiv: hep-ph/0311123].

[58] G. Degrassi, P. Gambino and P. Slavich, Comput. Phys. Commun. **179**, 759 (2008), [arXiv:0712.3265 [hep-ph]].

[59] CMS Collaboration, CERN/LHCC 2006-001 (2006).

[60] C. Lampen, ATL-PHYS-PROC-2009-122 (ATLAS Notes).

[61] pdg.lbl.gov

[62] The neutrino oscillation experiments include: S. Fukuda, *et al.* Phys. Lett.]**B433** (1998) 9; Phys. Rev. Lett. **81** (1998) 1562; *ibid.*, **82** (1999) 2644; Phys. Lett. **B467** (1999) 185; Phys. Rev. Lett. **85** (2000) 3999; Phys. Rev. Lett. **86** (2001) 5651, 5656; Phys. Lett. **B539** (2002) 179 (SuperK). Q. Ahmad *et al.*, Phys. Rev. Lett. **87** (2001) 071301; *ibid.* **89** (2002) 011301, 011302 (SNO).

[63] S. Dawson, C. B. Jackson, L. Reina, and D. Wackeroth, Mod. Phys. Lett. A **21**, 89 (2006), [hep-ph/0508293].

[64] D. Feldman, Z. Liu and P. Nath, Phys. Lett. B **662**, 190 (2008), [arXiv:0711.4591 [hep-ph]].

[65] G. Barenboim, P. Paradisi, O. Vives, E. Lunghi and W. Porod, JHEP **0804**, 079 (2008), [arXiv:0712.3559 [hep-ph]].

[66] B. Dudley and C. Kolda, [arXiv:0901.3337 [hep-ph]].

[67] [CDF and D0 Collaboration], ICHEP 2010, Paris, France, 21-28 Jul 2010; [arXiv: 1007.4587 [hep-ex]].

[68] CMS Collaboration, Phys. Lett. B **698**: 196-218, 2011. [arXiv: 1101.1628 [hep-ex]].

[69] ATLAS Collaboration, [arXiv: 1102.2357 [hep-ex]].

[70] ATLAS Collaboration, [arXiv: 1102.5290 [hep-ex]].

[71] T. Aaltonen *et al.* [CDF Collaboration], Phys. Rev. Lett. **100**: 101802, 2008; [arXiv: 0712.1708 [hep-ex]].

[72] A. Djouadi, M. Drees and J. L. Kneur, JHEP **0603**, 033 (2006), [arXiv:hep-ph/0602001].

[73] M. Misiak *et al.*, Phys. Rev. Lett. **98**: 022002, 2007. [arXiv: hep-ph/0609232].

[74] E. Barberio *et al.* [Heavy Flavor Averaging Group], [arXiv: 0808.1297 [hep-ex]].

[75] S. Bertolini, F. Borzumati, A. Masiero and G. Ridolfi, Nucl. Phys. B **353**, 591 (1991).

[76] P. Nath and R. L. Arnowitt, Phys. Lett. B **336**, 395 (1994), [arXiv:hep-ph/9406389]; F. Borzumati, M. Drees and M. M. Nojiri, Phys. Rev. D **51**, 341 (1995), [arXiv:hep-ph/9406390].

[77] G. Degrassi, P. Gambino and G. F. Giudice, JHEP **0012** (2000) 009, [arXiv:hep-ph/0009337]; F. Borzumati, C. Greub, T. Hurth and D. Wyler, Phys. Rev. D **62**, 075005 (2000), [arXiv:hep-ph/9911245]; D. A. Demir and K. A. Olive, Phys. Rev. D **65**, 034007 (2002), [arXiv:hep-ph/0107329]; A. J. Buras et.al., Nucl. Phys. B **659** (2003) 3, [arXiv:hep-ph/0210145]; M. E. Gomez, T. Ibrahim, P. Nath and S. Skadhauge, Phys. Rev. D **74** (2006) 015015, [arXiv:hep-ph/0601163]; G. Degrassi, P. Gambino and P. Slavich, Phys. Lett. B **635** (2006) 335, [arXiv:hep-ph/0601135].

[78] J. L. Hewett, Phys. Rev. Lett. **70**, 1045 (1993), [arXiv:hep-ph/9211256]; V. D. Barger, M. S. Berger and R. J. N. Phillips, Phys. Rev. Lett. **70**, 1368 (1993), [arXiv:hep-ph/9211260].

[79] R. Garisto and J. N. Ng, Phys. Lett. B **315**, 372 (1993), [arXiv:hep-ph/9307301].

[80] M. Davier, A. Hoecker, B. Malaescu, C. Z. Yuan and Z. Zhang, [arXiv:0908.4300 [hep-ph]].

[81] T. C. Yuan, R. L. Arnowitt, A. H. Chamseddine and P. Nath, Z. Phys. C **26**, 407 (1984); D. A. Kosower, L. M. Krauss and N. Sakai, Phys. Lett. B **133**, 305 (1983); J. L. Lopez, D. V. Nanopoulos and X. Wang, Phys. Rev. D **49**, 366 (1994), [arXiv:hep-ph/9308336]; J. L. Lopez, D. V. Nanopoulos and X. Wang, Phys. Rev. D **49**, 366 (1994), [arXiv:hep-ph/9308336]; T. Moroi, Phys. Rev. D **53**, 6565 (1996), [arXiv:hep-ph/9512396].

[82] A. Czarnecki and W. J. Marciano, Phys. Rev. D **64**, 013014 (2001), [arXiv:hep-ph/0102122].

[83] U. Chattopadhyay and P. Nath, Phys. Rev. Lett. **86**, 5854 (2001), [arXiv:hep-ph/0102157].

[84] L. L. Everett, G. L. Kane, S. Rigolin and L. T. Wang, Phys. Rev. Lett. **86**, 3484 (2001), [arXiv:hep-ph/0102145].

[85] A. D. Sakharov, Pisma Zh.Eksp.Teor.Fiz. **5**: 32-35,1967, JETP Lett. **5**: 24-27,1967, Sov.Phys.Usp. **34**: 392-393,1991.

[86] Arno A. Penzias, Robert Woodrow Wilson, Astrophys. J. **142**: 419-421, 1965. Eric Gawiser, Joseph Silk, Phys. Rept. **333**: 245-267, 2000, [arXiv: astro-ph/0002044].

[87] N. Jarosik et al. [WMAP Collaboration], [arXiv: 1001.4744 [astro-ph.CO]]; E. Komatsu et al. [WMAP Collaboration], Astrophys. J. Suppl. **180**, 330 (2009); D. N. Spergel et al. [WMAP Collaboration], Astrophys. J. Suppl. **170**, 377 (2007).

[88] Gerard Jungman, Marc Kamionkowski, Kim Griest, *Supersymmetric Dark Matter*, Phys. Rept. **267**: 195-373, (1996), [arXiv: hep-ph/9506380].

[89] Gianfranco Bertone, Dan Hooper, Joseph Silk, *Particle dark matter: Evidence, candidates and constraints*, Phys. Rept. **405**: 279-390, 2005, [arXiv: hep-ph/0404175].

[90] K. G. Begeman, A. H. Broeils and R. H. Sanders, 1991, MNRAS, 249, 523.

[91] K. Griest and D. Seckel, Phys. Rev. D **43** (1991) 3191; J. Edsjo and P. Gondolo, Phys. Rev. D **56**, 1879 (1997); J. R. Ellis, T. Falk and K. A. Olive, Phys. Lett. B **444** (1998) 367; J. R. Ellis, T. Falk, K. A. Olive and M. Srednicki, Astropart. Phys. **13**: 181-213, 2000.

[92] P. Nath and R. L. Arnowitt, Phys. Rev. Lett. **70**, 3696 (1993); Phys. Lett. B **299**, 58 (1993) [Erratum-ibid, B **307**, 403 (1993)]; J. L. Lopez, D. V.

Nanopoulos and K. J. Yuan, Phys. Rev. D **48**, 2766 (1993); H. Baer and M. Brhlik, Phys. Rev. D **53**, 597 (1996); V. D. Barger and C. Kao, Phys. Rev. D **57**, 3131 (1998).

[93] Edward A. Baltz, Joakim Edsjo, Phys. Rev. D **59**: 023511, 1998, [arXiv: astro-ph/9808243].

[94] Lars Bergstrom, Joakim Edsjo, Piero Ullio, Astrophys. J. **526**: 215-235, 1999, [arXiv: astro-ph/9902012]

[95] Daniel Feldman, Zuowei Liu, and Pran Nath, Phys. Rev. D **75**: 115001,2007. [arXiv: hep-ph/0702123]

[96] Daniel Feldman, Gordon Kane, and Ran Lu, Phys. Lett. B **687**: 363-370, 2010. [arXiv: 1002.2430 [hep-ph]].

[97] Marco Cirelli, Roberto Franceschini, Alessandro Strumia, Nucl. Phys. B 800: 204-220, 2008. [arXiv: 0802.3378 [hep-ph]].

[98] T. Delahaye, R. Lineros, F. Donato, N. Fornengo and P. Salati, Phys. Rev. D **77**, 063527 (2008), [arXiv: 0712.2312 [astro-ph]].

[99] P. Brun, G. Bertone, J. Lavalle, P. Salati, R. Taillet, Phys. Rev. D **76**, 083506 (2007), [arXiv: 0704.2543 [astro-ph]].

[100] R. Lemrani, **EDELWEISS** Collaboration *Phys. Atom. Nucl.* **69** (2006) 1967-1969.

[101] R. Bernabei *et. al.*, *AIP Conf. Proc.* **878** (2006) 91-98.

[102] D. S. Akerib *et. al.*, **CDMS** Collaboration, [arXiv: astro-ph/0609189].

[103] Z. Ahmed *et. al.*, Science **327**, 1619 (2010), [arXiv: 0912.3592 [astro-ph. CO]].

[104] J. Angle *et. al.*, **XENON** Collaboration, [arXiv: 0706.0039 [astro-ph]].

[105] E. Aprile *et. al.*, [XENON100 Collaboration], Phys. Rev. Lett. 105: 131302, 2010. [arXiv: 1005.0380 [astro-ph. CO]].

[106] E. Aprile *et. al.*, [XENON100 Collaboration], [arXiv: 1104.2549 [astro-ph. CO]].

[107] [PAMELA], Nature **458**, 607 (2009); Phys. Rev. Lett. **102**, 051101 (2009); Astropart. Phys. **34**, 1 (2010); Phys. Rev. Lett. **105**, 121101 (2010).

[108] [Fermi-LAT] Phys. Rev. Lett. **104**, 091302 (2010). [arXiv: 1001.4836 [astro-ph. HE]].

[109] S. Weinberg, Phys. Rev. D **19**, 1277 (1979); L. Susskind, Phys. Rev. D **20**, 2619 (1979).

[110] C. Quigg and R. Shrock, Phys. Rev. D **79**, 096002 (2009), [arXiv: 0901.3958 [hep-ph]].

[111] S. Dimopoulos and L. Susskind, Nucl. Phys. **B155**, 237 (1979); E. Eichten and K. Lane, Phys. Lett. **B90**, 125 (1980).

[112] C. T. Hill and E. H. Simmons, Phys. Rep. **381**, 235 (2003).

[113] R. Shrock, in M. Harada, M. Tanabashi, and K. Yamawaki, eds. *The Origin of Mass and Strong Coupling Gauge Theories, SGCT06* (World Scientific, Singapore, 2008), p. 227.

[114] R. S. Chivukula, M. Narain, and J. Womersley, in Particle Data Group, J. Phys. G **37** 1340, (2010)

[115] F. Sannino, Acta Phys. Polon. B **40**, 3533 (2009), [arXiv:0911.0931 [hep-ph]].

[116] S. Raby, S. Dimopoulos, and L. Susskind, Nucl. Phys. **B** 169, 373 (1980).

[117] Michael E. Peskin, Tatsu Takeuchi, Phys. Rev. D **46**: 381-409, 1992.

[118] G. Aad et al. (ATLAS Collab.), Phys. Rev. Lett. **105**, 161801 (2010).

[119] CMS Collab., Phys. Rev. Lett. **105**: 211801, 2010, [arXiv:1010.0203 [hep-ex]].

[120] T. Appelquist and J. Terning, Phys. Rev. D **50**, 2116 (1994), [arXiv: hep-ph/9311320].

[121] T. Appelquist and R. Shrock, Phys. Lett. B **548**, 204 (2002). [arXiv: hep-ph/0204141].

[122] Neil D. Christensen, and Robert Shrock, Phys. Rev. D **72**: 035013, 2005. [arXiv: hep-ph/0506155].

[123] T. Appelquist, M. Piai, and R. Shrock, Phys. Rev. D **69**, 015002 (2004). [arXiv: hep-ph/0308061].

[124] T. Appelquist, M. Piai, and R. Shrock, Phys. Lett. B **593**, 175 (2004); Phys. Lett. B **595**, 442 (2004).

[125] Thomas Appelquist, Robert Shrock, Phys. Rev. Lett. **90**: 201801, 2003. [arXiv: hep-ph/0301108].

[126] T. Appelquist, N. D. Christensen, M. Piai, and R. Shrock, Phys. Rev. D **70**, 093010 (2004).

[127] Ning Chen, and Robert Shrock, Phys. Rev. D 78: 035002, 2008. [arXiv: 0805.3687 [hep-ph]].

[128] E. Farhi and L. Susskind, Phys. Rev. D **20**, 3404 (1979).

[129] N. D. Christensen and R. Shrock, Phys. Lett. B **632**, 92 (2006); S. B. Gudnason, T. A. Ryttov, and F. Sannino, Phys. Rev. D **76**, 015005 (2007).

[130] H. Georgi, Nucl. Phys. B **156**, 126 (1979).

Appendix A

$\mathcal{N} = 1$ Rigid Supersymmetric Models

In this chapter, we will review two basic $\mathcal{N} = 1$ rigid supersymmetric theories for the realistic model building, namely the Wess-Zumino (WZ) theory and supersymmetric Yang-Mills (SYM) theory. Their generalization into Standard Model yields the supersymmetric Standard Model to be discussed in chapter (2). We start from reviewing the supersymmetric vacuum and where supersymmetry is broken in the rigid supersymmetric theories in Section (A.1). Then we discuss the WZ and SYM theories in Section (A.2) and (A.3) within the superspace. Our convention and details of the "superspace calculus" follows Ref. [2]. Other reviews include [1] [3].

A.1 Introduction to SUSY Vacuum

In rigid supersymmetry, the Hamiltonian is the sum of the squares of the SUSY generators[1]: $H = Q^\dagger Q$. Because of this, the energy of any state in the theory should be semi-positive definite. A SUSY vacuum state is defined such that $Q|\Omega\rangle = 0$. Hence it is clear that it has a vanishing vacuum energy $E_\Omega = 0$. Furthermore, one may notice that states of non-zero energy in the

[1]The SUSY generator is a two-component spinor, which is defined as: $Q_\alpha \equiv \int d^3x S_{0\alpha}$, with $S_{0\alpha}$ being the time component of the super-current $S_{\mu\alpha}$.

SUSY theory must be paired by the supercharge Q in the following fashion:

$$Q|b\rangle = \sqrt{E}|f\rangle \qquad Q|f\rangle = \sqrt{E}|b\rangle \tag{A.1}$$

However, this is not the case for $E = 0$ states. One is allowed to have any number of bosonic/fermionic states at $E = 0$ level. As one varies some parameter of the theory, some zero-energy states may make transitions into non-zero energy states and vice versa. However, there must be pair of bosons/fermions to transit between states. Under any variation of states, the quantity of $n_B^{E=0} - n_F^{E=0}$ is always unchanged. This quantum invariant is called *Witten index* [9, 10], denoted as $\Delta \equiv \ \mathrm{Tr}(-1)^F$. This quantity can be reliably computed in many different models. Its physical meaning is the following:

- For $\Delta \neq 0$, it must be either $n_B^{E=0} \neq 0$ or $n_F^{E=0} \neq 0$ or both. In any case, SUSY is unbroken.
- For $\Delta = 0$, there can be two sub cases. One may have $n_B^{E=0} = n_F^{E=0} \neq 0$, which means there are vacuum states with $E_\Omega = 0$; hence SUSY is unbroken. One may also have $n_B^{E=0} = n_F^{E=0} = 0$, i.e. all states in the spectrum must have $E > 0$; hence SUSY is broken.

One can also view from the perspective of the vacuum energy density in the SUSY theory, which is defined as the expectation value of the energy-momentum tensor:

$$\langle\Omega|T_{\mu\nu}|\Omega\rangle = E_\Omega \eta_{\mu\nu} \tag{A.2}$$

(where $\eta_{\mu\nu}$ is the flat-space metric) with the energy-momentum tensor in the SUSY theory being $T_{\mu\nu} = (\gamma_\mu)_{\alpha\beta}\{Q_\alpha, S_{\nu\beta}\}$. Hence for any non-zero E_Ω, this means SUSY is spontaneously broken. For the SUSY breaking case, an analogue of Goldstone's theorem can be formulated in terms of SUSY currents. By current algebra, one can write the anti-commutator from Eq. (A.2) into:

$$\langle\Omega|\{Q_\alpha, S_{\mu\beta}\}|\Omega\rangle = \int d^4x \partial_\rho \langle\Omega|TS_{\rho\alpha}(x)S_{\mu\beta}(0)|\Omega\rangle \tag{A.3}$$

To have a non-vanishing contribution from the (A.3), the two-point function $\langle\Omega|TS(x)S(0)|\Omega\rangle$ should behave as $1/r^3$ as $r \to \infty$. The only possible intermediate state is the spin 1/2 massless fermion, which is known as *Goldstino*. One can define the coupling between the Goldstino and the supercurrent through:

$$\langle\Omega|S_{\mu\alpha}|\psi_\beta\rangle = f(\gamma_\mu)_{\alpha\beta} \tag{A.4}$$

It is not hard to find that the coupling f is related to the vacuum energy density as: $E_\Omega = f^2$. In other words, for the SUSY-breaking vacuum with $E_\Omega \neq 0$, there should be a massless Golstino emerge with the coupling strength to the super-current being $f = \sqrt{E_\Omega}$.

A.2 Wess-Zumino Theory

The Wess-Zumino (WZ) theory, expressed in superspace form, contains a chiral supermultiplet $\Phi(x, \theta)$ (and its conjugate $\Phi^\dagger(x, \overline{\theta})$ in the superspace) with its general form as follows:

$$\mathcal{L} \quad = \quad \int d^4\theta \mathcal{K}(\Phi^\dagger, \Phi) + (\int d^2\theta \mathcal{W}(\Phi) + h.c.) \tag{A.5}$$

The first term in Eq. (A.5) is a real function of Φ, which is called *Kähler potential*. In other words, the chiral field must appear in the form of $f(\Phi^\dagger\Phi)$ in the Kähler potential. This function gives the kinematic terms for the scalar and spinor components of the supermultiplet. The simplest Kähler potential reads $\mathcal{K}(\Phi^\dagger, \Phi) = \Phi^\dagger\Phi$, which is called the *canonical Kähler potential*. The

second one is a holomorphic function[2] of Φ, which is called the *superpotential*. This term yields masses and interactions for the chiral fields.

The chiral supermultiplet contains three components: $\Phi = (\phi, \psi, F)$. One easy way is to define each component by the covariant derivatives in the superspace as:

$$\Phi|_{\theta=0} = \phi, \qquad D_\alpha \Phi|_{\theta=0} = \psi_\alpha, \qquad -\frac{1}{2} D^2 \Phi|_{\theta=0} = F \tag{A.6}$$

With this definition one can easily show that the canonical Kähler potential yields the following kinematic terms by performing the superspace integration:

$$\mathcal{L}_{\text{WZfree}} = \int d^4\theta \Phi^\dagger \Phi = -|\partial\phi|^2 - \overline{\psi}\sigma^\mu \partial_\mu \psi + \frac{1}{4}|F|^2 \tag{A.7}$$

The scalar potential of the WZ model $V(\phi^\dagger, \phi)$ is derived by varying the chiral field Φ in the superspace:

$$\begin{aligned} & \frac{\delta}{\delta\Phi}[\int d^2\theta(-\frac{1}{4}\overline{D}^2\Phi^\dagger)\Phi + \mathcal{W}(\Phi)] + h.c. = 0 \\ \Rightarrow \quad & F^*_{\text{sol}} = -2\frac{\partial \mathcal{W}}{\partial \Phi}|_{\theta=0} \qquad F_{\text{sol}} = -2\frac{\partial \mathcal{W}^\dagger}{\partial \Phi^\dagger}|_{\overline{\theta}=0} \end{aligned} \tag{A.8}$$

By substituting the solution (A.8) into the auxiliary part in the (A.7), one gets the scalar potential[3]:

$$V(\phi, \phi^\dagger) = \frac{1}{4}|F_{\text{sol}}|^2 = |\frac{\partial \mathcal{W}}{\partial \Phi}|^2 \tag{A.9}$$

[2]By 'holomorphic', we mean that $\mathcal{W}(\Phi)$ is a polynomial in Φ and does not contain the conjugated fields $\Phi^\dagger$.

[3]In the more general case where one can have multiple chiral fields Φ_i, the scalar potential reads: $V(\phi_i^\dagger, \phi_i) = (\mathcal{K}^{\Phi^\dagger\Phi})_{ij}(\partial^i \mathcal{W})(\partial^{\bar{j}} \mathcal{W}^\dagger)|_{\theta=\bar{\theta}=0}$, where $(\mathcal{K}^{\Phi^\dagger\Phi})_{ij} \equiv (\partial\mathcal{K}/\partial\Phi\partial\Phi^\dagger)^{-1}_{ij}$ is the inverse of the Kähler metric, and $\partial^i \mathcal{W} = \partial\mathcal{W}/\partial\Phi_i$.

This expression tells where does supersymmetry break in the WZ theory. From our previous discussion of the SUSY vacuum, it is obvious that when a non-vanishing vev of $\langle F \rangle \neq 0$ exists, one gets a positive-definite scalar potential in the vacuum. Hence this breaks the rigid SUSY. This type of breaking is called the *F-term breaking*.

A.3 Super Yang-Mills Theory

To describe the superfields in the gauge sector, one uses a hermitian vector[4] superfield $V \equiv V^a T^a$ for the gauge multiplet $(A^a_\mu, \lambda^a_\alpha, D^a)$. We shall also define the gauge covariant field strength W_α and its conjugates $\overline{W}_{\dot{\alpha}}$ (which are also shown to be chiral $\overline{D}_{\dot{\beta}} W_\alpha = 0$ and anti-chiral $D_\beta \overline{W}_{\dot{\alpha}} = 0$) as [5]:

$$W_\alpha \equiv \overline{D}^2 (e^{-V} D_\alpha e^V) \qquad \overline{W}_{\dot{\alpha}} \equiv D^2 (e^{-V} \overline{D}_{\dot{\alpha}} e^V) \tag{A.10}$$

Therefore, a gauge invariant pure SYM action in the superspace reads:

$$S_{\rm SYM} = \frac{1}{4} \int d^4x d^2\theta \mathrm{tr}(\mathrm{W}^\alpha \mathrm{W}_\alpha) + \mathrm{h.c.} \tag{A.11}$$

Each component of the vector supermultiplet is defined as:

$$\begin{aligned} D &= -2 D^\alpha W_\alpha|_{\theta=0} \qquad \lambda_\alpha = W_\alpha|_{\theta=\overline{\theta}=0} \\ A_\mu &= -\frac{1}{4} (\sigma_\mu)^{\alpha\dot{\beta}} [D_\alpha, \overline{D}_{\dot{\beta}}] V|_{\theta=\overline{\theta}=0} \end{aligned} \tag{A.12}$$

where each component is Lie-algebra valued. Then in the x-space, the SYM action reads:

[4] We define $V^\dagger = V$ for real vector multiplet. We also define the Lie algebra generator to be anti-hermitian as $(T^a)^\dagger = -T^a$, hence V^a is imaginary: $(V^a)^* = -V^a$. The gauge transformation of V is $\exp(V) \to \exp(\overline{\Lambda}) \exp(V) \exp(-\Lambda)$, where $\Lambda = \Lambda^a T^a$ and $\overline{\Lambda} \equiv -\Lambda^\dagger$ are the gauge transformation parameters in the superspace.

[5] The gauge transformation of the field strength reads: $W_\alpha \to \exp(\Lambda) W_\alpha \exp(-\Lambda)$, and one also has the equality $D^\alpha W_\alpha = \overline{D}^{\dot{\alpha}} \overline{W}_{\dot{\alpha}}$.

$$S_{\rm SYM} = {\rm tr}\int {\rm d}^4{\rm x}(-\frac{1}{4}{\rm F}_{\mu\nu}^2 - \frac{1}{2}\overline{\lambda}\gamma^\mu {\rm D}_\mu\lambda + \frac{1}{2}{\rm D}^2) \tag{A.13}$$

Similarly if $\langle D\rangle \neq 0$ is found, then the rigid SUSY breaks. This is called the *D-term breaking*.

Finally, we shall couple the matter chiral superfield [6] with the SYM field. A gauge-invariant action is easily obtained by generalizing the canonical Kähler potential in the WZ theory:

$$\int d^4x d^4\theta \Phi^\dagger (e^{gV})\Phi \tag{A.14}$$

which simply modifies the free WZ action (A.7) into the following interacting WZ action:

$$\begin{aligned}\mathcal{L}_{\rm int} &= -|D_\mu\phi|^2 - \overline{\psi}\sigma^\mu D_\mu\psi + \frac{1}{4}F^2 \\ &\quad -\sqrt{2}g((\phi T^a\psi)\lambda^a + h.c.) + g(\phi^* T^a\phi)D^a\end{aligned} \tag{A.15}$$

Combining the D-term from the (A.13), one can integrate out both F and D^a auxiliary fields to get:

$$\begin{aligned}\mathcal{L} &= -|D_\mu\phi|^2 - \overline{\psi}\sigma^\mu D_\mu\psi + V(\phi^\dagger,\phi) \\ &\quad -\sqrt{2}g((\phi T^a\psi)\lambda^a + h.c.) - \frac{g^2}{2}(\phi^* T^a\phi)^2\end{aligned} \tag{A.16}$$

[6] The gauge transformation for a chiral superfield goes as: $\Phi^a \to (e^\Lambda)^a{}_b\Phi^b$, where $\Lambda^a{}_b$ represents the gauge transformation parameter in the representation $\mathcal{R}$.

Appendix B

Gravity-mediated Supersymmetry Breaking Models

Since no supersymmetric partner of any known particle has been observed, supersymmetry must be broken in nature. Much important work on supersymmetric model building since the birth of the MSSM has been devoted to investigating the origin of supersymmetry breaking. In the discussion of chapter (2), many soft SUSY-breaking terms have been introduced in an *ad hoc* fashion. With more than one hundred free parameters introduced, the MSSM itself cannot be a predictive theory.

The spontaneous SUSY-breaking models cannot be achieved within the MSSM itself. Some separate hidden sector in addition to the MSSM (typically at some higher energy scale) is then introduced where SUSY can be spontaneously broken. The breaking of SUSY leads to a massless Goldstino to be absorbed by a gravitino. This led to the pioneering idea of coupling the supergravity into a realistic SUSY breaking model [20] [21] in early 1980's. The spontaneous SUSY breaking in a separate hidden sector is communicated to the MSSM sector via gravity. Hence, this leads to various soft breaking terms as we introduced in the previous discussion on the MSSM. Such a scheme of breaking the SUSY through a hidden sector and mediated by supergravity is

called the *SUGRA-mediation*.

B.1 Spontaneous SUSY breaking

We come to mention two spontaneous (rigid) SUSY-breaking models at the tree-level, either from the F-term breaking called O'Raifeartaigh model or from the D-term breaking called Fayet-Iliopoulos (FI) model. We shall explain why they are not realistic for the MSSM.

In the O'Raifeartaigh model, one introduces three different chiral supermultiplets into a superpotential:

$$\mathcal{W}(\Phi_1, \Phi_2, \Phi_3) \;=\; -k\Phi_1 + m\Phi_2\Phi_3 + \frac{y}{2}\Phi_1\Phi_3^2 \tag{B.1}$$

which translates into the following scalar potential:

$$V(\phi_1, \phi_2, \phi_3) \;=\; |k - \frac{y}{2}\phi_3^2|^2 + m^2|\phi_3|^2 + |m\phi_2 + y\phi_1\phi_3|^2 \tag{B.2}$$

without a consistent solution for $V(\phi_1, \phi_2, \phi_3) = 0$, hence the supersymmetry is broken at tree-level with such a superpotential. However, the mass spectrum[1] of this model follows the following supersymmetric sum rule:

$$\mathrm{STr}(\mathrm{m}^2) \equiv \sum_{\mathrm{j}} (-)^{2\mathrm{j}}(2\mathrm{j}+1)\ \mathrm{Tr}(\mathrm{m}_{\mathrm{j}}^2) = 0 \tag{B.3}$$

If the O'Raifeartaigh F-term breaking scheme were true for the MSSM fields, this implies the following relation between the electron and selectrons:

[1] Assuming that $m^2 \geq ky$, an expansion of the (B.2) around the $\langle\phi_1\rangle = \langle\phi_2\rangle = \langle\phi_3\rangle = 0$ yields the tree-level squared masses of: 0, m^2, and $m^2 \pm ky$. Meanwhile, the Weyl fermion squared masses are 0, m^2, and m^2. For the different case when $m^2 < ky$, one should expand the scalar potential in a different vacuum. This does not change the result of the supersymmetric sum rule.

$$2m_e^2 = m_{\tilde{e}_1}^2 + m_{\tilde{e}_2}^2 \tag{B.4}$$

However, no such scalar electrons with mass < 0.5 MeV were found in nature.

Another type of spontaneous SUSY-breaking model is by introducing a linear U(1) D-term. Combined with the D-term from the kinematic part of the SYM (A.13) and the interacting term (A.15), and also assuming a mass term (from the superpotential) for the scalar ϕ, one writes:

$$\mathcal{L}_{\rm FI} = \frac{1}{2}D^2 - m^2|\phi|^2 + gD(q|\phi|^2) - \kappa D \tag{B.5}$$

where q is the charge of ϕ. Since we are discussing the U(1) case, the interacting term from the (A.15) should be replaced with the $U(1)$ charge of the scalar field ϕ. Integrating out the auxiliary D field in the same way as we derive the (A.16), one gets the following FI-potential:

$$V_{\rm FI} = m^2|\phi|^2 + \frac{1}{2}(\kappa - gq|\phi|^2)^2 \tag{B.6}$$

Clearly this potential cannot vanish, hence SUSY is spontaneously broken. Again, such a D-term breaking is impossible in the MSSM. The only scalar fields that can enter the (B.6) are the sfermions charged under the $U(1)_Y$, while the MSSM superpotential (2.6) does not contribute the mass term. To have a non-vanishing scalar potential (B.6), one must have some of sfermions picking up non-zero vev's: $\langle\tilde{f}\rangle \neq 0$. If squarks or charged sleptons got non-zero vev's, this will lead to color/charge-breaking (CCB) SUSY breaking vacuum. However, the $\mathrm{SU}(3)_c \times \mathrm{U}(1)_{\rm em}$ is not a broken symmetry in nature[2]. Therefore, the FI D-term for $\mathrm{U}(1)_Y$ must be subdominant compared to other sources of superysmmetry breaking. Or one may consider the FI-type supersymmetry breaking by some other unknown U(1) gauge symmetry broken at very high

[2]Even if the sneutrinos pick up non-zero vev's, this FI D-term breaking leaves all gaugino fields massless, which makes it again unrealistic for the MSSM.

scale.

B.2 Supergravity GUT Model

We next review the SUGRA GUT model where the $\mathcal{N}=1$ SUGRA is coupled to chiral multiplets and vector multiplets. We shall recall that the full Lagrangian of the $\mathcal{N}=1$ rigid supersymmetric theory reads:

$$\mathcal{L}_{\text{rigid}} = \int d^2\theta(-\frac{1}{8}\overline{D}^2\Phi_i^\dagger(e^{gV})_{ij}\Phi_j + \mathcal{W}(\Phi_i) + \frac{1}{4}W_A^\alpha W_{A,\alpha}) + h.c. \quad \text{(B.7)}$$

Now we extend the discussion into the curved spacetime. This means that the (B.7) will be generalized into:

$$\mathcal{L} = \int d^2\theta(-\frac{1}{8}\overline{D}^2 K[\Phi_i^\dagger(e^{gV})_{ij}\Phi_j] + \mathcal{W}(\Phi_i) + \frac{1}{4}f^{AB}(\Phi_i)W_A^\alpha W_{B,\alpha}) \quad \text{(B.8)}$$

where K is a general real function and f^{AB} is a dimensionless analytic function of the chiral superfields. It will be convenient to re-write the Kähler potential function as:

$$\mathcal{K}(\Phi_i^\dagger(e^{gV})_{ij}\Phi_j) \equiv -3\log(-\frac{1}{3}\kappa^2 K(\Phi_i^\dagger(e^{gV})_{ij}\Phi_j)) \quad \text{(B.9)}$$

where we have defined $\kappa \equiv 1/M_{\text{pl}}$.

Meanwhile, the generalization into the $\mathcal{N}=1$ local supersymmetry means that one needs to include the gravitational fields. In the $\mathcal{N}=1$ supergravity, they are graviton field ${e_\mu}^m$ with its spin 3/2 superpartner gravitino ψ_μ. They together form the super vielbein field ${E_\Pi}^M = ({e_\mu}^m, \psi_\mu)$. Correspondingly, the usual Einstein scalar curvature R should be generalized to the superspace scalar curvature $\mathcal{R}$. Then the supergravity Lagrangian in terms of the $\mathcal{N}=1$ superspace reads:

$$\mathcal{L} \;=\; -\frac{3}{\kappa}\int d^2\theta E\mathcal{R} + h.c. \tag{B.10}$$

Or combining the (B.8) and the (B.10), one gets the full $\mathcal{N}=1$ Lagrangian for pure supergravity and its coupling to the chiral and vector superfields as:

$$\begin{aligned}\mathcal{L}_{\text{sugra}} \;=\; &\int d^2\theta E[\frac{3}{8\kappa^2}(\overline{D}^2 - 8\kappa\mathcal{R})\exp(-\frac{1}{3}\mathcal{K}[\Phi^\dagger e^{gV}\Phi]) \\ &+\mathcal{W}(\Phi) + \frac{1}{4}f^{AB}(\Phi)W_A^\alpha W_{B,\alpha}] + h.c.\end{aligned} \tag{B.11}$$

The final Lagrangian in the ordinary x-space is extremely lengthy after superspace integration from the (B.11), which contains bosonic kinematic term, fermionic kinematic term, the scalar potential term, the fermion mass term, and the four-fermion interaction term. In our following discussion, we shall combine the Kähler potential in the supergravity (B.9) with the superpotential into the following modified Kähler potential[3]:

$$\mathcal{G}(\Phi_i,\Phi_i^\dagger) \;\equiv\; \frac{1}{\kappa^2}(\mathcal{K}(\Phi_i,\Phi_i^\dagger) - \log(\kappa^6|\mathcal{W}(\Phi_i)|^2)) \tag{B.12}$$

We shall first mention a fermionic kinematic term for the gravitino ψ_μ as follows:

$$\mathcal{L}_{\text{FK}} \;=\; -\frac{e}{2\kappa}\exp(-\kappa^2\mathcal{G}/2)\overline{\psi}_\mu\sigma^{\mu\nu}\psi_\nu + ... \tag{B.13}$$

with $e \equiv \det e_\mu{}^m$ and ... being the irrelevant terms for our discussion. If the $\mathcal{N}=1$ local SUSY breaks spontaneously, the gravitino eats the goldstino to become massive (called the *Super-Higgs mechanism*). The spontaneous breaking of local SUSY means a non-vanishing vev of $\langle\mathcal{G}\rangle \neq 0$, with the gravitino

[3]The modified Kähler potential is invariant under the transformation: $\mathcal{K} \to \mathcal{K} + h(\Phi_i) + h^*(\Phi_i^\dagger)$ and $\mathcal{W} \to \exp(-h(\Phi_i))\mathcal{W}$.

mass reading:

$$m_{3/2} = \frac{1}{\kappa}\exp(-\kappa^2\langle\mathcal{G}\rangle/2) \tag{B.14}$$

As the rigid SUSY-breaking, one should have the spontaneous breaking of the local SUSY only when (at least) one auxiliary component of the superfields get non-vanishing vev's. In our consideration, the F-term of the chiral superfield reads:

$$F_i = \frac{1}{\kappa}\exp(-\kappa^2\mathcal{G}/2)(\mathcal{G}^{-1})_i{}^j\mathcal{G}_j + \frac{1}{4}f_k^{*AB}(\mathcal{G}^{-1})_i{}^k\lambda^A\lambda^B + ... \tag{B.15}$$

where we have:

$$\mathcal{G}_j \equiv \frac{\partial\mathcal{G}}{\partial\Phi^{j\dagger}}| \qquad \mathcal{G}^i{}_j \equiv \frac{\partial^2\mathcal{G}}{\partial\Phi_i\partial\Phi^{j\dagger}}| \tag{B.16}$$

and

$$f_k^{*AB} \equiv \frac{\partial f^{*AB}}{\partial\Phi^{k\dagger}}| \tag{B.17}$$

Next, the F-term scalar potential then reads:

$$V_F = -\exp(-\kappa^2\mathcal{G})[\frac{1}{\kappa^2}\mathcal{G}^i(\mathcal{G}^{-1})_i{}^j\mathcal{G}_j + \frac{3}{\kappa^4}] \tag{B.18}$$

Here we shall make an ansätz to split the chiral multiplet into the observed piece Z and the hidden piece Σ. We denote their lowest scalar components as (z, σ). The superpotential is separated into two parts correspondingly with the following modified Kähler potential $\mathcal{G}$ assumed:

$$\mathcal{G} = - Z^{i\dagger}Z_i - \Sigma^\dagger\Sigma - \frac{1}{\kappa^2}\log(\kappa^6|\mathcal{W}(z_i,\sigma)|^2) \quad \text{(B.19)}$$

$$\mathcal{W} = \mathcal{W}_o(Z_i) + \mathcal{W}_h(\Sigma) \quad \text{(B.20)}$$

With these assumptions and using that $\mathcal{K}(z_i, z^{i\dagger}, \sigma, \sigma^\dagger) = -\kappa^2(z^{i\dagger}z_i + \sigma^\dagger\sigma)$, the scalar potential (B.18) becomes:

$$e^{\mathcal{K}}V_F = \kappa^4|\mathcal{W}|^2(|z_i|^2 + |\sigma|^2) + |\frac{\partial\mathcal{W}_o}{\partial z_i}|^2 + \kappa^2(\mathcal{W}^* z_i(\partial^i\mathcal{W}_o) + h.c.)$$
$$+|\frac{\partial\mathcal{W}_h}{\partial\sigma}|^2 + \kappa^2(\mathcal{W}^*\sigma\frac{\partial\mathcal{W}_h}{\partial\sigma} + h.c.) \quad \text{(B.21)}$$

Notice that the $\partial^i\mathcal{W}_o \equiv \frac{\partial\mathcal{W}_o}{\partial Z_i}|_{\theta=0}$ and similar relations should be understood in this expression of the scalar potential. One can see a universal mass for all scalars z_i in the visible sector:

$$m_i^2 = \exp(-\langle\mathcal{K}\rangle)\kappa^4|\mathcal{W}|^2 = m_{3/2}^2 \equiv M_0^2 \quad \text{(B.22)}$$

In addition, the last term yields a universal trilinear coupling term among all scalar fields:

$$A_0 = e^{-\langle\mathcal{K}\rangle/2}\langle\frac{\sigma}{|\mathcal{W}|}\frac{\partial\mathcal{W}_h}{\partial\sigma}\rangle m_{3/2} \quad \text{(B.23)}$$

Finally, we shall give the gaugino mass from the crossing terms of the (B.15):

$$\mathcal{L}_\lambda = \frac{1}{4\kappa}e^{-\kappa^2\langle\mathcal{G}\rangle/2}\langle\mathcal{G}_j(\mathcal{G}^{-1})^j{}_k f^{AB,k}\rangle(\lambda^A\lambda^B) + h.c. \quad \text{(B.24)}$$

which yields the following gaugino masses:

$$m_\lambda^{AB} = \frac{1}{2} m_{3/2} \mathcal{R}e \langle \mathcal{G}_j (\mathcal{G}^{-1})^j{}_k f^{AB,k} \rangle \tag{B.25}$$

Unlike the scalar soft masses or the trilinear couplings, Eq. (B.25) does not imply the universality for gaugino masses. Notice that the $\mathcal{R}e f^{AB}$ is the coefficient of the gauge kinematic term $F^A_{\mu\nu} F^{\mu\nu,B}$, which is proportional to $1/g^2$. One can further assume the grand unification at the $M_U \simeq 10^{16}$ GeV, hence $\mathcal{R}e\langle f^{AB,k} \rangle \propto \delta^{AB}$ can be the simplest assumption. Thus, a universal gaugino mass can be assumed in the supergravity GUT model:

$$m_\lambda = M_{1/2} \tag{B.26}$$

Since f^{AB} is symmetric in the adjoint indices AB, the above statement is equivalent to the case when we only take the singlet contribution from the product of adj $\otimes$ adj $= \mathbf{1} + ...$ to the gaugino masses. Inclusion of non-singlet contributions denoted by ... leads to non-universality of the gaugino masses, i.e. there are different gaugino mass terms for different factor groups. The full discussion of the non-universal gaugino masses due to non-singlet terms from SU(5), SO(10), and E_6 gauge symmetries is presented in Ref [13]. In the text we have analyzed the collider signatures and dark matter implications in both mSUGRA models and SUGRA models with non-universal gaugino mass terms.